

WiMAX Cross Layer Capacity Optimization

BY

Siddharth Nair

A Thesis Presented to the
DEANSHIP OF GRADUATE STUDIES

KING FAHD UNIVERSITY OF PETROLEUM & MINERALS

DHAHRAN, SAUDI ARABIA

In Partial Fulfillment of the
Requirements for the Degree of

MASTER OF SCIENCE

In

Telecommunication Engineering

February, 2012

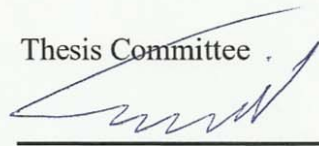
KING FAHD UNIVERSITY OF PETROLEUM AND MINERALS

DHAHRAN 31261, SAUDI ARABIA

DEANSHIP OF GRADUATE STUDIES

This thesis, written by Siddharth Nair under the directions of his thesis advisor and approved by his thesis committee, has been presented to and accepted by the Dean of Graduate Studies, in partial fulfillment of the requirements for the degree of **MASTER OF SCIENCE in TELECOMMUNICATIONS ENGINEERING.**

Thesis Committee

 25/2/12

Dr. Samir N. Al – Ghadhban (Advisor)



Dr. Mohammed A. Haleem (Co – advisor)



Dr. Salam A. Zummo (Member)



Dr. Tareq Y. Al – Naffouri (Member)

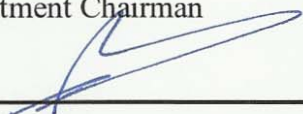


Dr. Ashraf S. Hasan Mahmoud (Member)



Dr. Ali A. Al – Shaikhi

Department Chairman



Dr. Salam A. Zummo

Dean of Graduate Studies

25/2/12

Date





Dedicated to My

Parents and My

Family Members



ACKNOWLEDGEMENT

I would like to acknowledge KFUPM for the support extended towards my research through its remarkable facilities and for providing me the opportunity to pursue graduate studies.

My deepest appreciation to my thesis advisor Dr. Samir Al-Ghadban and my thesis co-advisor Dr. Mohd. Abdul Haleem for their constant endeavor, guidance, positive criticism and the numerous moments of attention they devoted throughout this research work. Their valuable suggestions made this work interesting and knowledgeable for me. I extend my thanks for all the committee members for their constructive support and encouragement. I also owe thanks and recognition to my fellow RAs, course mates, colleagues and hostel friends for their help, motivation and support. Not all the names are possible to be mentioned here, but each one of them really made my stay at KFUPM joyful and memorable for lifetime. I am also obliged to thank all my friends especially Akber and Rizwan for their positive criticism. Finally, from the bottom of my heart, I thank my mother and father, and all my family members for their continuous love, encouragement, prayers, emotional and moral support throughout my life.

TABLE OF CONTENTS

ACKNOWLEDGEMENT.....	iv
LIST OF TABLES.....	viii
LIST OF FIGURES.....	ix
THESIS ABSTRACT (ENGLISH).....	xxi
THESIS ABSTRACT (ARABIC).....	xxii
CHAPTER 1: INTRODUCTION.....	1
1.1 INTRODUCTION.....	1
1.2 BACKGROUND	4
1.2.1 MIMO	6
1.2.2 OFDM	10
1.2.3 PRECODING	13
1.2.4 USER SCHEDULING.....	21
1.2.5 THEORETICAL BER	24
1.3 PROBLEM STATEMENT.....	27
1.4 THESIS CONTRIBUTIONS.....	28
1.5 THESIS ORGANIZATION	29

CHAPTER 2: LITERATURE REVIEW	30
2.1 CAPACITY ANALYSIS	31
2.2 PRECODING.....	33
2.3 USER SCHEDULING	39
CHAPTER 3: IEEE 802.16M CHANNEL MODEL.....	44
3.1 INTRODUCTION.....	45
3.2 STOCHASTIC CHANNEL MODELLING.....	45
3.3 CHANNEL BANDLIMITING UNIFORM SAMPLING.....	53
3.4 DOPPLER SHIFT.....	59
3.5 SPATIAL CORRELATION.....	66
3.6 SIMULATION METHODOLOGY.....	69
CHAPTER 4: HIERARCHICAL PRECODING	71
4.1 HIERARCHICAL PRECODING	72
4.1.1 FIXED RATIO POWER ALLOCATION	72
4.1.2 CAPACITY BASED POWER ALLOCATION	80
CHAPTER 5: ADAPTIVE EIGEN MODE REDUCTION.....	94
5.1 REDUCTION CRITERION.....	95
5.1.1 SNR CUTOFF	95
5.1.2 BER BASED CUTOFF	98
CHAPTER 6: FEEDBACK REDUCTION.....	103
6.1 FEEDBACK REDUCTION IN TIME.....	104

6.2 FEEDBACK REDUCTION IN FREQUENCY DOMAIN	115
CHAPTER 7: USER SCHEDULING.....	122
7.1 SCHEDULING CRITERIA	123
7.2 USER SELECTION FAIRNESS.....	126
CHAPTER 8: CONCLUSION AND FUTURE WORK	150
8.1 CONCLUSIONS.....	150
8.2 FUTURE WORK.....	152
APPENDIX	153
LIST OF ABBREVIATIONS	153
REFERENCES	155
VITA	160

LIST OF TABLES

Table 1.1: IEEE 802.16m OFDM parameters.....	12
Table 3.1: Urban macrocell channel NLOS model from the IEEE 802.16m EMD.....	49
Table 3.2: Suburban macrocell channel model as described in the IEEE 802.16m EMD.....	51
Table 3.3: Urban microcell channel model as described in the IEEE 802.16m EMD.....	52
Table 3.4: Spatial correlation parameters.	69

LIST OF FIGURES

Figure 1.1: MIMO configuration in a scattering environment.....	6
Figure 1.2: Transmit Antennas versus MIMO capacity.	9
Figure 1.3: Capacity gain per transmit antenna increase.	9
Figure 1.4: Channel representation in time (a) and frequency (b).	10
Figure 1.5: Frequency domain (a) and time domain (b) representation of an OFDM symbol.....	11
Figure 1.6: Visualization of power allocation using waterfilling algorithm.	13
Figure 1.7: Waterfilling solution with SNR = 20dB, 2x2 MIMO, 128 OFDM subcarriers.	15
Figure 1.8: BER versus SNR FOR 2X2 MIMO, 128 subcarrier OFDM system with waterfilling algorithm and QPSK modulation with IEEE 802.16m macrocell channel model.	15
Figure 1.9: SMSE minimization over 2x2 MIMO with 128 OFDM subcarriers and SNR=20dB.....	17

Figure 1.10: BER versus SNR FOR 2X2 MIMO, 128 subcarrier OFDM system with SMSE minimization algorithm and QPSK modulation with IEEE 802.16m macrocell channel model.	17
Figure 1.11: Schematic of SDMA channel.	18
Figure 1.12: Visualization of power allocation using multiuser waterfilling; 4 users, 8 transmit antennas, 2 receive antennas per user.	20
Figure 1.13: BER versus SNR comparison for a 2x2 MIMO, 128 OFDM subcarrier system for SU-MIMO and MU-MIMO configurations.....	20
Figure 1.14: CDF plot for spatial and frequency correlated channel capacity using spatio-frequency waterfilling with RR scheduling for 10 dB SNR.....	21
Figure 1.15: CDF plot for spatial and frequency correlated channel capacity using spatio-frequency waterfilling with greedy scheduling for 10 dB SNR.....	22
Figure 1.16: BER versus SNR for different scheduling algorithms for a 2x2, 128 subcarrier MIMO-OFDM system.....	23
Figure 1.17: Theoretical and simulation BER versus SNR curves for a 2x2 MIMO, 128 OFDM subcarrier system.....	26
Figure 1.18: CDF curves for eigen mode gains for different bit loading values.	27
Figure 3.1: A simple SISO configuration.	46
Figure 3.2: Rayleigh faded multipath channel.	47
Figure 3.3: Schematic diagram for non-uniform tap generation.....	48
Figure 3.4: Non uniform channel impulse response for the urban macrocell NLOS channel model.	50

Figure 3.5: Non uniform channel impulse response for the suburban macrocell NLOS channel model.	52
Figure 3.6: Non uniform channel impulse response for the urban microcell NLOS channel model.	53
Figure 3.7: Channel frequency response bandlimited by a bandlimiting filter.....	55
Figure 3.8: Channel bandlimiting and resampling.	56
Figure 3.9: Non uniform versus resampled multipath channel.	57
Figure 3.10: Frequency-flat channel frequency response, with time domain (a) and frequency domain (b) representation.	58
Figure 3.11: Frequency selective channel frequency response, with time domain (a) and frequency domain (b) representation.....	59
Figure 3.12: Jakes spectrum with Doppler shift of 200 Hz.	61
Figure 3.13: Jakes spectrum fir filter for Doppler shift 200 Hz.....	62
Figure 3.14: Schematic diagram for non-uniform tap generation with Jakes filter.	62
Figure 3.15: Correlated sample values.	63
Figure 3.16: Theoretical versus simulation autocorrelation of time samples for a Doppler shift of 350 Hz.....	64
Figure 3.17: Simulation PSD with Doppler shift of 350 Hz.....	64
Figure 3.18: Non-stationary channel impulse response over time.	65
Figure 3.19: Non-stationary channel frequency response over time.....	66
Figure 3.20: Channel correlation due to BS and MS antenna array position.	67
Figure 4.1: Fixed ratio - hierarchical precoding algorithm flowchart.	74

Figure 4.2: Hierarchical precoding with $R = 0.5$ for a 2x2 MIMO, 32 OFDM subcarrier system at 5dB	75
Figure 4.3: BER versus SNR comparison for a 2x2 MIMO, 128 subcarrier OFDM system with IEEE 802.16m urban macrocell channel model for BPSK constellation.	76
Figure 4.4: BER versus SNR comparison for a 2x2 MIMO, 128 subcarrier OFDM system with IEEE 802.16m urban macrocell channel model for 4 QAM constellation.	77
Figure 4.5: BER versus SNR comparison for a 2x2 MIMO, 128 subcarrier OFDM system with IEEE 802.16m urban macrocell channel model for 256 QAM constellation.	78
Figure 4.6: Average throughput per OFDM symbol versus SNR for a 2x2 MIMO, 128 subcarrier OFDM system with IEEE 802.16m urban macrocell channel model.	79
Figure 4.7: Throughput gain versus SNR for a 2x2 MIMO, 128 subcarrier OFDM system with IEEE 802.16m urban macrocell channel model.	80
Figure 4.8: C-HP waterfilling solution	82
Figure 4.9: Capacity based power allocation - HP	83
Figure 4.10: Capacity based hierarchical precoding algorithm flowchart.....	84
Figure 4.11: BER versus SNR for capacity based hierarchical precoding with cutoff capacity 2 bps/Hz for a 2x2 MIMO, 128 subcarrier OFDM system with IEEE 802.16m urban macrocell channel model.....	85
Figure 4.12: BER versus SNR for capacity based hierarchical precoding with cutoff capacity 4 bps/Hz for a 2x2 MIMO, 128 subcarrier OFDM system with IEEE 802.16m urban macrocell channel model.....	86

Figure 4.13: Throughput versus SNR for capacity based hierarchical precoding and WF for a 2x2 MIMO, 128 subcarrier OFDM system with IEEE 802.16m urban macrocell channel model.	86
Figure 4.14: Throughput gain versus SNR for C-HP for a 2x2 MIMO, 128 subcarrier OFDM system with IEEE 802.16m urban macrocell channel model.	87
Figure 4.15: BER versus SNR for C-HP C=4 AND MU precoding for a 2x2 MIMO, 128 subcarrier OFDM system with IEEE 802.16m urban macrocell channel model.	88
Figure 4.16: Throughput versus SNR FOR C-HP C=4, with MU precoding for a 2x2 MIMO, 128 subcarrier OFDM system with IEEE 802.16m urban macrocell channel model.	89
Figure 4.17: Throughput versus SNR with adaptive modulation, for a 2x2 MIMO, 128 subcarrier OFDM system with IEEE 802.16m urban macrocell channel model.	90
Figure 4.18: Throughput gain versus SNR with adaptive modulation for a 2x2 MIMO, 128 subcarrier OFDM system with IEEE 802.16m urban macrocell channel model.	90
Figure 4.19: BER versus SNR comparison with iterative WF algorithm for a 2x2 MIMO, 128 subcarrier OFDM system with IEEE 802.16m urban macrocell channel model.	91
Figure 4.20: Throughput versus SNR comparison with iterative WF algorithm for a 2x2 MIMO, 128 subcarrier OFDM system with IEEE 802.16m urban macrocell channel model.	92
Figure 4.21: Throughput gain versus SNR with respect to iterative WF algorithm for a 2x2 MIMO, 128 subcarrier OFDM system with IEEE 802.16m urban macrocell channel model.	92

Figure 5.1: Diagrammatic representation for AEMR algorithm with $S=15$ dB, using FR-HP with $R=0.5$ and a 2x2 MIMO, 128 subcarrier OFDM system with IEEE 802.16m urban macrocell channel model.....	96
Figure 5.2: BER versus SNR for FR-HP _{0.5} with AEMR _{S=15dB} for a 2x2 MIMO, 128 subcarrier OFDM system with IEEE 802.16m urban macrocell channel model.	97
Figure 5.3: Throughput versus SNR for FR-HP _{0.5} with AEMR _{S=15dB} for a 2x2 MIMO, 128 subcarrier OFDM system with IEEE 802.16m urban macrocell channel model.	98
Figure 5.4: BER Versus SNR FOR FR-HP WITH AEMR _{BERTh=10⁻²} for a 2x2 MIMO, 128 subcarrier OFDM system with IEEE 802.16m urban macrocell channel model.	99
Figure 5.5: Throughput versus SNR for FR-HP _{0.5} and AEMR _{BERTh=10⁻²} for a 2x2 MIMO, 128 subcarrier OFDM system with IEEE 802.16m urban macrocell channel model.	100
Figure 5.6: BER Versus SNR FOR C-HP ₂ WITH AEMR _{BERTh=10⁻²} for a 2x2 MIMO, 128 subcarrier OFDM system with IEEE 802.16m urban macrocell channel model.	101
Figure 5.7: Throughput versus SNR for C-HP ₂ with AEMR _{BERTh=10⁻²} for a 2x2 MIMO, 128 subcarrier OFDM system with IEEE 802.16m urban macrocell channel model.	101
Figure 6.1: Doppler shift autocorrelation function versus K.....	106
Figure 6.2: BER versus SNR performance comparison with WF algorithm for a 2x2 MIMO, 128 subcarrier OFDM system with IEEE 802.16m urban macrocell channel model, using QPSK constellation.....	107
Figure 6.3: BER versus SNR performance comparison with WF algorithm for a 2x2 MIMO, 128 subcarrier OFDM system with IEEE 802.16m urban macrocell channel model, using 4 QAM constellation.....	108

Figure 6.4: BER versus SNR performance comparison with WF algorithm for a 2x2 MIMO, 128 subcarrier OFDM system with IEEE 802.16m urban macrocell channel model, using 16 QAM constellation..... 108

Figure 6.5: BER versus SNR performance comparison with WF algorithm for a 2x2 MIMO, 128 subcarrier OFDM system with IEEE 802.16m urban macrocell channel model, using 256 QAM constellation..... 109

Figure 6.6: Throughput versus SNR performance comparison with WF algorithm for a 2x2 MIMO, 128 subcarrier OFDM system with IEEE 802.16m urban macrocell channel model, using BPSK constellation..... 110

Figure 6.7: Throughput versus SNR performance comparison with WF algorithm for a 2x2 MIMO, 128 subcarrier OFDM system with IEEE 802.16m urban macrocell channel model, using 4 QAM constellation..... 111

Figure 6.8: Throughput versus SNR performance comparison with WF algorithm for a 2x2 MIMO, 128 subcarrier OFDM system with IEEE 802.16m urban macrocell channel model, using 16 QAM constellation..... 111

Figure 6.9: Throughput versus SNR performance comparison with WF algorithm for a 2x2 MIMO, 128 subcarrier OFDM system with IEEE 802.16m urban macrocell channel model, using 256 QAM constellation..... 112

Figure 6.10: BER Versus SNR comparison for feedback reduction for $K = 0.1$ and doppler shift of 10 Hz with FR-HP_{0.5} and C-HP₂ for a 2x2 MIMO, 128 subcarrier OFDM system with IEEE 802.16m urban macrocell channel model. 113

Figure 6.11: Throughput versus SNR comparison for feedback reduction for $K = 0.1$ and doppler shift of 10 Hz with FR-HP_{0.5} and C-HP₂ for a 2x2 MIMO, 128 subcarrier OFDM system with IEEE 802.16m urban macrocell channel model. 114

Figure 6.12: BER Versus SNR for feedback reduction for $K = 0.1$ and doppler shift of 10 Hz with FR-HP_{0.5} for a 2x2 MIMO, 128 subcarrier OFDM system with IEEE 802.16m urban macrocell channel model, using 4 QAM constellation. 117

Figure 6.13: BER Versus SNR for feedback reduction for $K = 0.1$ and doppler shift of 10 Hz with FR-HP_{0.5} for a 2x2 MIMO, 128 subcarrier OFDM system with IEEE 802.16m urban macrocell channel model, using 16 QAM constellation. 118

Figure 6.14: BER Versus SNR for feedback reduction for $K = 0.1$ and doppler shift of 10 Hz with FR-HP_{0.5} for a 2x2 MIMO, 128 subcarrier OFDM system with IEEE 802.16m urban macrocell channel model, using 256 QAM constellation. 119

Figure 6.15: Throughput versus SNR for feedback reduction for $K = 0.1$ and doppler shift of 10 Hz with FR-HP_{0.5} for a 2x2 MIMO, 128 subcarrier OFDM system with IEEE 802.16m urban macrocell channel model. 120

Figure 7.1: Capacity CDF plot for time uncorrelated (a) and time correlated (b) channels, with round robin scheduling for a 2x2 MIMO, 128 subcarrier OFDM system with IEEE 802.16m urban macrocell channel model. 126

Figure 7.2: PDF for user scheduling using ORR scheduling algorithm and MaxMIMOCapc scheduling criterion, with 10 coherence times (a) and 100 coherence times (b) considered..... 128

Figure 7.3: PDF for user scheduling using greedy scheduling algorithm and MaxMIMOCapc scheduling criterion, with 10 coherence times (a) and 100 coherence times (b) considered.....	130
Figure 7.4: PDF for user scheduling using PF scheduling algorithm and MaxMIMOCapc scheduling criterion with 10 coherence times (a) and 100 coherence times (b) considered.	130
Figure 7.5: PDF for user scheduling using ORR scheduling algorithm and MaxMinSV scheduling criterion with 10 coherence times (a) and 100 coherence times (b) considered.	131
Figure 7.6: PDF for user scheduling using greedy scheduling algorithm and MaxMinSV scheduling criterion with 10 coherence times (a) and 100 coherence times (b) considered.	131
Figure 7.7: PDF for user scheduling using PF scheduling algorithm and MaxMinSV scheduling criterion with 10 coherence times (a) and 100 coherence times (b) considered.	132
Figure 7.8: PDF for user scheduling using ORR scheduling algorithm and MaxSNR scheduling criterion with 10 coherence times (a) and 100 coherence times (b) considered.	132
Figure 7.9: PDF for user scheduling using greedy scheduling algorithm and MaxSNR scheduling criterion with 10 coherence times (a) and 100 coherence times (b) considered.	133

Figure 7.10: PDF for user scheduling using PF scheduling algorithm and MaxSNR scheduling criterion with 10 coherence times (a) and 100 coherence times (b) considered. 133

Figure 7.11: BER versus SNR for FR-HP_{0.5} with user scheduling with 5 users and MaxMIMOCapc scheduling criterion, for a 2x2 MIMO, 128 subcarrier OFDM system with IEEE 802.16m urban macrocell channel model. 134

Figure 7.12: BER versus SNR for C-HP₂ with user scheduling with 5 users and MaxMIMOCapc scheduling criterion, for a 2x2 MIMO, 128 subcarrier OFDM system with IEEE 802.16m urban macrocell channel model. 136

Figure 7.13: BER versus SNR for FR-HP_{0.5} with user scheduling with 5 users and MaxSNR scheduling criterion, for a 2x2 MIMO, 128 subcarrier OFDM system with IEEE 802.16m urban macrocell channel model. 136

Figure 7.14: BER versus SNR for C-HP₂ with user scheduling with 5 users and MaxSNR scheduling criterion, for a 2x2 MIMO, 128 subcarrier OFDM system with IEEE 802.16m urban macrocell channel model. 137

Figure 7.15: BER versus SNR for C-HP₂ with user scheduling with 5 users and MaxMinSV scheduling criterion, for a 2x2 MIMO, 128 subcarrier OFDM system with IEEE 802.16m urban macrocell channel model. 138

Figure 7.16: BER versus SNR for FR-HP_{0.5} with user scheduling with 5 users and MaxMinSV scheduling criterion, for a 2x2 MIMO, 128 subcarrier OFDM system with IEEE 802.16m urban macrocell channel model. 139

Figure 7.17: BER versus SNR for FR-HP_{0.5} with user scheduling with 5 users and MinES scheduling criterion, for a 2x2 MIMO, 128 subcarrier OFDM system with IEEE 802.16m urban macrocell channel model..... 140

Figure 7.18: BER versus SNR for C-HP₂ with user scheduling with 5 users and MinES scheduling criterion, for a 2x2 MIMO, 128 subcarrier OFDM system with IEEE 802.16m urban macrocell channel model..... 140

Figure 7.19: Throughput versus SNR for FR-HP_{0.5} with user scheduling with 5 users and MaxMIMOCapc scheduling criterion, for a 2x2 MIMO, 128 subcarrier OFDM system with IEEE 802.16m urban macrocell channel model. 141

Figure 7.20: Throughput versus SNR for C-HP₂ with user scheduling with 5 users and MaxMIMOCapc scheduling criterion, for a 2x2 MIMO, 128 subcarrier OFDM system with IEEE 802.16m urban macrocell channel model. 142

Figure 7.21: Throughput versus SNR for FR-HP_{0.5} with user scheduling with 5 users and MaxSNR scheduling criterion, for a 2x2 MIMO, 128 subcarrier OFDM system with IEEE 802.16m urban macrocell channel model..... 142

Figure 7.22: Throughput versus SNR for C-HP₂ with user scheduling with 5 users and MaxSNR scheduling criterion, for a 2x2 MIMO, 128 subcarrier OFDM system with IEEE 802.16m urban macrocell channel model..... 143

Figure 7.23: Throughput versus SNR for FR-HP_{0.5} with user scheduling with 5 users and MaxMinSV scheduling criterion, for a 2x2 MIMO, 128 subcarrier OFDM system with IEEE 802.16m urban macrocell channel model..... 144

Figure 7.24: Throughput versus SNR for C-HP ₂ with user scheduling with 5 users and MaxMinSV scheduling criterion, for a 2x2 MIMO, 128 subcarrier OFDM system with IEEE 802.16m urban macrocell channel model.....	145
Figure 7.25: Throughput versus SNR for FR-HP _{0.5} with user scheduling with 5 users and MinES scheduling criterion, for a 2x2 MIMO, 128 subcarrier OFDM system with IEEE 802.16m urban macrocell channel model.	146
Figure 7.26: Throughput versus SNR for C-HP ₂ with user scheduling with 5 users and MinES scheduling criterion, for a 2x2 MIMO, 128 subcarrier OFDM system with IEEE 802.16m urban macrocell channel model.	147
Figure 7.27: BER versus SNR for MU scheduling using WF precoding with MaxMinSV scheduling criterion and greedy scheduling algorithm. 4 users are chosen from a set of 16, for a 2x2 MIMO, 128 subcarrier OFDM system with IEEE 802.16m urban macrocell channel model.	148
Figure 7.28: BER versus SNR for MU scheduling using WF precoding and 16 QAM constellation with MaxMinSV scheduling criterion and greedy scheduling algorithm. 4 users are chosen from a set of 16, for a 2x2 MIMO, 128 subcarrier OFDM system with IEEE 802.16m urban macrocell channel model.....	149
Figure 7.29: Throughput versus SNR for MU scheduling using WF precoding with MaxMinSV scheduling criterion and greedy scheduling algorithm. 4 users are chosen from a set of 16, for a 2x2 MIMO, 128 subcarrier OFDM system with IEEE 802.16m urban macrocell channel model.....	149

THESIS ABSTRACT (ENGLISH)

NAME : SIDDHARTH NAIR

TITLE : WiMAX Cross Layer Capacity Optimization

DEGREE : MASTER OF SCIENCE

MAJOR : TELECOMMUNICATION ENGINEERING

DATE : JANUARY, 2012

The IEEE 802.16 standard, also known as WiMAX, is an upcoming wireless standard that allows data rates of up to 1 Gb/s. WiMAX can provide last mile connectivity by replacing wired communication channels, without any reduction in data throughput compared to wireline networks. This high data rate requires large bandwidths, which can cause deterioration in the signal due to frequency and time selectivity. In order to overcome these problems, precoding is used in conjunction with OFDM and MIMO in order to overcome the signal deterioration that is caused by the wideband channel. Precoding techniques such as waterfilling allow for optimal power allocation, thereby improving the error performance of a fixed constellation system, at the cost of reduced utilization of available channels. This thesis presents a novel precoding technique that allows an improvement in the utilization of available channels, with minimal effect on the error performance of the system. A realistic channel that is correlated in time, frequency and across the spatial domain is used to evaluate the proposed algorithms. Finally, the effect of feedback reduction and user scheduling on existing and proposed algorithms is studied.

Keyword: *Precoding, OFDM, MIMO, WiMAX, feedback reduction, user scheduling.*

MASTER OF SCIENCE DEGREE

KING FAHD UNIVERSITY OF PETROLEUM AND MINERALS

Dhahran, Saudi Arabia

THESIS ABSTRACT (ARABIC)

الاسم: سيدهارت ناير

عنوان الرسالة: تحسين سعة الطبقة المتقاطعة في تقنية الواي ماكس

ماجستير في العلوم : درجة

التخصص: هندسة الاتصالات

تاريخ التخرج :يناير 2012

إن معيار هيئة مهندسي الكهرباء والالكترونيات رقم (IEE 802.16) والمعروف باسم واي ماكس (WiMAX) هو معيار الجيل المستقبلي من للاتصالات اللاسلكية التي سرعة نقل البيانات فيها إلى 1 جيجا بت ؟ ثانية . يمكن لتقنية واي ماكس أن تزود الاتصال اللاسلكي ضمن ميل بدون أي نقص في نقل معدل نقل البيانات . الكم الهائل من سرعة نقل البيانات يتطلب عرض نطاق كبير جدا والذي بدوره قد يتسبب في تدهور حالة الإشارة بسبب تحديد الترددات المسموحة في قناة الواي ماكس . للتغلب على هذه المشاكل ، يمكن الجمع بين تقنية التضمين الترددي المتعامد (OFDM) وتقنية الإدخالات والإخراجات المتعددة (MIMO) من أجل التغلب على التدهور في الإشارة الناتج عن القناة عريضة النطاق . تقنيات مثل تشفير السقوط المائي (Precoding waterfilling) تسمح لتخصيص القدرة الأمثل، وبالتالي تحسين أداء نظام الكوكبة ثابتة، على حساب تقلص استخدام القنوات المتاحة .

هذه الأطروحة تقدم تقنية تشفير قبلية حديثة تتيح تحسنا في الاستفادة من القنوات المتاحة ، مع تأثير ضئيل على أداء خطأ في النظام . وتستخدم قناة واقعية يتبسط في التردد والوقت وعبر المجال المكاني لتقييم الخوارزميات المقترحة . أخيرا، تم دراسة وتقييم تأثير التغذية المرتدة ، وجدولة المستخدمين المقترحة سابقا والمقترحة في هذه الرسالة .

الرئيسية الكلمات: *المرتدة التغذية تخفيض , المستخدم جدولة , WiMAX , MIMO , OFDM , Precoding*

متطلب لنيل درجة الماجستير في العلوم

جامعة الملك فهد للبترول والمعادن

الظهران، المملكة العربية السعودية

CHAPTER 1

INTRODUCTION

1.1 INTRODUCTION

The IEEE 802.16 is a wireless standard for broadband internet access that provides data rates comparable to DSL or other cable-modem based connections [1]. The advantage of wireless broadband internet access over wireline broadband internet access is the cost of providing last mile connectivity. Wireless broadband can be setup easily in areas with limited or no wireline communication infrastructure such as optical fiber cable or copper cable [2].

In this thesis, the channel model used is the model as described in IEEE 802.16m evaluation methodology document [3]. The model assumes channel correlation in

frequency, across the spatial domain and in time due to Doppler shift. These constraints cause the channel to behave differently than an independent, identically distributed Gaussian channel model that is not correlated in any dimension. As a lot of the research in this field is done assuming an uncorrelated Gaussian channel, the effects of a realistic channel model on the proposed algorithms are not studied. In this thesis, the IEEE 802.16m channel model is the basis on which all the algorithms are developed.

IEEE 802.16 proposes bandwidths of up to 20MHz. With such a high bandwidth, the multipath structure of the channel manifests as frequency selectivity [4]. The 802.16m update is expected to offer up to 1Gbps fixed speeds. The multipath channel makes it difficult to achieve such high data rates. Thus, we need to design a transceiver that can take advantage of the channel, and allow high data throughput. The IEEE 802.16m standard proposes Multiple Input Multiple Output (MIMO), Orthogonal Frequency Division Multiplexing (OFDM) and Orthogonal Frequency Division Multiple Access (OFDMA) to provide high data rates to multiple users.

Precoding is a method of compensating for distortions caused by the channel at the transmitter. Two such methods are studied in the thesis. The first is waterfilling, which maximizes the sum channel capacity, and second is sum of mean square error minimization. Both allocate power to the available channels such that the respective criterion is maximized. Waterfilling allows a big gain in bit error rate performance. However, one major disadvantage of waterfilling precoding is that it leaves out certain channels whose gain to noise ratio is less than a cutoff value. On the other hand, sum of mean square minimization precoding allows relatively more channels to transmit, at the

cost of deteriorated bit error rate performance. This thesis proposes a new precoding technique, hierarchical precoding, uses both waterfilling and sum of mean square minimization precoding in order to reduce the number of discarded channels, while keeping the system performance within an acceptable range. Also, adaptive eigen mode reduction is proposed to overcome the performance deterioration caused by hierarchical precoding.

The optimal solution for precoding requires perfect channel knowledge at the transmitter. This channel knowledge is fed back by the receiver to the transmitter, which means that resources need to be spared for feedback purposes. However, in a realistic channel, the channel is correlated over time and in the frequency domain. This correlation can be exploited to reduce the amount of feedback required, thus freeing resources being used for feedback. Due to the multipath nature of the channel, frequency correlation is induced in the channel. This implies that the subcarrier gains of an OFDM symbol would be correlated. This property of the channel can be used to reduce the feedback in the frequency domain. Similarly, the channel gain is correlated in time due to Doppler effect. This correlation can be exploited by allowing feedback to the transmitter to be sent every few symbols, as opposed to every symbol in the optimal case. This reduction in feedback causes the precoding to become suboptimal and deteriorates performance. In this thesis, the effect of feedback reduction on the established precoding techniques as well as the proposed precoding technique is studied.

In high mobility scenarios, the channel is changing continuously. So, scheduling users according to a static algorithm does not produce optimal results [5]. In order to approach

the Shannon capacity limit, realistic and dynamic user/OFDM subcarrier scheduling schemes need to be used. Various user scheduling criteria and algorithms have been proposed in literature that aims at maximizing the performance of the system by exploiting user diversity. In a correlated channel, the question of fairness comes into the picture. If a user has a bad channel, that user will continue to have a bad channel for some time, as well as across the OFDM subcarriers. If users are selected according to the quality of their channel only, then this user who has a relatively low gain channel will not be able to transmit until his channel state improves. This kind of scheduling would be unfair to users that have a bad channel, and allow just a subset of users to contend for resources, but would maximize its performance.

In this thesis, various scheduling criteria and scheduling algorithms are compared, using the proposed precoding techniques, on the basis of performance and user fairness. In the section that follows, a brief introduction to the physical layer system model, as used in the IEEE 802.16m standard, is presented. In the later sections, a concise explanation for precoding and user scheduling are presented.

1.2 BACKGROUND

Before describing the IEEE 802.16m physical layer system model, few new terms are to be defined. A communication channel, also known as channel, is defined as the medium through which the communication takes place. In wireless communication, this medium is the radio waves that are transmitted from the transmitter's antenna and received at the

receiver. The problem with radio waves as a communication medium is that they can get reflected, scattered and diffracted due to obstacles. This causes attenuated and time delayed copies of the signal to be received at the receiver. This type of channel is called a multipath channel, and is described in detail in the IEEE 802.16m channel model chapter (Section 3.1). This type of channel causes delayed symbol copies of the current symbol to interfere with subsequent symbols. This causes inter-symbol interference (ISI), and degrades the performance of the communication system. The amount of ISI present in a symbol depends on how long the symbol is, in time, compared to the maximum delay caused by the channel, called the maximum excess delay. If the symbol duration is much larger than the maximum excess delay, all the delayed copies of the current symbol will be received within the current symbol, eliminating ISI. On the other hand, if the symbol duration is less than the maximum excess delay, the delayed copies of the current symbol will interfere with subsequent symbols.

The multipath channel causes different frequencies to have varying gain in the frequency domain. This is called frequency selectivity, which means that the channel selectively attenuates certain frequencies more than others. The opposite of this is a frequency flat channel, where all frequencies are equally attenuated. The time domain channel representation of a flat fading channel is a single path channel, where there is no ISI due to multipath. The IEEE 802.16m standard proposes bandwidths of up to 20 MHz, with the least bandwidth being 1.25MHz [3]. The high bandwidth implies that the symbol transmission rate can be very high. But in a multipath channel, ISI will be high, causing more errors at the receiver. To overcome this problem, the standard allows the use of

multiple antennas at the transmitter and receiver, known as Multiple Input Multiple Output (MIMO), and Orthogonal Frequency Division Multiplexing (OFDM). In the following sections, a brief background about MIMO, OFDM, various precoding algorithms and user scheduling is presented.

1.2.1 MIMO

MIMO means using multiple antennas at the transmitter and the receiver. A 4x4 MIMO configuration is shown in Figure 1.1. The scatterers are hindrances between the transmitter and the receiver, causing multiple delayed and attenuated copies of the signal to be received at the receiver.

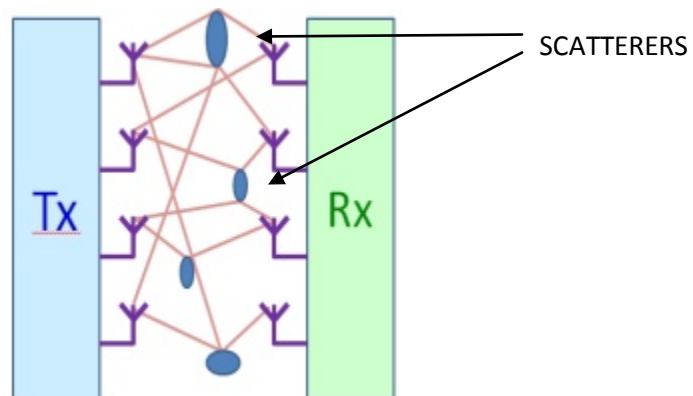


Figure 1.1: MIMO configuration in a scattering environment.

In [6], Rayleigh *et al* show that, in a multipath environment, the capacity of the MIMO configuration increases log linearly with the increase in the number of transmit antennas, assuming that the number of delayed multipath taps are greater than the number of transmitters used.

Assume that, in a multipath channels, the total number of delayed paths is ‘ L ’. Let us also assume that ‘ N ’ symbol samples were transmitted, and ‘ $N+\mu$ ’ samples are received. Here, it is assumed that the channel is not sampled at the same sampling rate as the input signal. This means that the delayed taps in the delay time for each tap of the multipath channel is not necessarily a multiple of the input signal sampling period. In this case, Rayleigh shows in [6] that the number of parallel channels that can be created in the communication channel, \mathbb{K} , is bounded by

$$\mathbb{K} \leq \text{Min}\{L, (N + \mu) * M_R, N * M_T\}. \quad (1.1)$$

Here, M_T is the number of transmit antennas, and M_R is the number of receive antennas. If it assumed that the channel taps delays are a multiple of the input sampling period, and assuming only one symbol sample is transmitted ($N=1$), (1.1) reduces to

$$\mathbb{K} \leq \text{Min}\{L, L * M_R, M_T\}. \quad (1.2)$$

If $L \leq M_T$ implies $\mathbb{K} \leq L$, where it is assumed that $M_R \geq 1$. What this means is that the number of parallel channel dimensions will have an upper bound at $\mathbb{K} \leq L$. This means that the capacity of the systems is fixed and is independent of the number of transmitter or receiver antennas.

If, on the other hand, $L > M_T$ implies $\mathbb{K} \leq M_T$. This is a crucial result because it says that the number of parallel spatial channel dimensions, and therefore capacity, is bounded by the number of transmit antennas if and only if the number of multipath taps is greater than the number of transmit antennas. This result shows that a MIMO system not only overcomes the problem of multipath, but uses it to its advantage, where a large number of

delayed multipath taps allows a log linear increase in capacity with an increase in the number of transmit antennas. The IEEE 802.16m standard allows 2, 4 and 8 antenna configuration at the base station (BS), and a minimum of 2 antennas at the mobile station (MS).

The MIMO capacity, as given in [6], is given in (1.3). The system model for which (1.3) holds is for a MIMO system, whose channel Matrix, defined as H , has \mathbb{K} singular values, represented as λ_k . The channel matrix's elements are assumed to be an independent, identically distributed (i.i.d.) complex Gaussian. An i.i.d. complex Gaussian channel matrix implies a large number of multipath components [6]. The channel capacity, C is given as

$$C = \sum_{k=1}^{\mathbb{K}} \log_2(1 + (P_k \lambda_k^2) / \sigma^2) \text{ bits / transmission.} \quad (1.3)$$

Here, λ_k^2 is the square of the singular values of the channel matrix, P_k is the power assigned to the k^{th} spatial channel, and σ^2 is the noise power. Here, \mathbb{K} is the total number of parallel spatial channel dimensions available as described in (1.1). Using (1.1) and (1.3), it can be seen that the capacity of a channel, for a given power allocation and noise power, increases linearly with increase in number of transmit antennas. Figure 1.2 shows capacity versus transmitter antennas used. The following observations can be made.

1. The capacity increases linearly with increase in number of antennas.
2. The slope, or the capacity gain, increases with increase in SNR. This is shown in

Figure 1.3.

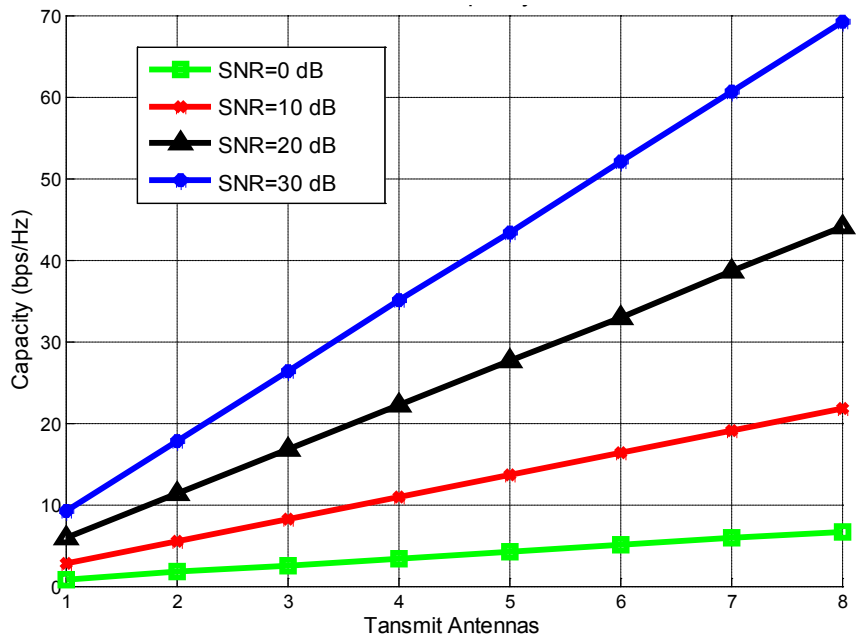


Figure 1.2: Transmit Antennas versus MIMO capacity.

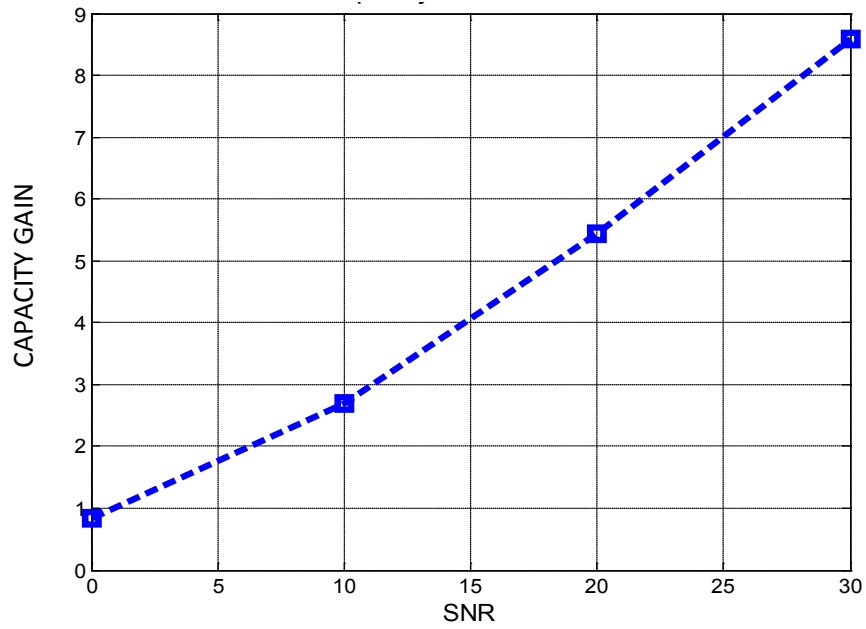


Figure 1.3: Capacity gain per transmit antenna increase.

1.2.2 OFDM

Figure 1.4 (a) shows a channel with large multipath taps is shown, with its frequency domain representation in figure 4 (b). It can be seen that in the frequency domain, each frequency bin is attenuated by a different amount. This causes distortion in the received signal that manifests itself as ISI in the time domain. (OFDM) overcomes this problem by dividing the available bandwidth into orthogonal, non overlapping regions such that the gain within each region is nearly constant.

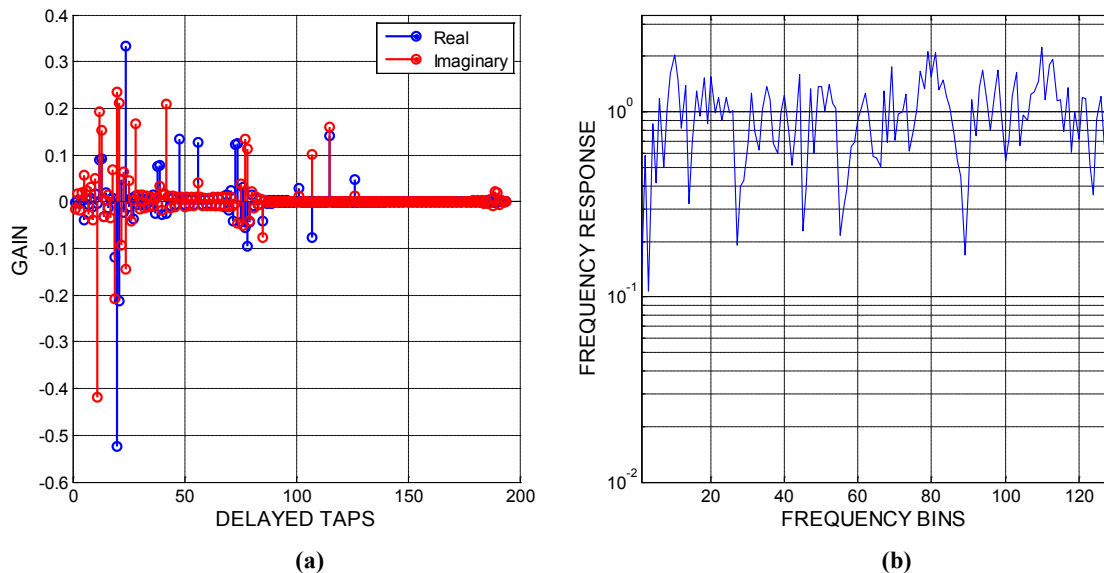


Figure 1.4: Channel representation in time (a) and frequency (b).

The available bandwidth is divided into ' N ' parallel subcarriers. Each subcarrier is then modulated with data, and all the subcarriers are superimposed and transmitted. This is similar to frequency division multiplexing (FDM), except the fact that in OFDM the subcarriers are spaced such that, after modulation, the main lobe of any subcarrier in the frequency domain coincides with zero crossing points of the rest of the subcarriers. This

allows subcarriers to be closer to each other without the need of guard bands as in the case of FDM. This conversion can easily be done by taking the fast fourier transform (FFT) of the input signal, and passing it through a digital to analog convertor to produce the baseband OFDM signal. To mitigate the effects of multipath, OFDM utilizes cyclic prefix (CP), which converts the linear convolution of the OFDM time domain signal with the multipath channel, to a circular convolution [4]. The CP has to be more than the maximum excess delay, given in terms of samples. For a channel that has a large maximum excess delay, the CP could become prohibitively large. To overcome this, the OFDM symbol duration can be increased, so as to make sure that majority of the OFDM symbol is comprised of useful data.

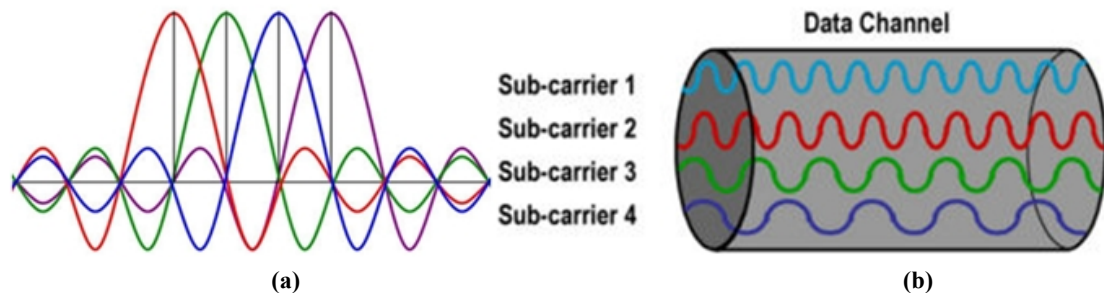


Figure 1.5: Frequency domain (a) and time domain (b) representation of an OFDM symbol.

Making the OFDM symbol excessively large is not always a good option if the user is mobile, causing the channel to vary over time. This effect of channel variation over time is due to doppler spread, which imposes a limit on the maximum symbol duration. Doppler spread is the spreading of the input signal frequency spectrum due to movement of the transmitter, receiver or the environment. This spreading of the frequency spectrum manifests itself as variations in the channel over time. The inverse of the doppler spread gives us, roughly, the amount of time for which the channel will remain constant [7]. This

time is called coherence time. Thus, the OFDM symbol length needs to be long enough to be able to mitigate multipath, but need to be shorter in duration than the coherence time to ensure a quasi-static channel for that particular OFDM symbol. In the IEEE 802.16m system model, the OFDM parameters are given in detail, and those are discussed in Table 1.1.

Table 1.1: IEEE 802.16m OFDM parameters.

Nominal Channel Bandwidth (MHz)	5	7	8.75	10	20
FFT Size	512	1024	1024	1024	2048
Sub-carrier Spacing (kHz)	10.93750	7.812500	0.765625	10.937500	10.937500

The capacity of a MIMO-OFDM system is a modification of (1.3), given as follows. The system model is the same as that used for (1.3).

$$C = \sum_{n=1}^S \sum_{k=1}^K \log_2(1 + (P_{n,k} \lambda_{n,k}^2) / \sigma^2) \text{ bits / transmission} \cdot \quad (1.4)$$

$\lambda_{n,k}^2$ are the square of singular values of the n^{th} subcarrier's channel matrix, $P_{n,k}$ is the power assigned to the k^{th} spatial subchannel on the n^{th} subcarrier and 'S' is the total number of subcarriers in the OFDM symbol. (1.4) adds all the capacity values per-OFDM subcarrier per spatial channel in order to get the total channel capacity.

1.2.3 PRECODING

WATERFILLING

Waterfilling over four eigen channels is shown in Figure 1.6. Here, ψ is the waterfilling level, which depends on the total power constraint. P_1, P_2, P_3 are the power levels allotted to subchannels 1, 2 and 3, respectively. The power values, P_1, P_2, P_3 , are constrained as $\sum_{i=1}^4 P_i = 0$. It can also be inferred that $P_4 = 0$. This will maximize the theoretical achievable capacity for the given channel.

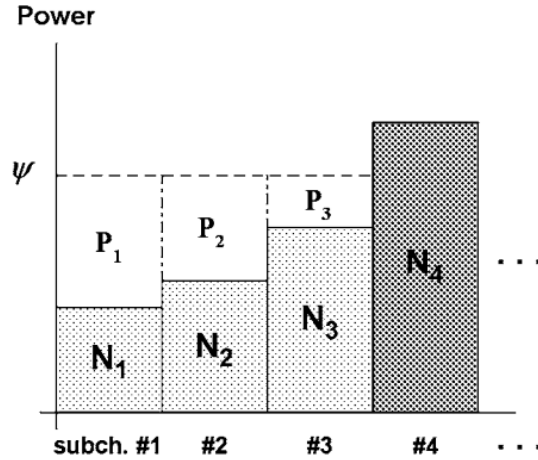


Figure 1.6: Visualization of power allocation using waterfilling algorithm.

For known channel state information (CSI), waterfilling capacity can be given as follows.

$$C = \sum_{i=1}^M \log_2 \left(1 + \frac{\lambda_{X,i}}{\sigma^2} \lambda_{H,i}^2 \right), \quad (1.5)$$

$$\lambda_{X,i} = \left(\psi - \frac{\sigma^2}{\lambda_{H,i}^2} \right)^+, \quad (1.6)$$

$$\sum_{i=1}^M \lambda_{X,i} = P_T, \quad (1.7)$$

$$(s)^+ = \begin{cases} s, & \text{if } s > 0 \\ 0, & \text{if } s \leq 0 \end{cases} \quad (1.8)$$

where $\lambda_{X,i}$ are the eigen values of the autocorrelation matrix of the input sequence, x and ψ is the waterfilling cutoff, such that all eigen subchannels whose noise to channel gain ratio, $\frac{\sigma^2}{\lambda_{H,i}^2}$, is greater than the waterfilling cutoff are not allocated any power. (1.6) and (1.7) are solved for the waterfilling cutoff level, ψ . Here, P_T is the total power that can be allocated. An important point to note is that, at high SNR, $\frac{\sigma^2}{\lambda_{H,i}^2} \approx 0$. Therefore, power will be constant across all eigen subchannels. Once ψ has been calculated, $\lambda_{X,i}$ are easy to find using (1.6). $\lambda_{X,i}$ is the power allocated to the eigen subchannel i . Figure 1.7 shows two dimensional waterfilling done over 128 OFDM and a 2x2 MIMO configuration. Note that all eigen channels above the waterfilling level have not been assigned any power.

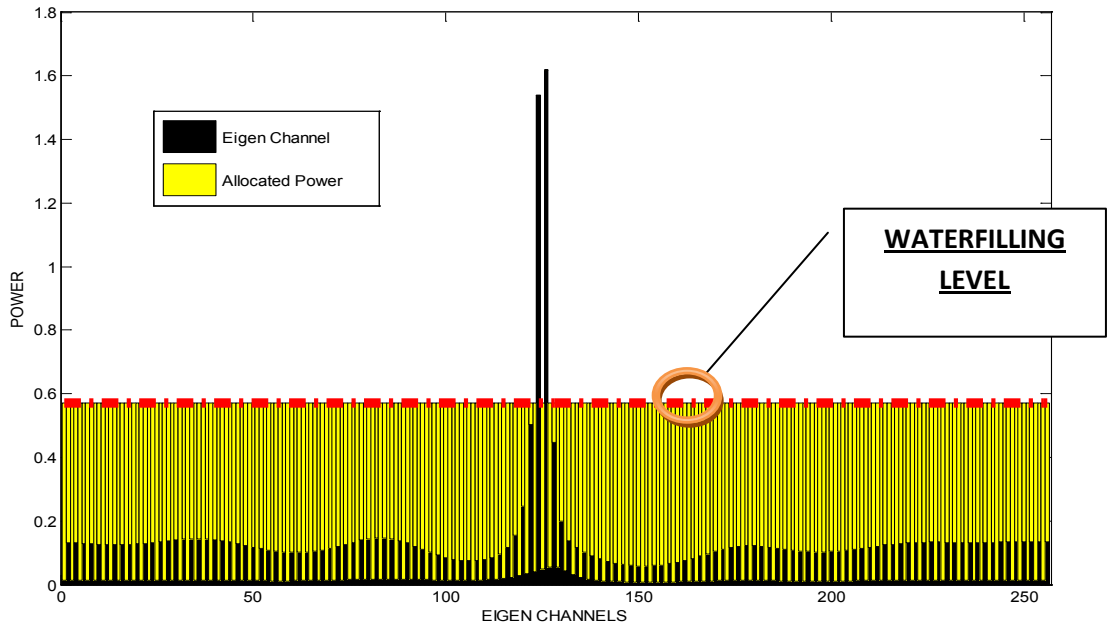


Figure 1.7: Waterfilling solution with SNR = 20dB, 2x2 MIMO, 128 OFDM subcarriers.

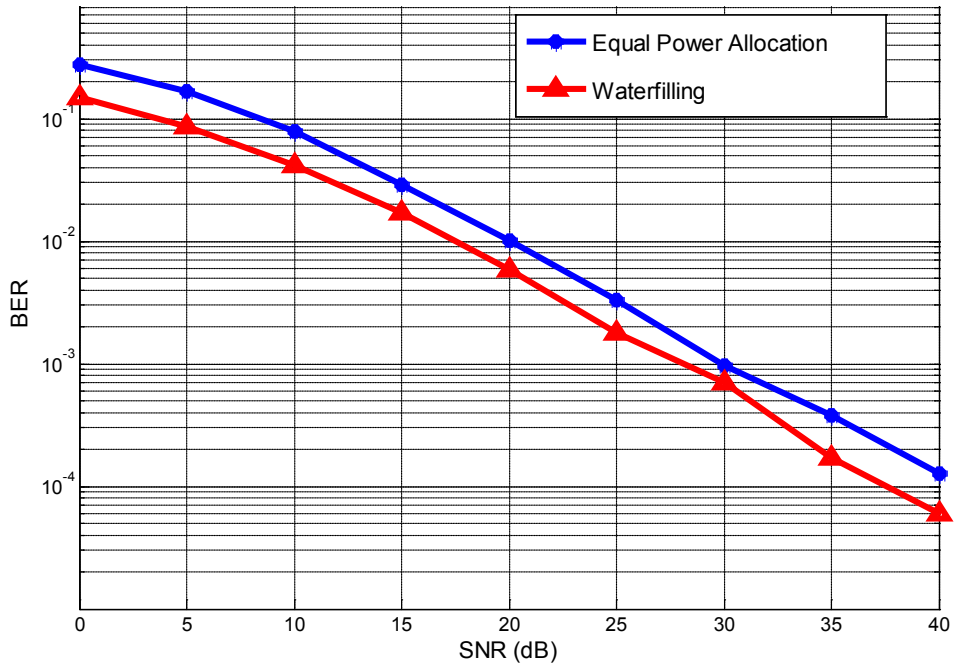


Figure 1.8: BER versus SNR FOR 2X2 MIMO, 128 subcarrier OFDM system with waterfilling algorithm and QPSK modulation with IEEE 802.16m macrocell channel model.

SMSE MINIMIZATION

The SMSE minimization equations are similar to those given for the waterfilling solution, i.e., (1.6) and (1.7). The following equations are used to find the SMSE minimization solution.

$$\lambda_{X,i} = \psi \frac{\sigma}{\lambda_{H,i}} - \frac{\sigma^2}{\lambda_{H,i}^2}, \quad (1.9)$$

$$\text{subject to } \sum_{i=1}^M \lambda_{X,i} = P_T. \quad (1.10)$$

From (1.9) it can be deduced that at high SNR, $\frac{\sigma^2}{\lambda_{H,i}^2} \approx 0$. It can thus be deduced that at high SNR, the amount of power allocated to each eigen subchannel is inversely proportional to the gain associated with the eigen subchannel, that is $\lambda_{H,i}^2$. Recall that in waterfilling the power allocated to each eigen mode or subchannel is directly proportional to the eigen subchannel gain, $\lambda_{H,i}^2$. This means that at high SNR, SMSE minimization acts as *inverse* waterfilling. Figure 1.9 shows a visual representation of SMSE minimization power allocation over a 2x2 MIMO configuration with 128 subcarriers. In Figure 1.10, BER performance of SMSE minimization is shown. It can be deduced from the plots that SMSE minimization performs better at low SNR compared to equal power allocation.

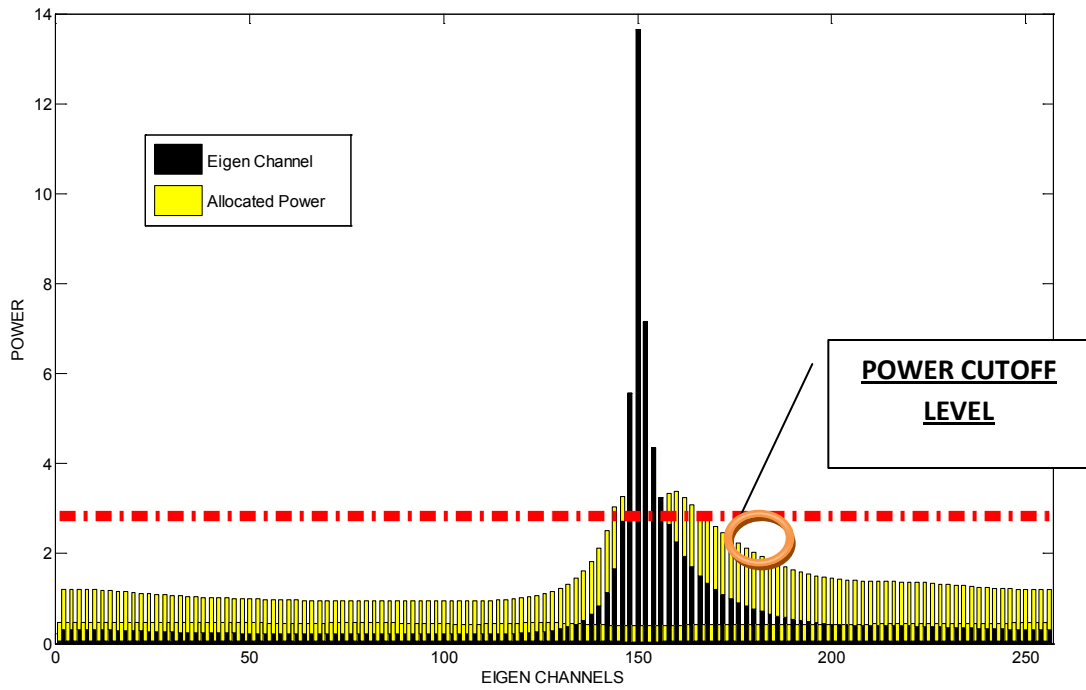


Figure 1.9: SMSE minimization over 2x2 MIMO with 128 OFDM subcarriers and SNR=20dB.

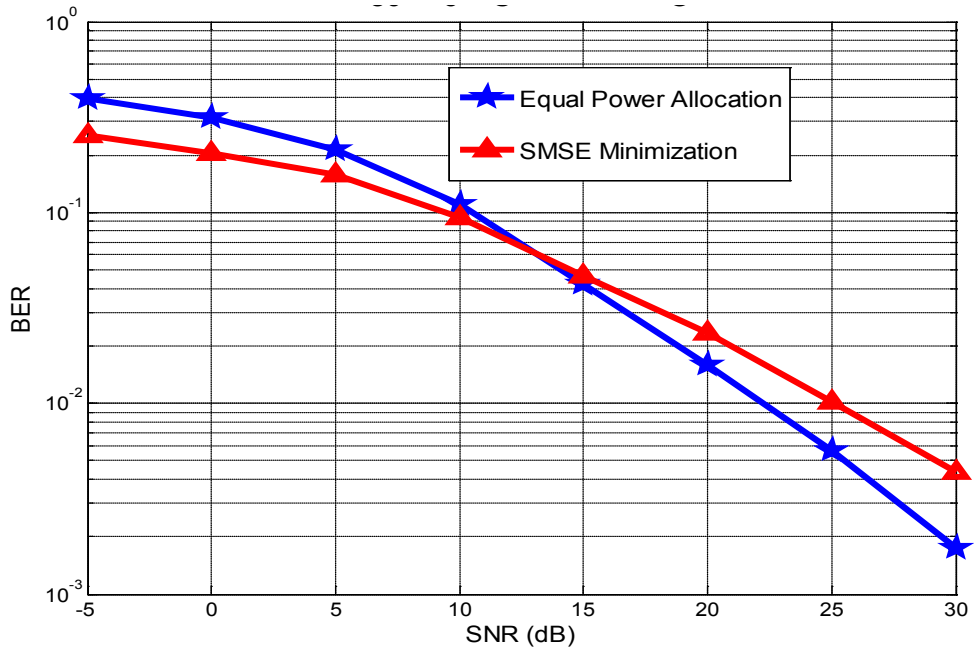


Figure 1.10: BER versus SNR FOR 2X2 MIMO, 128 subcarrier OFDM system with SMSE minimization algorithm and QPSK modulation with IEEE 802.16m macrocell channel model.

SPACE DIVISION MULTIPLE ACCESS (SDMA) USING NULL SPACE STEERING

SDMA allows multiple users to transmit on the same frequency. The users are distributed in space. This is done by precoding the users' respective data such that the data of one user falls in the Null Space of the other users. This form of precoding is called Null Space Steered Precoding because the data of one user falls in the null space of the other users, thereby nullifying the inter-user interference.

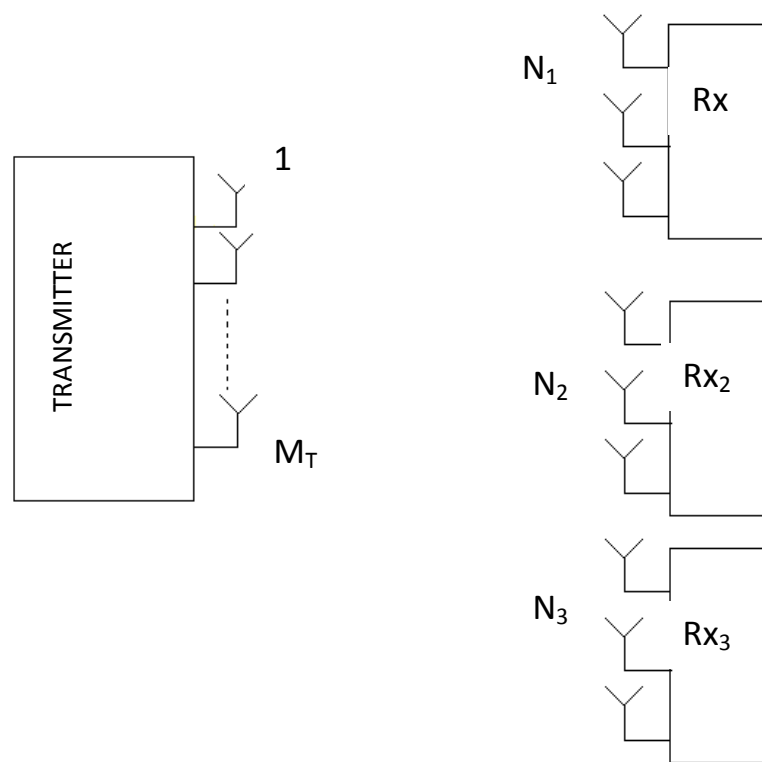


Figure 1.11: Schematic of SDMA channel.

Let us assume that each user has a channel, H_u , of size $N_{Rx} \times M_{Tx}$, where N_{Rx} are the number of receive antennas for user ' u ', and M_{Tx} are the number of transmit antennas at

the base station (BS). To induce orthogonality amongst users, a matrix of orthonormal vectors, M_{Null}^u , is generated for user 'u', such that this matrix is orthogonal to the rest of the users' respective channels.

To do so, first a matrix is created for the user 'u', $H'_u = [H_1^H H_2^H \dots H_{u-1}^H H_{u+1}^H \dots H_{U-1}^H H_U^H]^H$. Here, $(*)^H$ is the Hermitian function and U is the total number of users. Once H'_u has been created for each user, the null space vectors for each of these matrices are calculated. These vectors are orthonormal, and are orthogonal to H'_u columns. The null space matrix formed here is M_{Null}^u , for the user 'u'. The new orthogonal channel matrix, $H_{u|Orth}$, is calculated as follows.

$$H_{u|Orth} = H_u * M_{Null}^u \cdot \quad (1.11)$$

Once the users are made orthogonal, normal power allocation schemes, such as waterfilling, can be applied to all the users put together. Figure 1.12 shows a visual representation of the waterfilling algorithm applied to a multiuser scenario. Here, we see 4 users, each with 2 receive antennas, using an OFDM symbol of length 24. Each user uses all the available subcarriers. Comparing plots in Figure 1.8 and Figure 1.13, it can be seen that the BER performance with waterfilling is the same for both SU and MU systems. This implies that there is no interference amongst the users. In other words, the users have been made orthogonal to each other, and therefore they can communicate with the BS without any interference from the other users. The plots shown in figure 13 also imply that the user channels are not degraded in any way after orthogonalization, and are simply orthogonal to the other users.

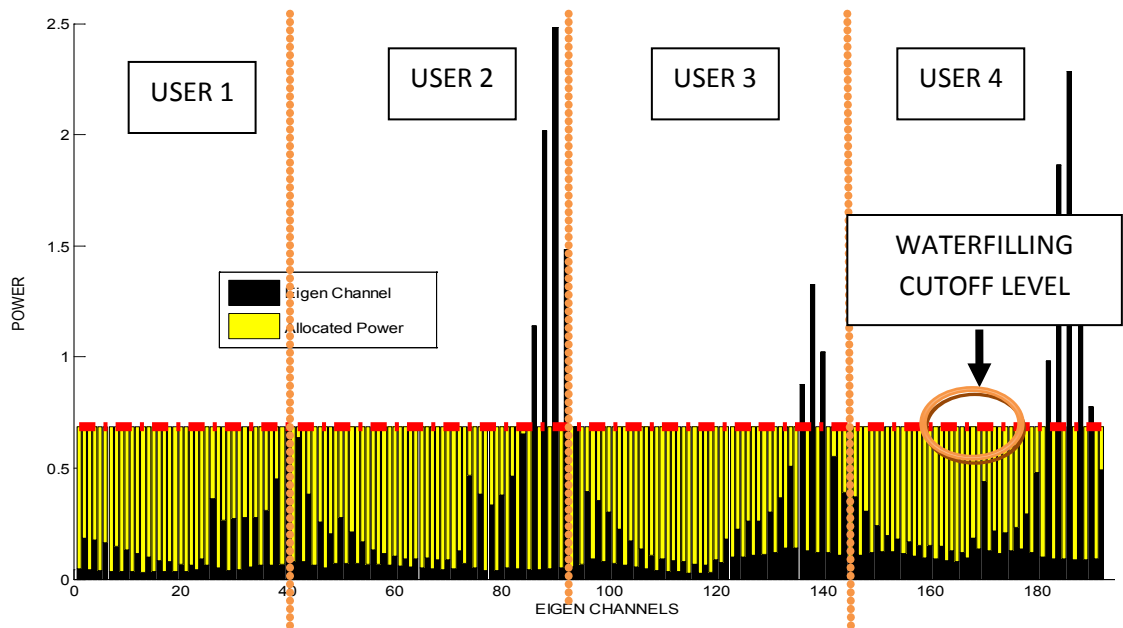


Figure 1.12: Visualization of power allocation using multiuser waterfilling; 4 users, 8 transmit antennas, 2 receive antennas per user.

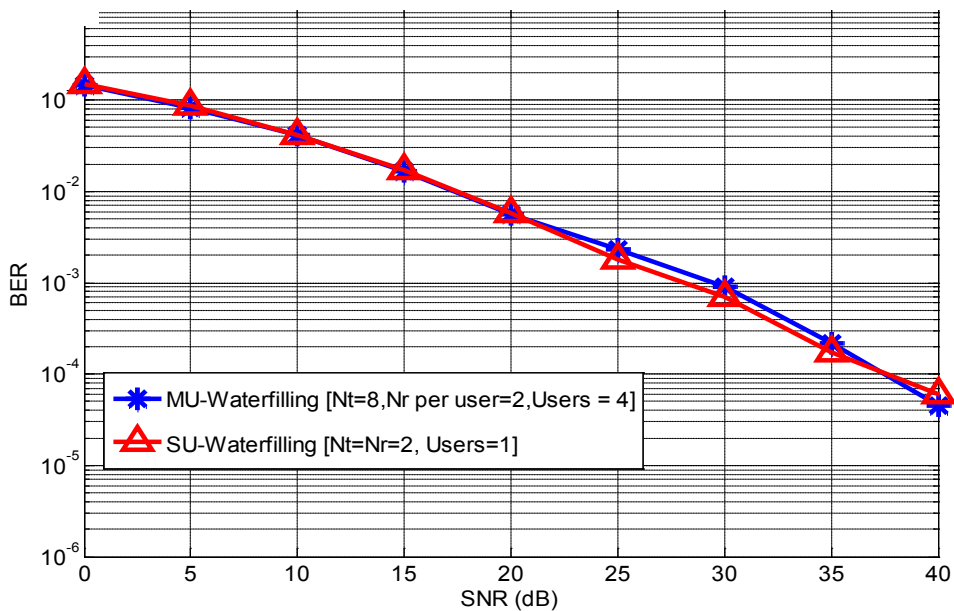


Figure 1.13: BER versus SNR comparison for a 2x2 MIMO, 128 OFDM subcarrier system for SU-MIMO and MU-MIMO configurations

1.2.4 USER SCHEDULING

In the previous chapter, user scheduling was discussed. In this chapter, a few results showing the effect of user scheduling are shown. The following figures show the performance gains due to user scheduling techniques. Figure 1.14, a cumulative distribution function (CDF) plot, shows the effect a frequency correlated channel has on the channel capacity. The abscissa is the capacity in bits/sec/Hz, and the ordinate gives the probability of the channel capacity being less than the abscissa value.

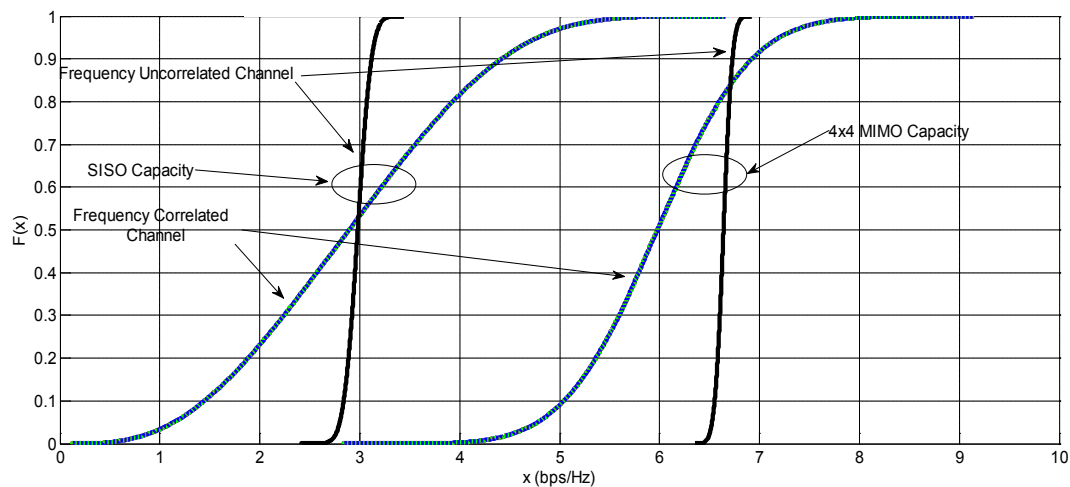


Figure 1.14: CDF plot for spatial and frequency correlated channel capacity using spatio-frequency waterfilling with RR scheduling for 10 dB SNR.

The frequency uncorrelated channel capacity has small variance in its values because per subcarrier capacity gain averages out if each subcarrier in an OFDM symbol is assumed to have uncorrelated gain with respect to the rest of the subcarriers. On the other hand, if the subcarrier gain is correlated in frequency, the entire channel (across all the OFDM

subcarriers) would either have a low gain or high gain, on average. This can be seen as a large amount of variance in capacity values.

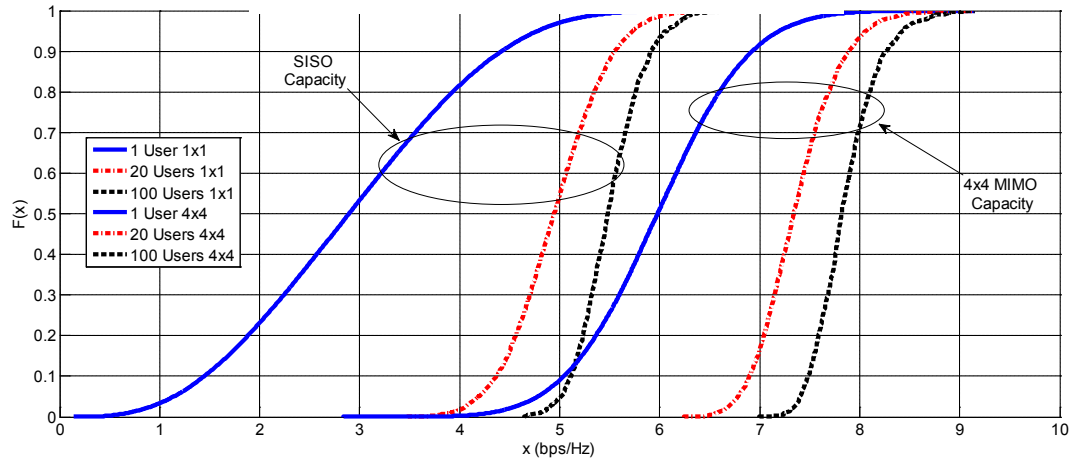


Figure 1.15: CDF plot for spatial and frequency correlated channel capacity using spatio-frequency waterfilling with greedy scheduling for 10 dB SNR.

Figure 1.15 shows cumulative distribution function (CDF) curve for capacity values, for greedy scheduling with different parameters. The abscissa is the capacity in bits/sec/Hz, and the ordinate gives the probability of the channel capacity being less than the abscissa value. The solid blue plot shows the capacity CDF curve when no scheduling is used, i.e., one user is considered at any given time, and therefore, there is no user scheduling that can be done. The red and black plots show that the capacity of the system increases as the number of users considered for contention for any given transmission period is increased. The criterion here is maximum channel capacity. The user with the highest channel capacity is allowed to transmit. It can be seen from the plots that, for a SISO channel, the probability that the channel capacity is less than 5 bits/sec/Hz is about 0.98 for round robin scheduling (where one user is considered), which means that the probability of the

capacity being greater than 5 bits/sec/Hz is $1-0.98=0.02$. For greedy scheduling with a set of 20 users to choose from, the probability of the capacity being greater than 5 bits/sec/Hz is increased to $1-0.5=0.5$. With 100 users, the same probability has jumped to $1-0.05=0.95$. Thus, it can be seen that the capacity of the system increases with increase in the number of users considered for scheduling.

The effect of scheduling is also seen on BER curves, as shown in Figure 1.16. Here, the effect of choosing the best scheduling algorithm is seen. Scheduling criteria are chosen according to [8]. ‘*VBLAST*’ criterion takes into account the *VBLAST* capacity of each user, allowing the user with the highest capacity to transmit in a given timeslot. The channel used here is the Macrocell Channel model given in [3], with no spatial correlation. We see that proportional fair (PF) algorithm produces similar results to those got using the Greedy scheduling policy.

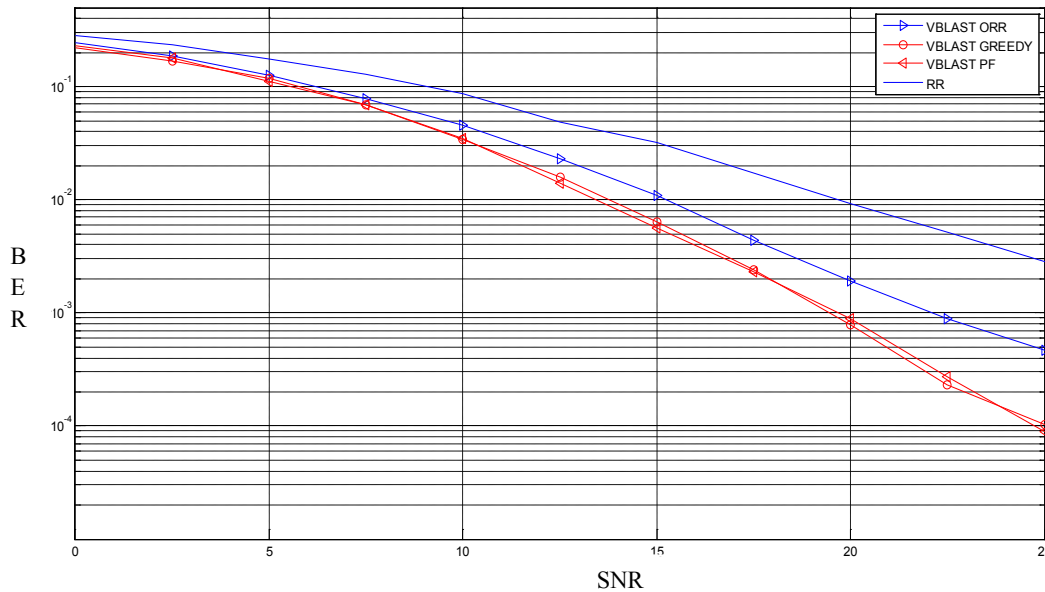


Figure 1.16: BER versus SNR for different scheduling algorithms for a 2x2, 128 subcarrier MIMO-OFDM system.

1.2.5 THEORETICAL BER

In [9], Letaief *et al* have given a closed-form solution for bit error probability, or bit error rate (BER) for M-QAM and M-PSK modulation in an additive white Gaussian noise (AWGN) channel. The AWGN channel is of the following form.

$$y = h * x + n \quad (1.12)$$

Here, x is the input symbol, n is the additive white Gaussian noise, y is the received signal and h is the channel gain. The receiver is assumed to have perfect channel knowledge, and can compensate for the attenuation factor h using automatic gain control (AGC). Thus, h can be dropped from (1.12). In an AWGN channel, the signal can be assigned a signal-to-noise ratio (SNR), and the BER can be given terms of average received SNR.

$$P(e) \cong \frac{4(\sqrt{M} - 1)}{\sqrt{M}} * \frac{1}{\log_2 M} \sum_{i=1}^{\sqrt{M}/2} Q \left\{ (2i - 1) * \sqrt{3 * \frac{E_b \log_2(M)}{(M - 1)N_o}} \right\} \quad (1.13)$$

Let $E_S = E_b \log_2(M)$, where E_S is the energy of each symbol. This energy is a function of the power allocated to the symbol transmitted on the given channel using the waterfilling algorithm that maximizes capacity, or sum of mean square error (SMSE) minimization algorithm.

Let $\gamma_k = \frac{E_b \log_2(M)}{N_o}$ Here, γ_k is the instantaneous SNR on the 'k'th eigen mode. For fading channels,

$$P(e)|_{fading} = \int_0^{\infty} P(e|\gamma) \cdot p(\gamma) d\gamma, \quad (1.14)$$

where, $p(\gamma)$ is the channel fading gain PDF. The instantaneous SNR can also be defined as

$$\gamma_k = \frac{P_k \lambda_k^2}{\sigma^2}. \quad (1.15)$$

Here, P_k will be constant for Equal Power Allocation, and will vary for Waterfilling and SMSE Minimization Algorithms. P_k is dependent on the WF cutoff power level as well as the Eigen mode Gain, which is the eigenvalue of $H^H * H$, where H is the channel Matrix. As the PDF of γ_k is way complicated, the closed-form solution for is hard to compute. Therefore, it is better to store BER Versus SNR values in a table and used to perform bit loading. Figure 1.17 shows BER Versus SNR curves for a 2x2 MIMO OFDM system with OFDM symbol size of 128 subcarriers. Waterfilling power allocation is applied here. It can be seen that the theoretical BER, given by (1.13), closely follows the simulation values even for SNR as low as 15 dB. Also, it can be seen that the approximation in (1.13) becomes better at higher modulation schemes. Beyond 20 dB, the BER curves for 256 QAM are indistinguishable.

Figure 1.18 shows the dependency of the bit loading value on the eigen mode gain. The bit loading value, $m = \log_2(M)$, is chosen such that the $BER < BER_{Req}$, where BER_{Req} is the required BER value. Here, $BER_{Req} = 10^{-3}$. The conclusions drawn for waterfilling hold for SMSE minimization as well. The power allocated to each eigen mode is a random variable, which is dependent on the eigen value of $H^H * H$, ($= [SVD(H)]^2$). Due to the

fact that deriving the closed-form solution for BER for the given SNR is very complicated, a better option is to use stored BER Versus SNR values.

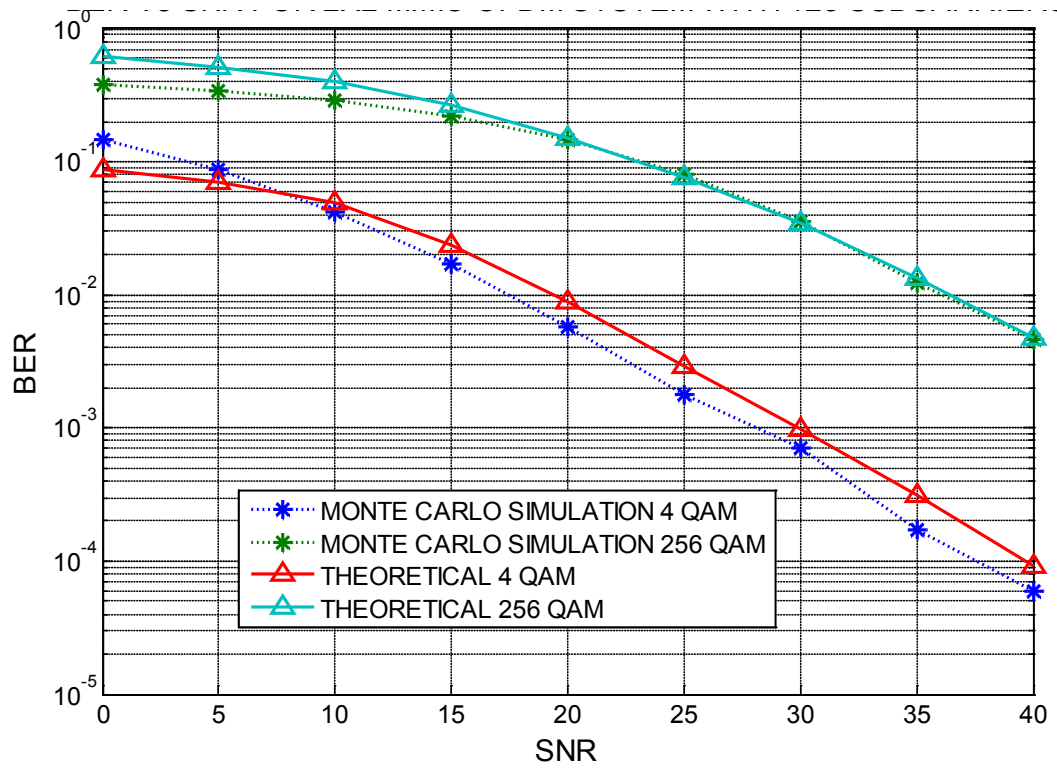


Figure 1.17: Theoretical and simulation BER versus SNR curves for a 2x2 MIMO, 128 OFDM subcarrier system.

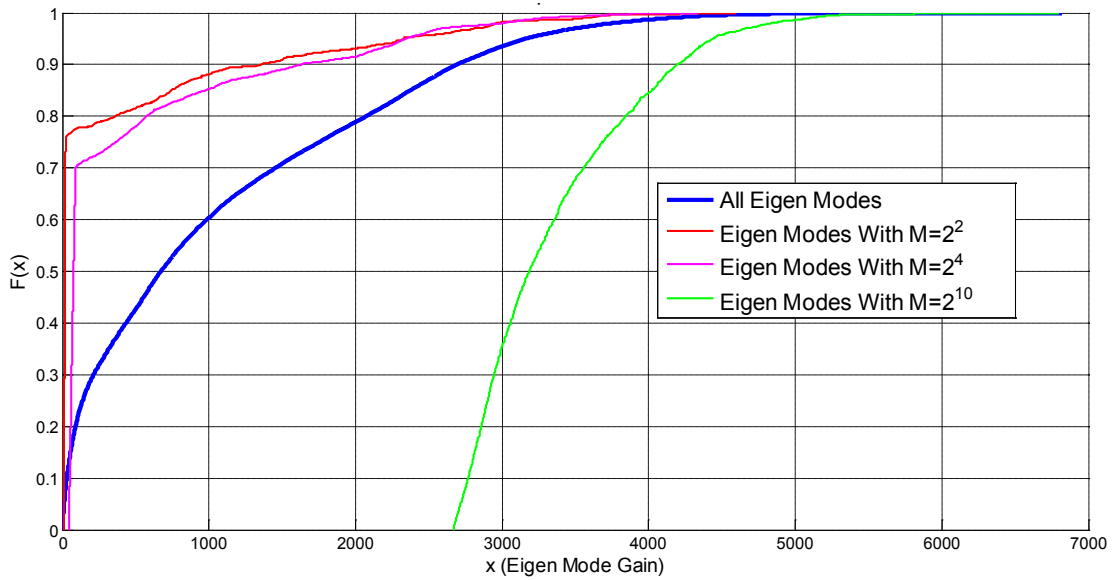


Figure 1.18: CDF curves for eigen mode gains for different bit loading values.

1.3 PROBLEM STATEMENT

The WF precoding algorithm improves the performance of a communication system, but does so by not allowing certain eigen modes to transmit. This reduces the number of eigen modes that are available. SMSE minimization allows more number of eigen modes to transmit compared to WF, but suffers from deteriorated performance at high SNRs of 15 dB or higher. The problem this thesis focuses on is to allow more number of eigen modes to transmit while keeping the performance degradation to a minimum.

1.4 THESIS CONTRIBUTIONS

This thesis proposes a new precoding technique for boosting eigen mode utilization, hierarchical precoding (HP). The results show that using HP improves the system throughput for a SU-MIMO OFDM system at low signal-to-noise ratios (SNRs), with minimal bit error rate performance degradation. The system is tested using a realistic communication channel model, and is shown to perform well under the conditions of channel correlation in the frequency, time and spatial domains.

In addition adaptive eigen mode reduction (AEMR) algorithm is proposed, which uses selective diversity to improve the bit error rate performance of the system. HP degrades the BER performance of a MIMO OFDM system, compared to WF. The algorithm picks optimal channels such that the bit error rate performance is improved.

Further, the effect of feedback reduction is studied on a SU-MIMO OFDM system with WF and HP precoding. Precoding is performed at the transmitter, which requires the receiver to feedback channel information to the transmitter. This thesis shows system performance results with reduced feedback from the receiver, causing imperfect precoding at the transmitter due to imperfect channel knowledge.

Finally, the effects of user scheduling in the frequency domain using OFDMA, and in the spatial domain using SDMA are also studied. Various scheduling algorithms and scheduling criteria are taken into consideration, and their respective performance is studied.

1.5 THESIS ORGANIZATION

The rest of the thesis is organized as follows. Chapter 2 presents a review of published research work. Chapter 3 introduces the channel model used throughout this thesis, and discusses the methods used to generate a realistic, correlated channel. Chapter 4 also introduces the simulation methodology, the assumptions made and the parameters chosen. Chapter 4 presents the proposed Hierarchical Precoding algorithm. Chapter 5 presents the proposed adaptive eigen mode reduction algorithm. Chapter 6 presents the performance evaluation of the proposed algorithms under the assumption of reduced feedback to the transmitter. Chapter 7 presents performance of the algorithms with user scheduling. Finally, Chapter 8 concludes the study, and proposes future direction of work.

CHAPTER 2

LITERATURE REVIEW

In this chapter, a thorough literature review is presented. The chapter is divided into sections, and each section discusses and presents literature review pertaining to one topic. Section 2.1 presents a review of research work done in the fields of capacity analysis, section 2.2 discusses research papers related to precoding and section 2.3 provides an overview of the research work done in the field of user scheduling.

2.1 CAPACITY ANALYSIS

SINGLE-USER/MULTIUSER MIMO

MIMO capacity analysis has been studied exhaustively in literature. For a single-user MIMO (SU-MIMO) setup, Rayleigh *et al* [6] extend the single-user SISO capacity to derive the MIMO capacity. The paper shows that the capacity of a channel, for a given power allocation and noise power, increases linearly with increase in number of transmit antennas. Paulraj [10] shows that a multipath channel can be advantageous in a MIMO scenario, in terms of the ergodic capacity as well as outage capacity, assuming the delayed multipath taps increase the angular spread of the received. In [11], Goldsmith *et al* show the effect of channel knowledge on the capacity of a SU-MIMO system. With perfect channel knowledge, the channel is reduced to a set of parallel, non-interfering spatial subchannels, where the gain of each path corresponds to the singular values of the channel matrix. Transmit power allocation can then be done equally among all transmit antennas, or according to the gain on each of the parallel eigen channels, under the constraint of total transmitted power.

Multuser (MU) MIMO configuration allows multiple users to communicate over the same frequency, but on different spatial subchannels. The users need to be orthogonal to each other in order to eliminate inter-user interference. This can be done by multiplying each user's input signal with a nulling matrix such that it falls in the null space of the rest of the users' channels. This process is known as space division multiple access (SDMA),

and is covered in detail in Section 1.2.3. For the MU-MIMO configuration, Cioffi *et al.*, in [12], show the effect multiple antennas can have on a MU-MIMO configuration for the uplink. The authors show that the receiver antenna dimensions at the BS enable multiple users to transmit simultaneously. On the other hand, the transmitter antenna dimensions per user enable users to increase their throughput. The paper [12] highlights how system designers can tradeoff sum capacity to allow more users, and vice versa. In [13], Fujimoto *et al.* have shown that, in a channel with spatial correlation between antennas, MU-MIMO performs better than SU-MIMO. This is due to the fact that spatial correlation degrades performance. Therefore, allowing multiple independent orthogonal users to transmit reduces the overall spatial correlation, thereby improving performance.

MIMO OFDM

OFDM can be used in conjunction with MIMO to provide better throughput. In [6], discrete matrix multitone (DMMT) coding is proposed, which bears a strong resemblance to MIMO-OFDM. In [6] the capacity of a MIMO-OFDM system is shown to be the sum of per-OFDM subcarrier MIMO capacities [6]. [10] gives the ergodic capacity of a MIMO-OFDM channel as the sum of capacities calculated using the eigen values of the channel matrix as the channel gains. In [14], the capacity for a MIMO OFDMA system is derived. The per-user capacity is shown to be the sum of capacities of all MIMO channels for the subcarriers allotted to each user.

2.2 PRECODING

Precoding is the process of compensating for spatial interference caused by the channel at the transmitter. This requires channel knowledge at the transmitter. The ‘*quality*’ of channel information dictates the performance of the precoding filter. Visotsky *et al* [15] show the effect of imperfect channel knowledge on the capacity of the channel. Visotsky *et al* show that the knowledge of the mean eigen channel gains at the transmitter performs equally well to the case with optimal beamforming with perfect channel knowledge if the feedback from the receiver is not error prone. In [16], Paulraj *et al* show that, assuming perfect channel knowledge at the transmitter, adding a precoder and a decoder at the transmitter and receiver, respectively, decouples the channel into eigen sub-channels. Also, it was shown that, at high SNRs, the precoder and decoder filters completely eliminate interference between spatial channels. In [17], generalized optimum precoder and decoder filters are designed. Windpassinger *et al* [18] show that non-linear precoding performs better than linear precoding, with the drawback of increased complexity of the transmitter and receiver design.

To simplify the problem of designing the generalized optimum precoder and decoder, certain assumptions are made in [17]. Firstly, perfect channel state information at the transmitter (CSIT) and receiver (CSIR) is assumed. The receiver can have perfect CSIR by using a training sequence in order to get channel information. Perfect CSIT is achieved by allowing the receiver to feedback channel state information (CSI) to the transmitter. Secondly, flat fading channels are assumed. IEEE 802.16m utilizes OFDM,

which converts the wideband channel frequency non-selective. For this to hold true, the cyclic prefix for an OFDM symbol needs to be longer than the maximum channel delay (See Section 1.2.2). Finally, a full-rank channel matrix is assumed. A multipath channel is assumed, which produces a full-rank channel matrix. Under these assumptions, jointly optimal precoding and decoding filters can be designed to satisfy different design constraints as follows.

- Maximize capacity – Waterfilling is shown to be the optimal solution.
- Minimize sum of symbol estimation errors – Sum of mean square error (SMSE) is minimized across subchannels.

Precoding can be done for SU-MIMO, as well as for MU-MIMO broadcast channel transmission, where multiple users transmit/receive simultaneously.

WATERFILLING AND SMSE MINIMIZATION PRECODING

Capacity maximization solution needs the precoding to follow the waterfilling solution, where each eigen subchannel is assigned power proportional to its gain. Waterfilling simply assigns more power to eigen channels that have larger path gain. The effectiveness of waterfilling depends on the *quality* of CSIT. If the transmitter has no knowledge of the MIMO transmission channel, the total power will be distributed equally amongst all transmitter antennas. If however the transmitter *knows* the channel, using feedback from the receiver, it can assign more power to the transmitter that has more path

gain. This method of power allocation is known as waterfilling algorithm [6]. In [19], Jiang *et al.* have given a closed-form solution for MIMO – OFDM channel capacity, assuming each OFDM subcarrier is assigned to one user. Here, waterfilling is done across spatial and OFDM subchannels. In [20], Münz *et al.* provide waterfilling solution for a SISO – OFDMA system, where the user with the best channel is assigned the subcarrier. Maung *et al.* [14] give an adaptive algorithm that provides different users different data rates. This is done to make sure that strong users do not hog the bandwidth all the time.

SMSE solution minimizes the SMSE across all the subchannels. In [16], precoding and decoding filters are designed such that SMSE is minimized, with a total transmit power constraint. At high SNR, the SMSE minimization solution allocates power inversely proportional to the respective eigen channel gain. This is the inverse of waterfilling, where eigen channels get power proportional to their gain. Hence, SMSE minimization solution is also known as inverse waterfilling solution. Paulraj *et al.* [17] designed the precoder and decoder filter design in order to either maximize capacity or minimize SMSE.

Karaa *et al.* [21] have proposed the joint SMSE minimization and power allocation algorithm for a MU-MIMO OFDM, where the users are allocated spatial subchannels. The following assumptions are made to make sure that the uplink and downlink links are resolvable.

- The number of total transmit antennas at the user's mobile station must be greater than or equal to the number of data streams assigned to him.

- The total number of data streams assigned to all users must be less than or equal to the number of transmit antennas at the base station

SMSE is minimized over all OFDM subcarriers and spatial subchannels, using a joint power allocation algorithm that allocates power across the OFDM subcarriers as well as across spatial subchannels to minimize the SMSE, constrained by the total transmit power. In [22], Liang *et al.* have used the Schmidt orthogonalization method to find precoding orthonormal basis vectors for each user, such that each user is orthogonal to the rest. Each user's precoding matrix falls in the nullspace of the rest of the users. This allows each user to be completely orthogonal to each other, block diagonalizing the channel. Yang *et al.* [23] give the precoding and decoding filter design algorithms for MIMO-SDMA system that either maximizes the signal to interference plus noise ratio (SINR), with the constraint of total transmittable power, or minimizes total transmitted power, with the constraint of minimum target SINR per user. In their paper [24], Li *et al* exploit the effect of slow fading channels to reduce feedback from the receiver, and use the past channel knowledge at the transmitter to extrapolate the precoding matrix.

MULTIUSER PRECODING

MU-MIMO precoding is done such that there is no inter-user interference. This property bears a striking resemblance to SDMA, wherein each user is assigned different spatial channels, and orthogonality is achieved through precoding. In order to allow multiple users to transmit simultaneously over the same subcarrier frequency, the users' data needs to be precoded such that each user's channel is effectively orthogonal to the rest of

the users. In [25], Zhong *et al* have described a user orthogonalization algorithm that implements space division multiple access (SDMA) that allows multiple users to transmit over the same carrier frequency. SDMA allows multiple access channels to be created in the spatial domain. This is equivalent to orthogonal subcarriers used in OFDM, except that the users are made orthogonal in the spatial domain. The algorithm is similar to Schmidt orthogonalization as described in [22]. Choi [26] gives a reduced feedback MU-precoding algorithm, that uses interpolation to reduce the amount of feedback required from the receiver. Due to this interpolation and feedback reduction, the system performance is reduced, and the effect of feedback reduction on the system performance is also studied in [26]. Tejera *et al* [27] give a suboptimal MU precoding technique for allowing multiple users to transmit simultaneously in the spatial and frequency domain. The paper also presents a reduced complexity zero forcing subchannel orthogonalization and allocation algorithm. In [28], Wang *et al* propose a MU precoding algorithm that takes the noise power into consideration when performing block diagonalization of the users. The proposed algorithm improves the system performance at low SNRs.

In [29], Chan *et al* have given a capacity maximization solution for multiuser SDMA MIMO OFDMA configuration. The best solution is one where each eigen subchannel is given to the best user for that particular eigen subchannel. The solution, however, is complicated, and the paper gives two suboptimal solutions that perform close to the optimal solution. The first solution proposed is to allow all users to transmit, and allotting different number of eigen subchannels per user such that the capacity is maximized. The maximum number of eigen modes that can be assigned to each user are equal to the

number of receive antennas used by the user. This is done to make sure that the system is not undetermined. For example, if the number of transmitting antennas assigned to a user is greater than the number of receiver antennas, the system would be underdetermined as there would be more unknowns (i.e. transmitted symbols) than equations to solve for them. If the total number of receive antennas per user is defined as N_R , then the number of assignable eigen modes for that user will be less than or equal to N_R . Thus, all combinations of receive antennas for each user would have to be considered when maximizing the total capacity. This method is tedious on its own, but the complexity is lower when compared to the optimal solution. The second solution proposed in [29] is to fix the number of eigen subchannels per user, and choose a subset of users from the whole user set such that capacity is maximized. Here the capacity would be maximized for a particular subset of users, which is found using a brute force method, wherein all possible user subsets are considered and the subset that maximizes the capacity is chosen. Henarejos *et al* [30] have considered a similar problem as [29], with an additional constraint of heterogeneous traffic with queue management. This paper proposes a suboptimal scheduler that reduces the delay experienced by heterogeneous data sources with finite queue backlog.

In [31], the authors have given a MU-MIMO user selection algorithm such that the capacity is maximized. The algorithm chooses a subset of users from the user superset that are the most orthogonal to each other. Recall that in SDMA, where the users that transmit on the same carrier frequency but on different spatial channels, each user needs to be orthogonal to the rest of the selected users in order to minimize inter-user

interference. So, in [31], the given algorithm chooses the user subset that minimizes the inter-user interference and maximizes the capacity. Capacity maximization can be achieved through waterfilling across the spatial and frequency domains, across all users. This algorithm gives a significant improvement in capacity with increase in the number of total users.

2.3 USER SCHEDULING

The subject of user scheduling has been studied extensively in literature. Here, users that satisfy a given criteria, such as maximum carrier to interference ratio (CIR), are allowed to transmit. This allows the user with the best channel to transmit at any given time, thus reducing the error probability, which boosts the throughput of the channel. The paper [32] gives a suboptimal, zero forcing based MU-MIMO user scheduling algorithm that achieves a significant fraction of the sum capacity attained using the optimal MU-MIMO precoding, that is, dirty paper coding. Greedy scheduling is implemented, which chooses the best user subset from a given set of users. If we assume a slow fading channel, the channel for each user will change slowly over a period of time. This implies that a user with a good channel might continue to have a good channel for quite some time. Thus, that particular user will be hogging the bandwidth and the users whose channels are worse will not get a chance to communicate. Choosing the best user according to some criteria is known as Greedy Scheduling, and this gives us the best achievable theoretical capacity for multiuser scheduling. Here, we are assuming that one user is chosen to transmit over the medium at any time. The greedy scheduling technique is not fair to all

users. Therefore, a number of scheduling techniques have been studied and implemented which provide some amount of fairness to all users.

The simplest form of scheduling is Round Robin (RR) scheduling, wherein all users are allotted sequential time slots for transmission. RR does not consider any criteria for user scheduling. Therefore, it has the lowest achievable capacity. Greedy scheduling is exactly the opposite of RR scheduling. Here, the best user, selected according to given criteria, is allowed to transmit in a given time slot. Greedy algorithm achieves the best capacity, but is not fair in the sense that a user with a constantly bad channel will not be able to transmit at all. Opportunistic Round Robin (ORR) scheduling takes the best of RR and greedy scheduling. In ORR scheduling, the best user is selected for a given transmission time slot. The difference for Greedy scheduling is that a user that has ‘*won*’ in the previous time slot is not allowed to contend for the present time slot. This continues till all users have transmitted, and the process begins again. ORR allows all users to have roughly the same throughput (bits/s/Hz), assuming that each user is transmitting at the same ‘*Bit Rate*’. If the users are transmitting different modulation symbols (QPSK, BPSK, 16 QAM, etc.) the actual throughput per user will vary. To overcome this, we can ‘*weigh*’ each user’s scheduling criterion metric (CIR, MIMO Capacity, etc.) with the amount of data, in bits, that the user has transmitted. This allows fairness if each user is using a different signal constellation to modulate its data. This scheduling algorithm is known as Proportional Fair (PF) scheduling. Liu *et al* [33] propose a joint spatial and frequency PF user scheduling algorithm. In this paper, users are selected such that the sum capacity is maximized, with the constraints of total transmittable power and

proportional fairness. In [34], Chan *et al* compare the performance of multicarrier-CDMA (MC-CDMA) with MIMO-OFDMA, with fairness constraints. This paper shows that MIMO-OFDMA system has higher sum capacity than the MC-CDMA system, for a given fairness constraint.

Shen *et al.* [35] give a multiuser OFDMA scheduling scheme wherein each user is guaranteed a certain required data rate. Till now, it is assumed that all users will have infinite amount of data to be transmitted. In [36], Chandrashekar gives a user scheduling algorithm that takes into account bursty traffic from users. Zhong *et al.*, in [25], have proposed a user scheduling algorithm, with quality of service (QoS) constraints such as target BER per user and total power that can be assigned over all users, OFDM subchannels and spatial eigen modes. Two algorithms are developed, to maximize the capacity, while keeping the complexity low. In [37], Papoutsis *et al.* give an algorithm that guarantees minimum number of OFDM subcarriers per user. Their results show that fairness can be achieved at the cost of capacity. The results show that as the minimum guaranteed OFDM subcarriers per user increases, the fairness increases with certain loss in the sum capacity. On the other hand, as the minimum subcarriers per user tends to zero, the capacity is maximized, but at the cost of fairness. Till now, we have seen user selection being done through exhaustive iteration through all the possible users. In [38], Dao *et al.* have reduced the complexity of the problem by choosing users that satisfy a certain criterion. Thus, for large number of users, complexity is greatly reduced with minimal drop in performance.

In [39], Conte *et al* have proposed a low complexity joint scheduling and beamforming technique called Projection Based Greedy (PBG) algorithm. Here, perfect channel state information at the receiver and the transmitter is assumed. Equal power distribution is assumed. Simply put, the algorithm chooses subcarriers iteratively, and allots data to them if transmission on the subcarrier increases the overall throughput of the system. With a fixed maximum transmit power available, the average SINR will decrease with increase in allotted subcarriers. Hence, PBG algorithm iteratively finds the point beyond which adding subcarriers to the scheduled subcarriers' list will decrease the average SINR, and therefore, decrease the throughput. The results in the paper show similar performance to two other algorithms that perform an exhaustive search amongst available subcarriers, but with reduced complexity.

In [29] capacity maximization using SDMA is studied. Here, multiple users are chosen from a given user set, such that the sum capacity is maximized. Thomas *et al* [40] present a user selection algorithm that switches from allotting users spatial channels to allotting frequency channels if it is not feasible to allot spatial channels to the users. This algorithm shows gains of up to 7 dB in frame error rate performance, while keeping the feedback requirements and computational complexity within reasonable limits.

Shrivastava *et al* [41] have proposed a joint scheduling and random beamforming technique, with reduced feedback. Each user is assumed to have perfect channel state information (CSI), but the transmitter does not. The multiuser precoding matrices for all subcarriers are preset and indexed, and it is assumed that the transmitter (base station) and the receivers (mobile station) have these matrices stored. The receiver feedbacks

signal to interference plus noise ratio (SINR) per subcarrier and the index of the precoding matrix to be used. The transmitter then chooses the user with the highest SINR for each subcarrier, and uses the precoding matrix sent by that user to transmit data. Feedback reduction is done by dividing the total subcarriers into blocks, such that the bandwidth of each block does not exceed the coherence bandwidth. The users just send the SINR value for the centre frequency for each block, and the user with the highest SINR for that block gets to transmit on that block. The results show that the average throughput for a given number of users is higher than the algorithm where SINR is calculated at the base station and perfect user orthogonality using null steering is performed [39].

CHAPTER 3

IEEE 802.16m CHANNEL

MODEL

In this thesis, the IEEE 802.16m channel model is used for the evaluation of the proposed algorithms. Firstly, the channel modeling approach is described. Next, The channel model parameters are described in [3], are stated. Finally, the evaluation methodology, that describes the receiver design and the channel parameters used throughout the thesis, are defined.

3.1 INTRODUCTION

The 802.16m evaluation methodology document [3] describes two ways of implementing channel modeling. The first is the deterministic channel model. Here, the channel is modeled based on a very specific setup, such as the environment, the transmitter and receiver location and the antenna type. This model creates a channel for system evaluation that is very site-specific. This channel model does not allow system evaluation under different channel conditions. Therefore, this type of channel model is not used for system level evaluation.

The second type is the stochastic channel modeling. Here, only channel statistics, such as correlation, mean and variance, while the channel instants themselves are random. This type of channel model is conducive to simulation type system evaluation, because channel instants that reflect the ‘best case’ or ‘worst case’ scenarios can be created just by changing the channel statistics. This method is used in this thesis for channel modeling.

3.2 STOCHASTIC CHANNEL

MODELLING

In Figure 3.1, a very simple single input single output (SISO) system is shown.

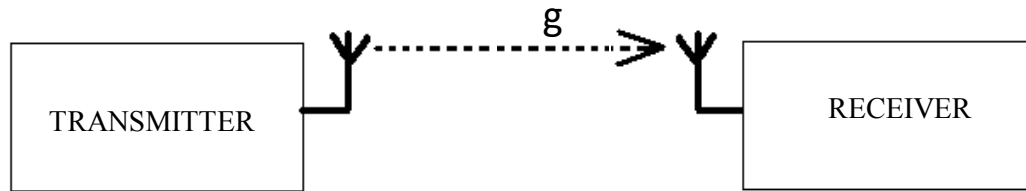


Figure 3.1: A simple SISO configuration.

Here, we see a simple communication system with just one path between the transmitter and receiver, whose path gain is 'g'. Here, 'g' can have a non-zero variance and mean, but it is assumed to be a random value. The EMD [3] takes this random value from a Gaussian probability function (PDF), and that is what is used in this thesis.

A more realistic model than what is described above would be a channel that assumes that multiple paths exist between the transmitter and the receiver. These paths can be delayed with respect to one another, thus causing multiple delayed copies of the transmitted signal to reach the receiver. In Figure 3.2, four delayed paths with different gains are shown. Path number 1 reaches the receiver the quickest, while the rest are reflected off different reflectors, and reach the receiver with different gains. The Figure 3.2 (B) shows the power value of each path that is received over time. In a stochastic channel model, the mean power for each of these taps is given. The instantaneous channel instants created have these tap values chosen from the Gaussian PDF, and are weighed according to their respective path power. This channel with multiple, time delayed paths is called a Multipath Channel, and the model used here, that uses the Gaussian PDF to choose the complex path gains, is known as the Rayleigh multipath channel model.

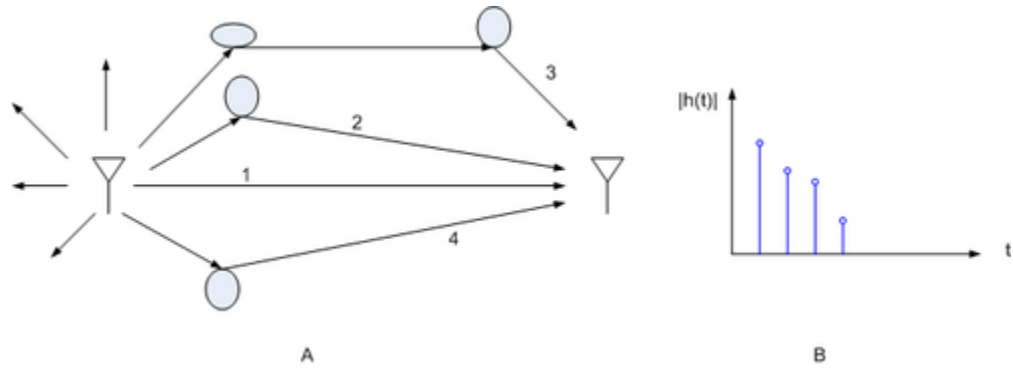


Figure 3.2: Rayleigh faded multipath channel.

A multipath Rayleigh fading channel is implemented as a finite impulse response (FIR) filter is given by (3.1) as

$$h(t) = \sum_{l=1}^L \alpha_l(t) * e^{(\tau - \tau_l(t))}. \quad (3.1)$$

Here, $h(t)$ is the baseband channel impulse response at time t , L is the total number of multipath taps, $\alpha_l(t)$ is the l^{th} tap gain, and $\tau_l(t)$ is the l^{th} tap delay.

The time lag between the first received tap and the last one is called maximum excess delay. It is a measure of how frequency selective channel is. If the maximum excess delay of a channel is large compared to the input symbol period, there will be a lot of inter symbol interference caused due to the multipath channel because delayed copies of the previously received symbols will interfere with the present received symbol. Conversely, if the maximum excess delay is much less than the input symbols period, all the delayed copies of the present symbol will be received within the current symbol, eliminating the inter-symbol interference.

The IEEE 802.16m Evaluation Methodology Document (EMD) [3] provides a detailed channel model, which is followed throughout in this work. The assumptions for the channel model, as given in the EMD, are as follows.

1. Total number of Multipath Taps, 'L', for a given propagation scenario (line of sight (LOS) urban macrocell, non LOS (NLOS) urban macrocell, etc.) is constant over time
2. The tap delays, τ_l , do not change over time.
3. The tap gains, $\alpha_l(t)$, can change with time, due to Doppler Spread. Doppler Effect will be dealt with in detail in Section 3.4.

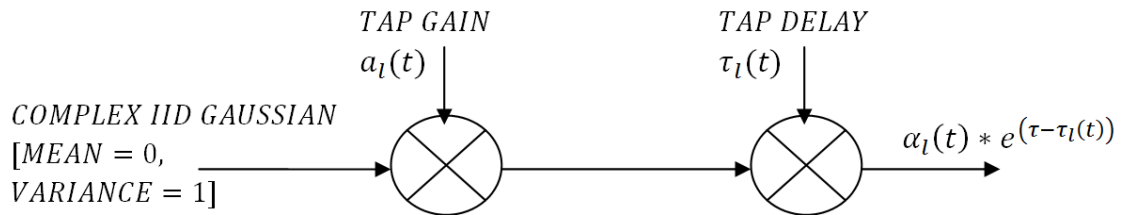


Figure 3.3: Schematic diagram for non-uniform tap generation.

The Figure 3.3 shows how an instantaneous tap is generated. First, a random, IID complex Gaussian value with zero mean and unit variance is generated, which is then multiplied by the average gain for that particular tap. This value is then delayed according to the delay value for the given tap. This whole procedure is repeated for each tap to be created. The tap delay and tap gain values are assumed fixed, and the channel variations are due to the IID Gaussian values used. The statistics of a channel are dictated by the

propagation scenario and the radio environment [3]. The EMD [3] defines channel models for different propagation scenarios, which are described now.

URBAN MACROCELL CHANNEL MODEL

In this model, the mobile station is located at street level, with the base station on the top of a high rise, clearly above the surrounding buildings. There may or may not be a clear line of sight (LOS) between the mobile station (MS) and the base station (BS). Each tap is assumed to be composed of a number of rays that have similar power, delay, angle of arrival (AoA) and angle of departure (AoD). Thus, a cluster of such similar rays can be assumed as a single tap. The urban macrocell channel model for the non line of sight (NLOS) scenario, as described in [3], has the following values, given in table 3.1. Note that the power values are not normalized.

Table 3.1: Urban macrocell channel NLOS model from the IEEE 802.16m EMD.

Cluster #	Delay (ns)			Power (dB)		
1	0			-6.4		
2	60			-3.4		
3	75			-2.0		
4	145	150	155	-3.0	-5.2	-7.0
5	150			-1.9		
6	190			-3.4		
7	220	225	230	-3.4	-5.6	-7.4
8	335			-4.6		
9	370			-7.8		
10	430			-7.8		
11	510			-9.3		
12	685			-12.0		
13	725			-8.5		
14	735			-13.2		
15	800			-11.2		
16	960			-20.8		

Cluster #	Delay (ns)	Power (dB)
17	1020	-14.5
18	1100	-11.7
19	1210	-17.2
20	1845	-16.7

Figure 3.4 shows a channel instant of the urban macrocell model. Here, it can be seen that the amplitude of each tap decreases with time. Also, although the instantaneous values of each of the taps are random, the asymptotic average power of each tap will be equal to the respective average per tap power given in table 3.2.

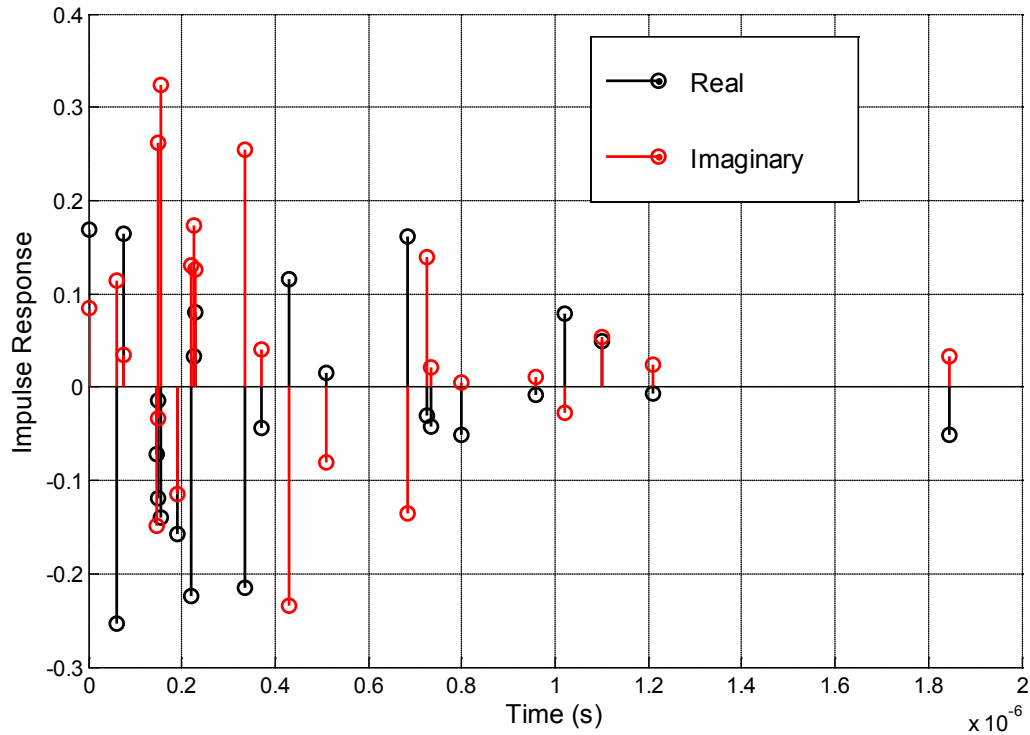


Figure 3.4: Non uniform channel impulse response for the urban macrocell NLOS channel model.

SUBURBAN MACROCELL CHANNEL MODEL

This model is similar to the urban macrocell model, except that the buildings are assumed to be shorter in height, usually 4 floors or lower.

Table 3.2: Suburban macrocell channel model as described in the IEEE 802.16m EMD.

Cluster #	Delay (ns)			Power (dB)		
1	0	5	10	-3.0	-5.2	-7.0
2	25			-7.5		
3	35			-10.5		
4	35			-3.2		
5	45	50	55	-6.1	-8.3	-10.1
6	65			-14		
7	65			-6.4		
8	75			-3.1		
9	145			-4.6		
10	160			-8		
11	195			-7.2		
12	200			-3.1		
13	205			-9.5		
14	770			-22.4		

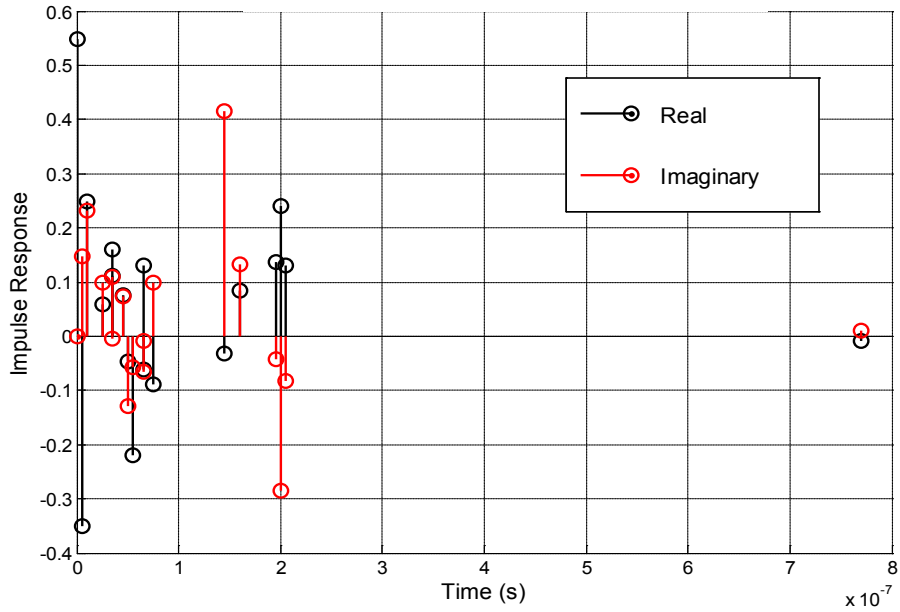


Figure 3.5: Non uniform channel impulse response for the suburban macrocell NLOS channel model.

URBAN MICROCELL CHANNEL MODEL

The MS and the BS are located lower than the tops of the surrounding buildings. This hinders the wave propagation, thereby reducing the area covered by the BS. The buildings and the streets are laid out in a Manhattan style grid.

Table 3.3: Urban microcell channel model as described in the IEEE 802.16m EMD.

Cluster #	Delay (ns)			Power (dB)		
1	0			-1		
2	90	95	100	-3.0	-5.2	-7.0
3	100	105	110	-3.9	-6.1	-7.9
4	115			-8.1		
5	230			-8.6		
6	240			-11.7		
7	245			-12.0		
8	285			-12.9		

Cluster #	Delay (ns)	Power (dB)
9	390	-19.6
10	430	-23.9
11	460	-22.1
12	505	-25.6
13	515	-23.3
14	595	-32.2
15	600	-31.7
16	615	-29.9

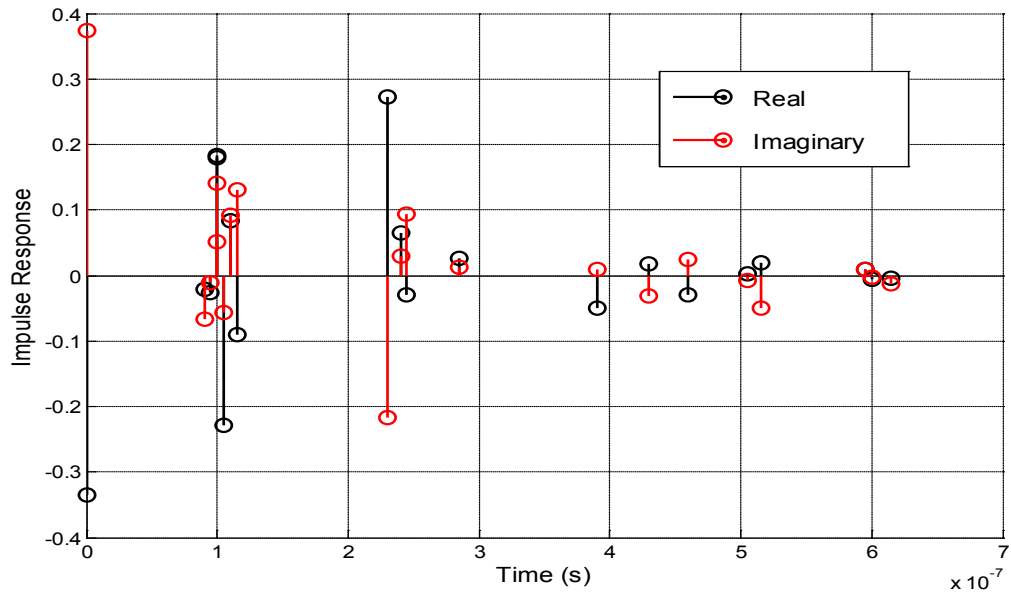


Figure 3.6: Non uniform channel impulse response for the urban microcell NLOS channel model.

3.3 CHANNEL BANDLIMITING

UNIFORM SAMPLING

All the models that are discussed up to this point are temporally non uniform, i.e., the taps are not equally spaced. In order to implement the channel model, the channel needs to be resampled uniformly at the sampling rate equal to the sampling rate of the

transmitted signal. Also, because the channel is of finite length in time, it is going to be infinite in frequency. To overcome these two problems, the channel needs to be bandlimited to the bandwidth of the transmitted signal, and then resampled to get a uniformly distributed channel. The problem, however, with bandlimiting a channel is that it will extend to infinity in the time domain. To overcome this problem, the channel can be limited in time by simply removing taps beyond a certain time threshold. If the threshold is taken to be large enough, the distortion caused due to time limiting will be minimal.

In Figure 3.7, a sample channel frequency response is shown, along with a bandlimiting filter, whose bandwidth is equal to the channel bandwidth. Here, it is assumed that the channel bandwidth and the transmitted signal bandwidth is the same. This is a mild assumption, because if the channel bandwidth is less than the signal bandwidth, some part of the signal will be lost when transmitted through the channel. The baseband channel bandwidth is shown to be equal to $BW/2$, where BW is the RF channel bandwidth. In the frequency domain, the channel frequency response is simply multiplied with the bandlimiting filter. This process translates to a convolution of the channel in the time domain with a sinc filter. The sinc function extends in time from negative infinity to positive infinity, therefore, by bandlimiting the channel, the channel has also been extended in time.

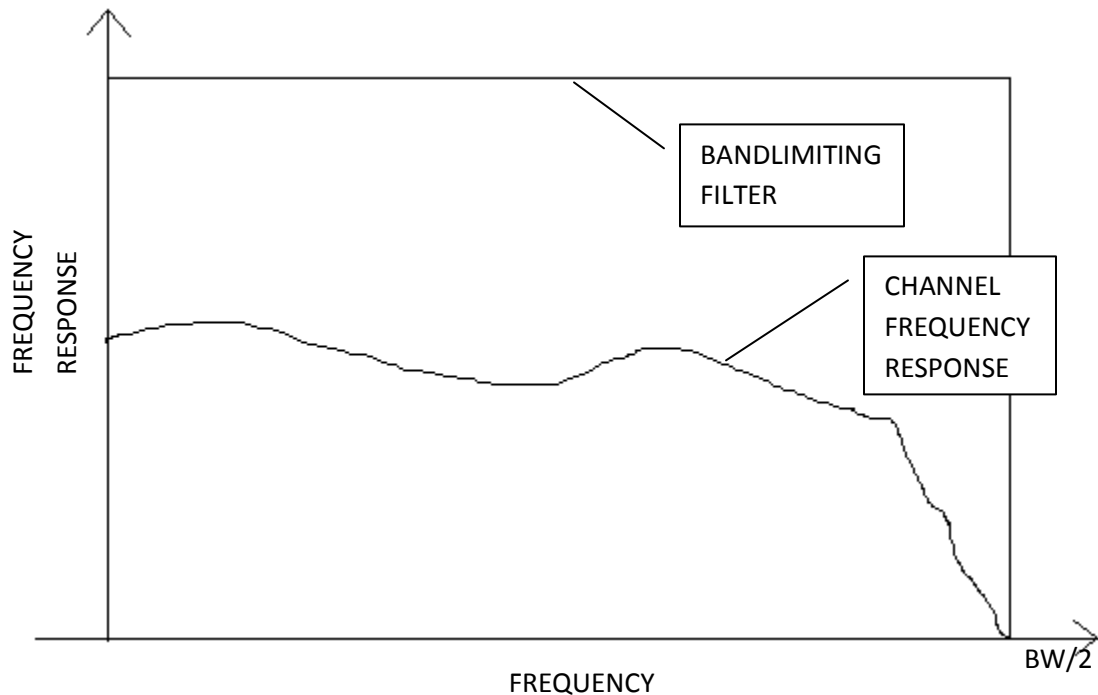


Figure 3.7: Channel frequency response bandlimited by a bandlimiting filter.

Till now, the channel is continuous in the time domain. As the input signal is a sampled signal, the channel needs to be sampled as well. The baseband bandwidth of the input signal is $BW/2$. This implies that the minimum sampling rate for the input signal, and therefore the channel, is $2 \cdot BW/2 = BW$. In the time domain, the process of sampling at a uniform rate translates to convolution with an impulse train, whose frequency is equal to the sampling frequency. In simple terms, the sampled channel's samples are calculated by convolving time shifted sinc function with the channel, where the time shift is equal to the sampling period.

In Figure 3.8, $T=1/BW$ is the sampling time, and the variable n represents time samples, $-\infty < n < \infty$. As ' n ' goes from negative infinity to positive infinity, the channel will be stretched out in time.

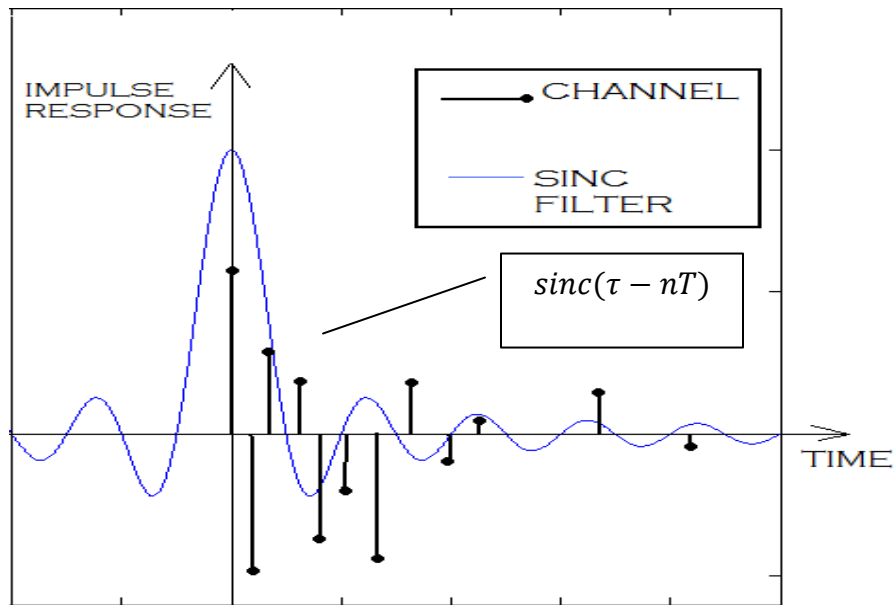
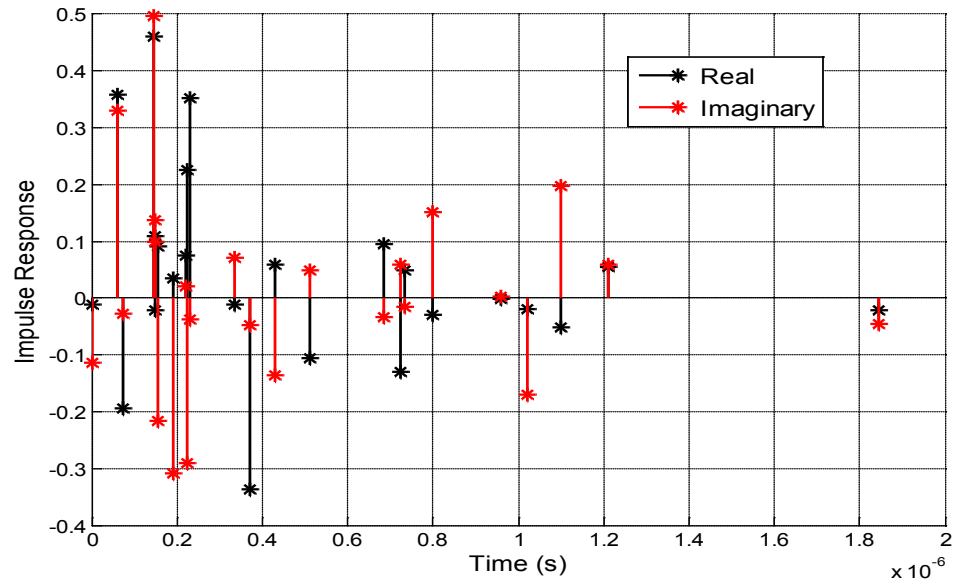


Figure 3.8: Channel bandlimiting and resampling.

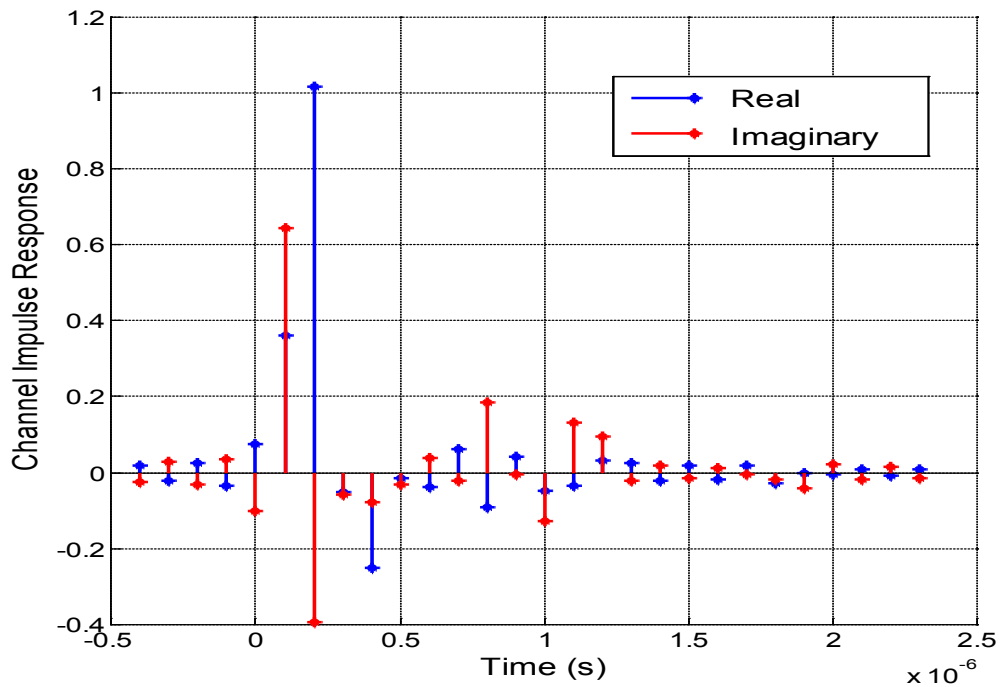
Figure 3.9 shows the non-uniform Rayleigh faded multipath channel on top, and the uniformly sampled, and bandlimited channel on the bottom. From the Figure 3.9, it can be deduced that the number of channel multipath as seen after uniform sampling is a function of sampling period.

If the sampling time is much less than the maximum excess delay, the resampled channel will have multiple delayed taps with high gain. Conversely, if the sampling period is much longer compared to the maximum excess delay, the delayed multipath taps will not be significantly large. Channels whose delayed multipath taps are insignificant compared to the centre tap will have no inter-symbol interference and, therefore, will have a flat frequency response. This type of channel is called a Frequency Flat Fade channel. If the delayed taps in a multipath channel are significant compared to the centre tap, the

channel will have a varying frequency response. Such a channel is called a frequency Selective Faded channel, because it affects different frequencies differently.



(a)



(b)

Figure 3.9: Non uniform versus resampled multipath channel.

In Figure 3.10, the maximum excess delay is $2 \cdot 10^{-6}$ s, while the sampling period is 10^{-5} s. As the sampling period is much larger compared to the maximum excess delay, the frequency response, which is the fast Fourier transform of the channel for 128 frequency bins, has very minimal ripples, which are present due to insignificant but non zero delayed channel taps. In Figure 3.11, the maximum excess delay is the same as before, but the sampling period has been reduced to 10^{-8} s. This choice of a very low sampling period causes a large number of multipath taps with significant gain. This translates to a frequency selective channel.

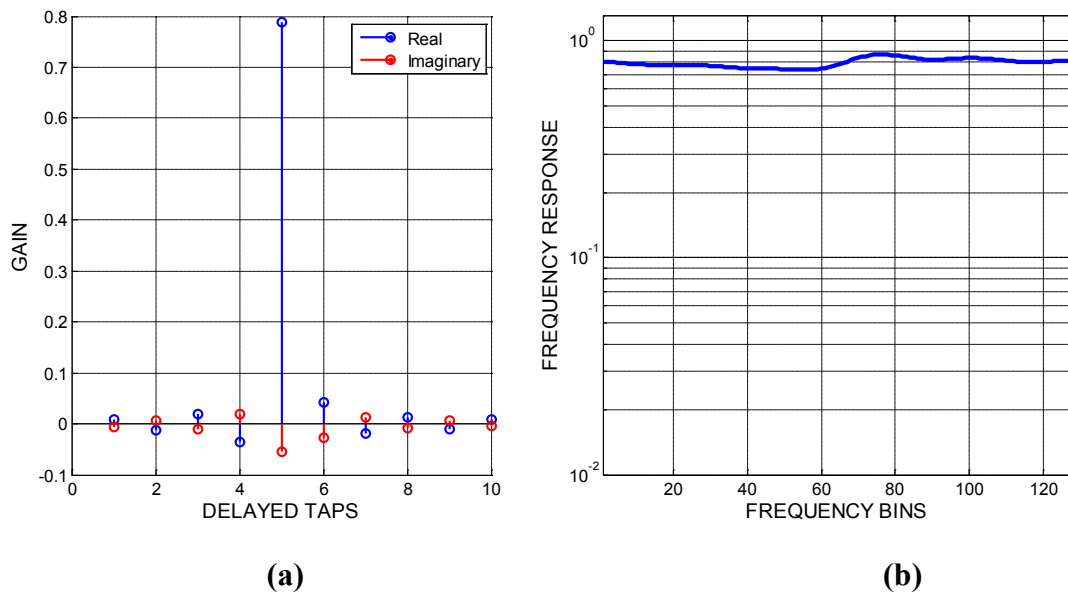


Figure 3.10: Frequency-flat channel frequency response, with time domain (a) and frequency domain (b) representation.

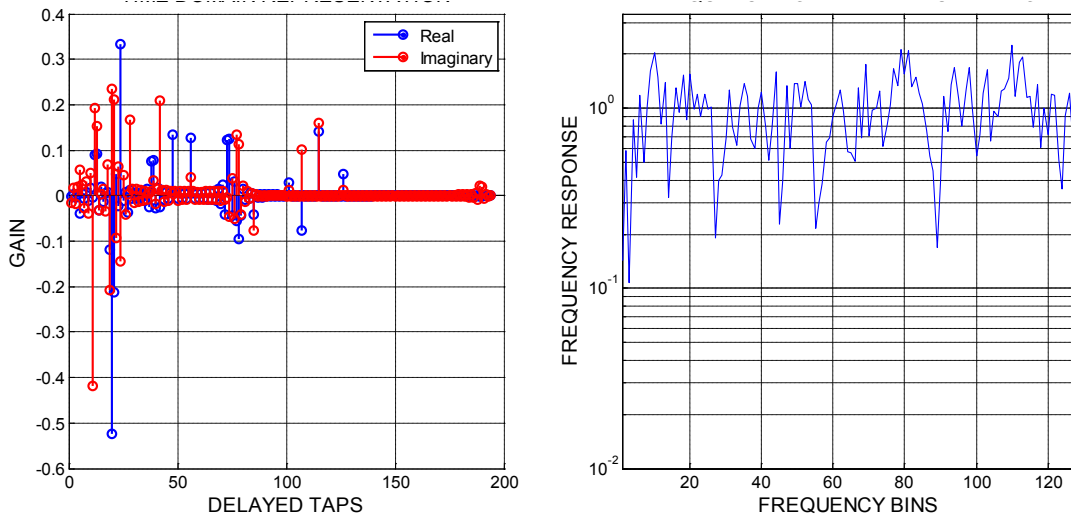


Figure 3.11: Frequency selective channel frequency response, with time domain (a) and frequency domain (b) representation..

3.4 DOPPLER SHIFT

The multipath model described above produces a channel at a given time instant. It does not, however, give a relationship between channel instants that are separated in time. For example, a snapshot of the channel at time ' t ' and another at time ' $t + \Delta t$ ' are separated by time ' Δt '. The relationship between the two channel instants is given by Doppler shift.

Doppler shift is caused due to relative motion between the transmitter and the receiver. The relative motion between the transmitter and the receiver causes the transmitted signal's bandwidth to expand by a certain amount, f_d , which is given as

$$f_d = \left(\frac{v}{c}\right) * f_c. \quad (3.2)$$

Here, v is the relative velocity in ms^{-1} , c is the speed of light in ms^{-1} and f_c is the center frequency. This variation in frequency is called Doppler Effect and the shift in frequency, f_d , is called Doppler shift. Due to this shift in frequency, the transmitted signal's frequency response is expanded. This expansion in the frequency domain manifests itself as more variations in the time domain. With no Doppler shift, the channel will remain constant over time. But with Doppler shift, the different channel instants will be correlated over time. In the channel model given in the EMD [3], it is assumed that the taps in any given channel instant are independent of each other, but are correlated across different channel instants across time. Therefore, each tap's gain in a given channel instant is independent of the rest of the taps' gains, but over multiple channel instants that particular tap's gain will be constant if the Doppler shift is zero, or will be correlated for non zero Doppler shift.

Doppler shift is described best in terms of its power spectral density (PSD), which is the Fourier transform of the correlation function of each tap. The IEEE 802.16m EMD [3] describes the PSD used for the standard as a bell shaped spectrum, given as

$$S(f) = \begin{cases} 1 - 1.72f_o^2 + 0.785f_o^4, & |f_o| \leq 1 \\ 0, & |f_o| > 1 \end{cases}; \text{where } f_o = \frac{f}{f_d}, \quad (3.3)$$

where f is the frequency shift from the carrier frequency, and f_d is the doppler shift. In the channel model used, each tap is composed of a number of rays. These rays have approximately equal angles of departure (AoDs), angles of arrival (AoAs) and delays, and therefore can be put together as one tap, assuming the receiver is in the far field of the transmitter. If the total number of rays in a given cluster is taken to be $N_c + N_s$, where

subscript ‘c’ stands for coherent rays, and subscript ‘s’ stands for the variable rays that vary according to the Doppler PSD $S(f)$, given above. The process of simulating the Doppler Effect is rather time consuming. And because the rays that make up a cluster can be taken as one single tap [3], each tap can have the Jakes spectrum with similar results. Jakes doppler PSD is given as

$$S(f) = \begin{cases} \frac{1}{2\pi f_d \sqrt{1 - \left(\frac{f}{f_d}\right)^2}}, & |f| \leq f_d \\ 0, & |f| > f_d \end{cases} \quad (3.4)$$

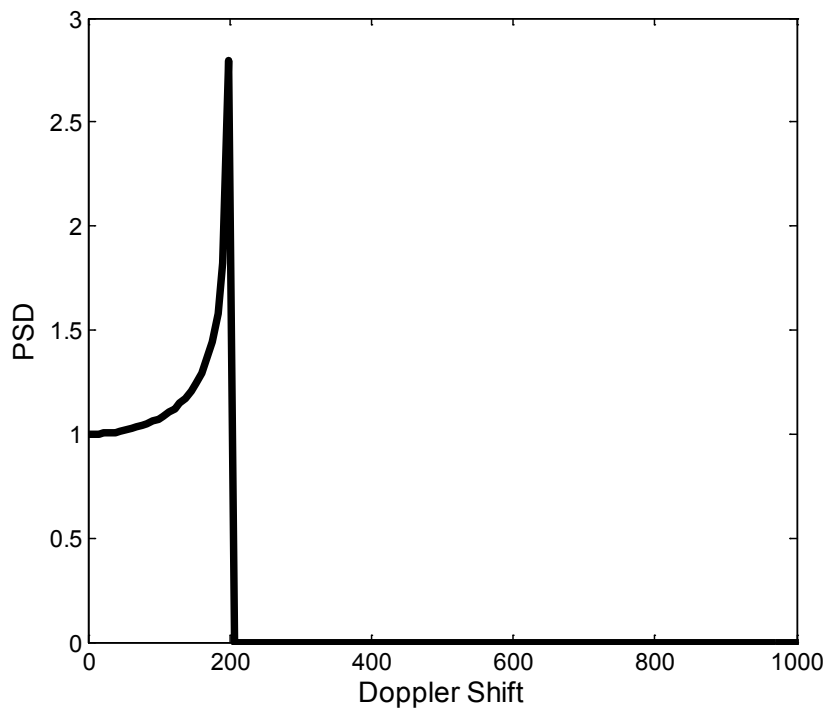


Figure 3.12: Jakes spectrum with Doppler shift of 200 Hz.

Figure 3.13 shows the time domain representation of the Jakes Spectrum.

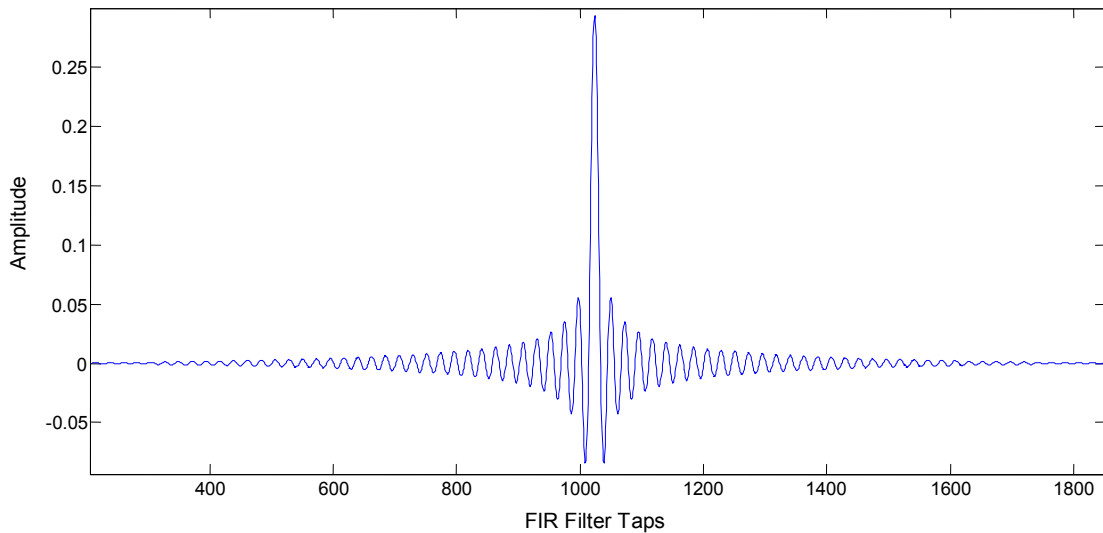


Figure 3.13: Jakes spectrum fir filter for Doppler shift 200 Hz.

The Jakes Spectrum FIR filter takes an IID complex Gaussian random value, and filters it using the FIR filter shown to produce a correlated value, which is then scaled by the tap gain and delayed to produce the required tap value. The filter's initial condition is set to IID complex Gaussian values, and is persistent across all correlated samples. In order to reset the system such that the samples are no longer correlated with the previous values, the filter's initial condition is simply reset to IID complex Gaussian.

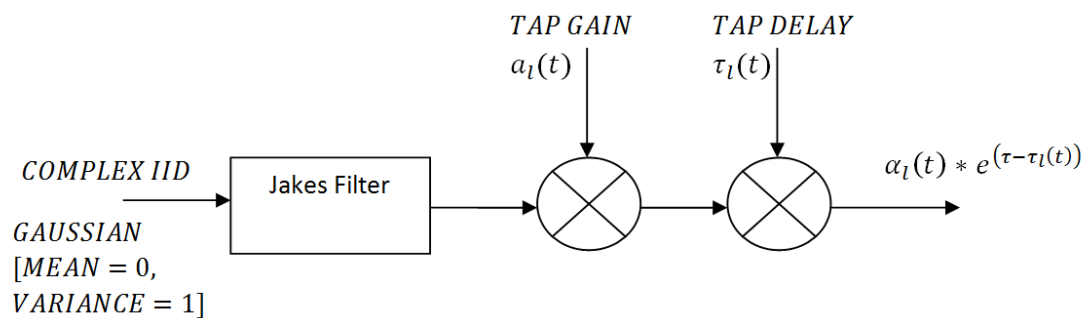


Figure 3.14: Schematic diagram for non-uniform tap generation with Jakes filter.

Figure 3.15 shows how the channel gain varies over time due to doppler shift. This phenomenon is called Time Selectivity.

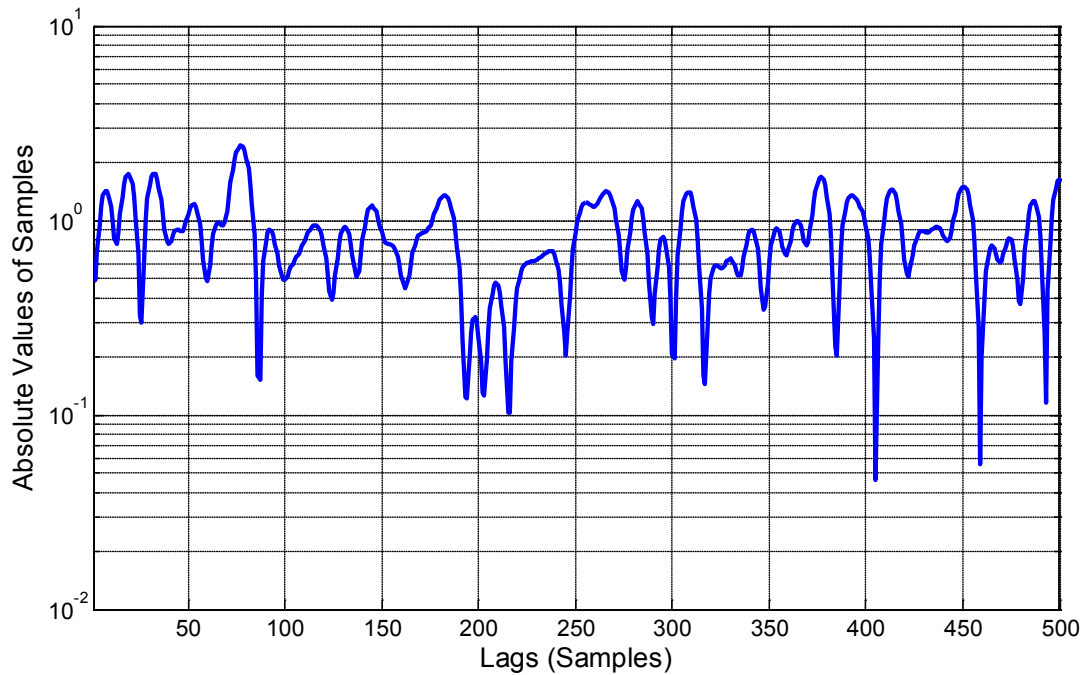


Figure 3.15: Correlated sample values.

The autocorrelation function is of the following form.

$$\rho(\Delta t) = J_0(2\pi f_d \Delta t). \quad (3.5)$$

Here, Δt is the time lag between correlated time samples and $J_0(\cdot)$ is zero order Bessel function. Figure 3.16 compares the theoretical correlation function with the simulation one. It can be seen that the simulation curve closely follows the theoretical one. Doppler shift is set to $f_d=350$ Hz. In Figure 3.17, it can be seen that the PSD peaks at $351\text{Hz} \approx 350$ Hz. The error is possibly due to the fact that the number of sample values taken was 10,000. Asymptotically, the simulation PSD will peak at 350 Hz.

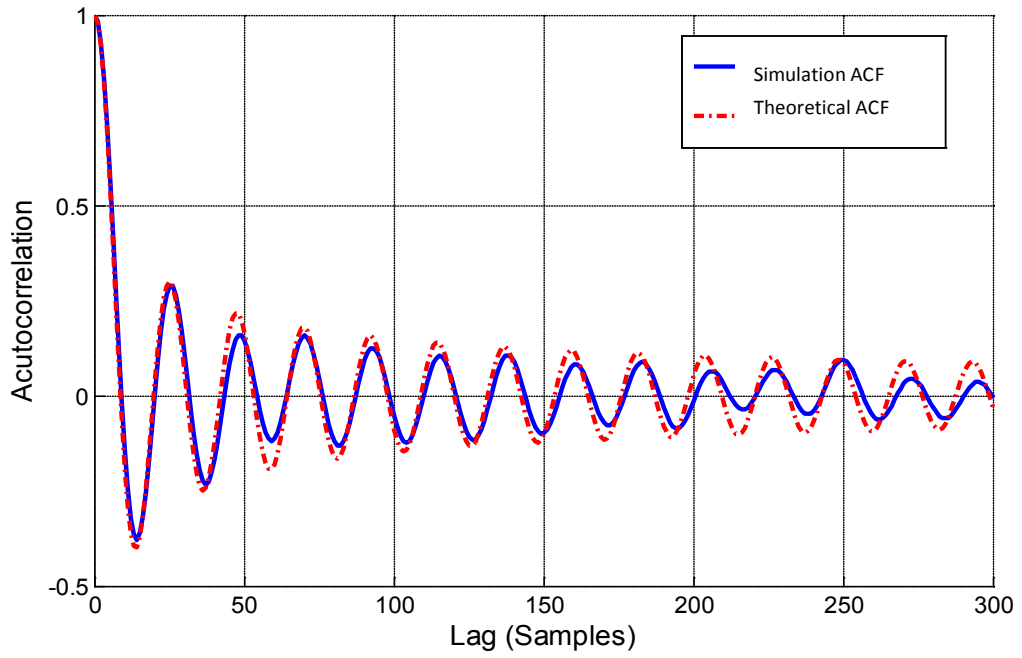


Figure 3.16: Theoretical versus simulation autocorrelation of time samples for a Doppler shift of 350 Hz.

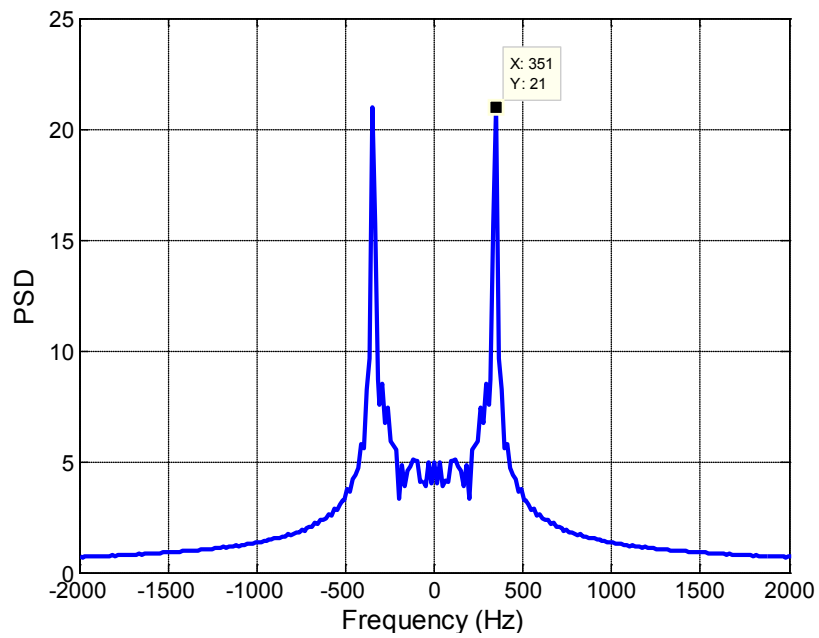


Figure 3.17: Simulation PSD with Doppler shift of 350 Hz.

Figure 3.18 shows the channel impulse response. Tau is the delay with respect to the first received tap. Time axis shows different times at which channel impulse response is measured. The channel taps are correlated in time due to doppler shift, as can be seen from the figure below. The multipath nature of the channel causes correlation in the frequency domain. In Figure 3.19 the channel frequency response is plotted against time and frequency.

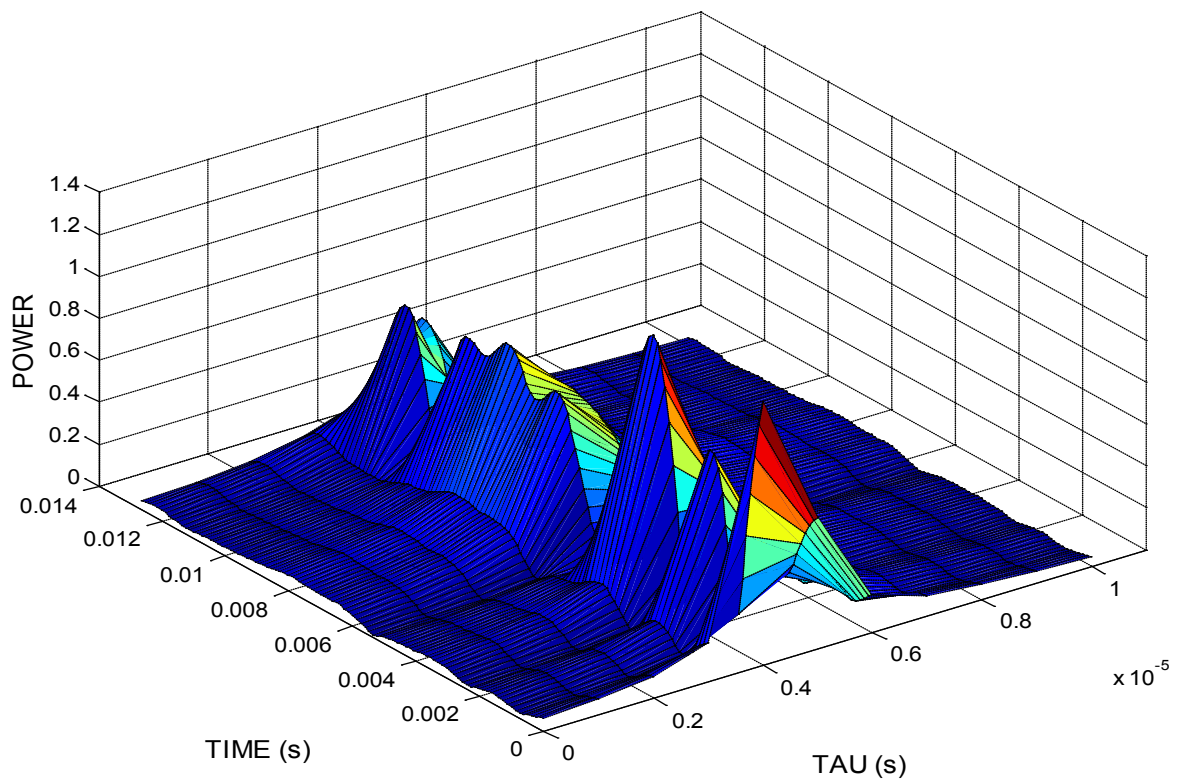


Figure 3.18: Non-stationary channel impulse response over time.

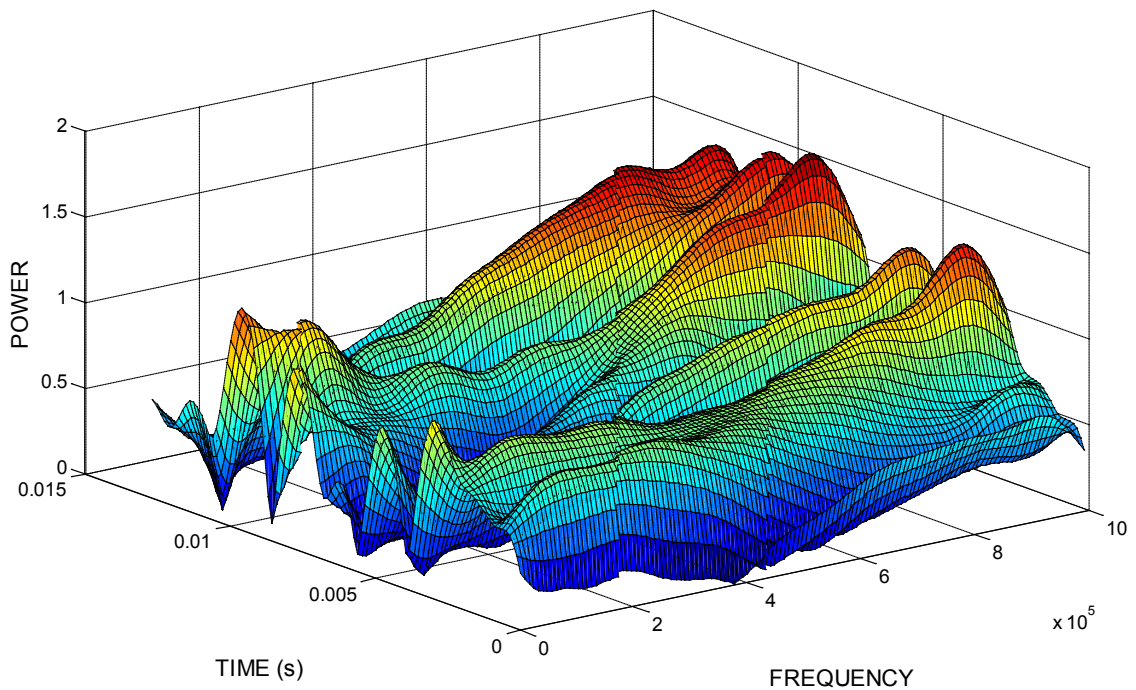


Figure 3.19: Non-stationary channel frequency response over time.

3.5 SPATIAL CORRELATION

Spatial correlation is the correlation between antennas at each end of the communication channel. This spatial correlation is a function of the AoA, AoD and angular spread (AS) of each tap (cluster). The angular spread refers to the variation in the AoAs and AoDs of each ray within a particular tap. Recall that in the channel model defined till now, each multipath tap (cluster) is assumed to be a combination of rays which have similar power, AoAs and AoDs. Here, a Laplacian power angular distribution is assumed [3]. Hence, using the values of per tap AS, mean AoA and mean AoD, the correlation coefficient

between any two antennas at the BS and the MS, respectively, can be calculated. The antennas are assumed to be omnidirectional.

In Figure 3.20, a visual representation of all the factors that affect spatial correlation is given. Each cluster is assumed to be composed of multiple rays, and each cluster has a mean AoA, AoD and angular offset $\Delta_{k,BS}$ for each of the rays or subpaths that make up that cluster. The correlation coefficients are given in (3.6) and (3.7).

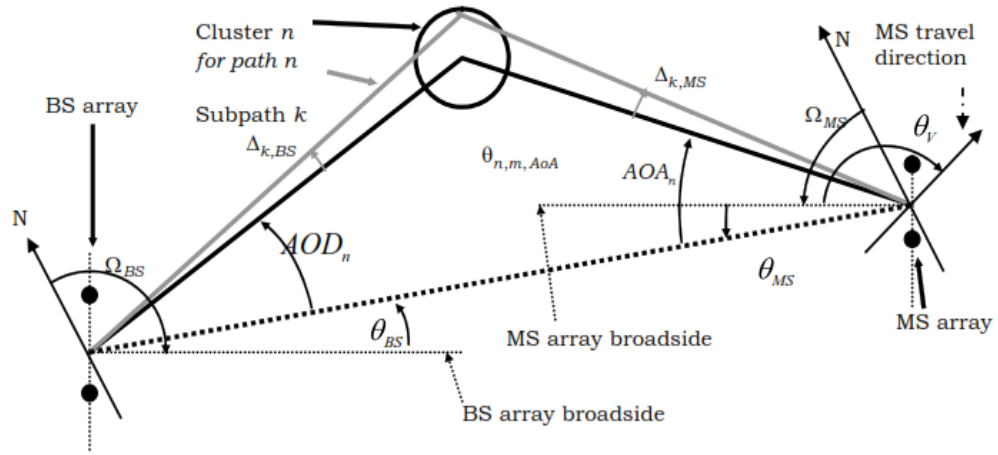


Figure 3.20: Channel correlation due to BS and MS antenna array position.

$$r_{n,BS}(p, q) = \int_{-\infty}^{\infty} f(\alpha) \exp\left\{j \frac{2\pi d_{BS}}{\lambda} (p - q) \sin(\theta_{BS} + AOD_n + \alpha)\right\} d\alpha \quad (3.6)$$

$$r_{n,MS}(p, q) = \int_{-\infty}^{\infty} f(\beta) \exp\left\{j \frac{2\pi d_{MS}}{\lambda} (p - q) \sin(\theta_{MS} + AOA_n + \beta)\right\} d\beta \quad (3.7)$$

Here, α is the angular offset around the mean AoD, β is the angular offset around the mean AoA, d_{BS}, d_{MS} are the antenna spacing at the BS and MS, respectively, λ is the wavelength, $r_n(p, q)$ is the correlation coefficient between the antennas p and q and $f(*)$ is the angular offset PDF.

The angular offset PDFs are given as

$$f(\alpha) = \frac{1}{AS_{BS,Path}\sqrt{2}} \exp\left[-\frac{\sqrt{2}|\alpha|}{AS_{BS,Path}}\right] \quad (3.8)$$

$$f(\beta) = \frac{1}{AS_{MS,Path}\sqrt{2}} \exp\left[-\frac{\sqrt{2}|\beta|}{AS_{MS,Path}}\right] \quad (3.9)$$

In order to reduce complexity, each tap is assumed to be composed of just 20 rays, each with a random angular offset value. This approximation reduces the integration in the correlation equations into a summation. The integration in the spatial correlation equation reduces to a simple summation.

$$r_{n,BS}(p, q) = \frac{1}{20} \sum_{k=1}^{20} \exp\left\{\frac{j2\pi d_{BS}}{\lambda} (p - q) \sin(AoD_n + \alpha)\right\} \quad (3.10)$$

$$r_{n,MS}(p, q) = \frac{1}{20} \sum_{k=1}^{20} \exp\left\{\frac{j2\pi d_{MS}}{\lambda} (p - q) \sin(AoA_n + \alpha)\right\} \quad (3.11)$$

The angular offset for the k^{th} path is given by

$$\alpha = \Delta_k * AS_{BS,Path} \quad (3.12)$$

$$\beta = \Delta_k * AS_{MS,Path} \quad (3.13)$$

Δ_k is defined in the table 3.4.

Table 3.4: Spatial correlation parameters.

SUB-PATH k	Δ_k
1,2	± 0.0447
3,4	± 0.1413
5,6	± 0.2492
7,8	± 0.3715
9,10	± 0.5129
11,12	± 0.6797
13,14	± 0.8844
15,16	± 1.1481
17,18	± 1.5195
19,20	± 2.1551

3.6 SIMULATION METHODOLOGY

The urban macrocell channel model with a 2x2 MIMO, 128 subcarrier OFDM system configuration is used for system evaluation. The input symbol rate is taken to be 10^6 symbols/sec, with the sampling rate equal to 1 MHz. The downlink scenario is assumed, where the transmitter is the base station, and the receiver is the mobile station. Spatial correlation is assumed, with transmitter antenna spacing taken as 4 times the center frequency's wavelength, and receiver antenna spacing is taken to be 0.5 times the center

frequency's wavelength. The receiver is assumed to use zero forcing equalization in order to equalize the effect of the channel.

If H is a $M_R \times N_T$ channel matrix, where M_R is the number of receiver antennas N_T is the number of transmit antennas, then the system model is assumed to be as given in (3.14).

$$y = Hx + n \quad (3.14)$$

At the receiver, the received signal, y , is multiplied with W in order to retrieve the original signal, x . W is defined in (3.15). W is the pseudo-inverse of H .

$$W = (H^H H)^{-1} H^H \quad (3.15)$$

Here, $[*]^H$ is Hermitian Function.

CHAPTER 4

HIERARCHICAL PRECODING

In this chapter, the proposed algorithm, hierarchical precoding (HP), is presented. The precoding techniques discussed in chapter 1 allow for capacity maximization (using WF) or SMSE minimization (using SMSE precoding). These precoding techniques, however, leave out eigen modes that do not satisfy the criterion set by the precoding technique, that is, the cutoff level. In a MU scenario, this translates to a reduction in the number of users that can be allowed to transmit using MU precoding. HP reduces the number of unused eigen modes, both for SU and MU cases, while keeping the BER performance deterioration within usable limits. In the following section, HP is introduced, and its BER and throughput performance is compared with WF.

4.1 HIERARCHICAL PRECODING

This thesis proposes a precoding technique called Hierarchical Precoding (HP), and compares its performance with precoding techniques mentioned in Chapter 1. The results show a significant increase in throughput performance, compared to the WF and SMSE precoding algorithms.

Hierarchical Precoding, as the name suggests, implements different precoding techniques in an hierarchical manner. Figure 1.10 (Section 1.2.3) shows BER Versus SNR curve for SMSE minimization precoding. It can be seen that SMSE minimization precoding performs better at low SNR values. Thus, HP proposes using SMSE minimization for eigen modes with low eigen subchannel gain to noise ratio (EGNR), while applying waterfilling to high EGNR eigen modes. Power allocation can be done according to some criterion. In Section 4.1.1, two such methods are described.

4.1.1 FIXED RATIO POWER ALLOCATION

The simplest way to perform HP is to preallocate fixed amounts of power for WF and SMSE, respectively, and performing power allocation iteratively, starting with waterfilling, and then applying SMSE.

As stated before, HP is an iterative implementation of WF and SMSE precoding. In Fixed Ratio power allocation (FR-HP), the amount of power allocated for waterfilling and SMSE is fixed. Let this ratio be R . this means that the, if the total power is P_T , power

allocated for WF is $P_T R$, while the power allocated for SMSE will be $P_T(1-R)$. Precoding is done based on the eigen mode gain values of the channel matrix multiplied by its Hermitian, or the square of the channel matrix's singular values. The eigen mode gain is defined as the variance of the eigen mode gains. As the channel matrix is defined using random values generated using the Gaussian PDF with zero mean and unit variance, the eigen mode gains will also have an asymptotic unit variance. In FR-HP, the eigen modes are divided in the same ratio as the total power. For instance, if the total number of eigen modes is M , then the number of modes that will be use WF will be MR , and the number eigen modes assigned for SMSE minimization would be $M(1-R)$.

Figure 4.1 shows the FR-HP algorithm in the form of a flowchart. In Figure 4.2, FR-HP is visually represented. R is taken to be 0.5. The communication system is a 2X2 MIMO OFDM system with 32 subcarriers. The channel model is the urban macrocell channel model, as described in Chapter 3. It can be seen that the eigen subchannels with low noise to gain ratio (NGR) have been allocated power using waterfilling, while the ones with a high NGR are assigned power using SMSE. The average SNR is taken to be 5dB.

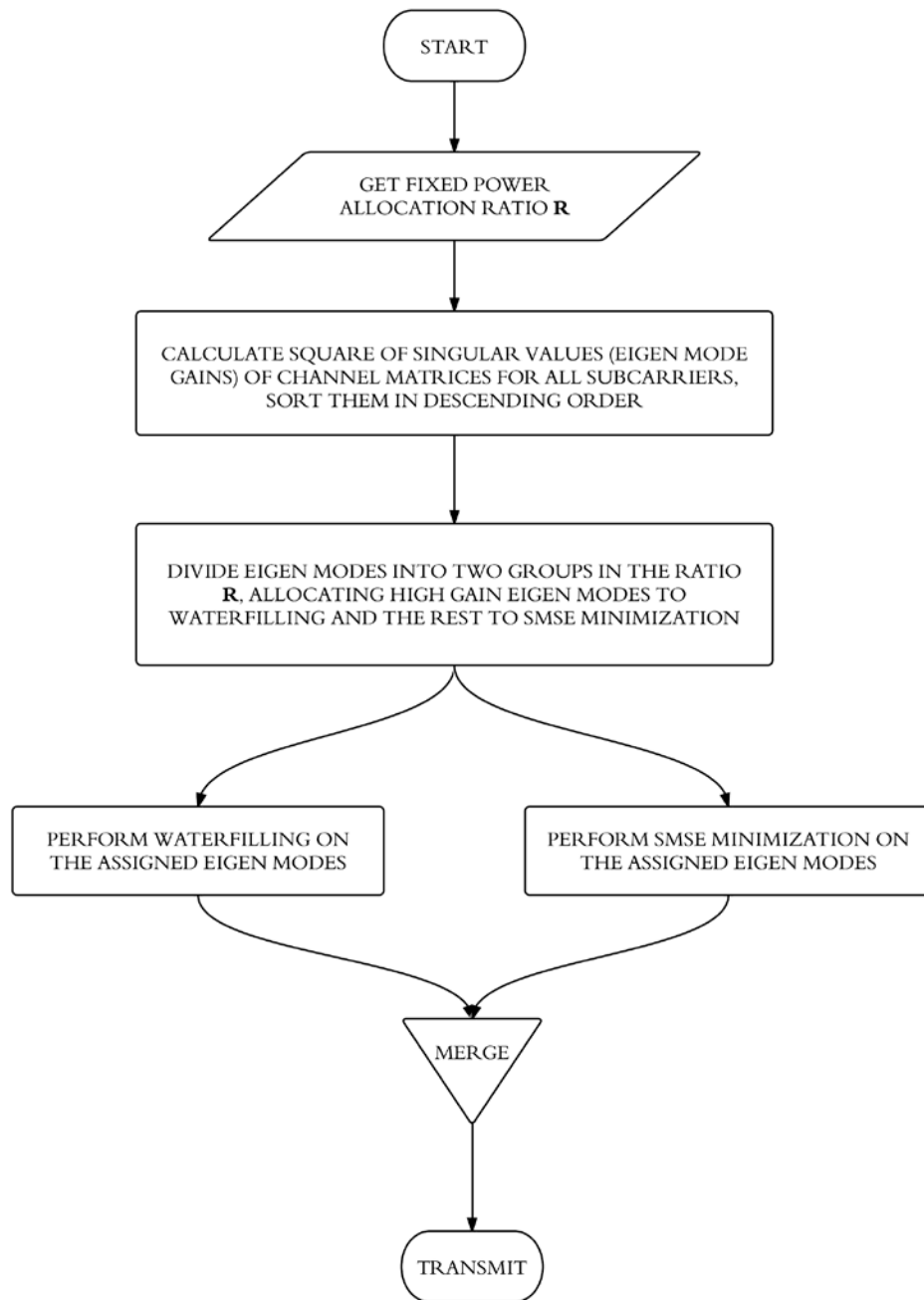


Figure 4.1: Fixed ratio - hierarchical precoding algorithm flowchart.

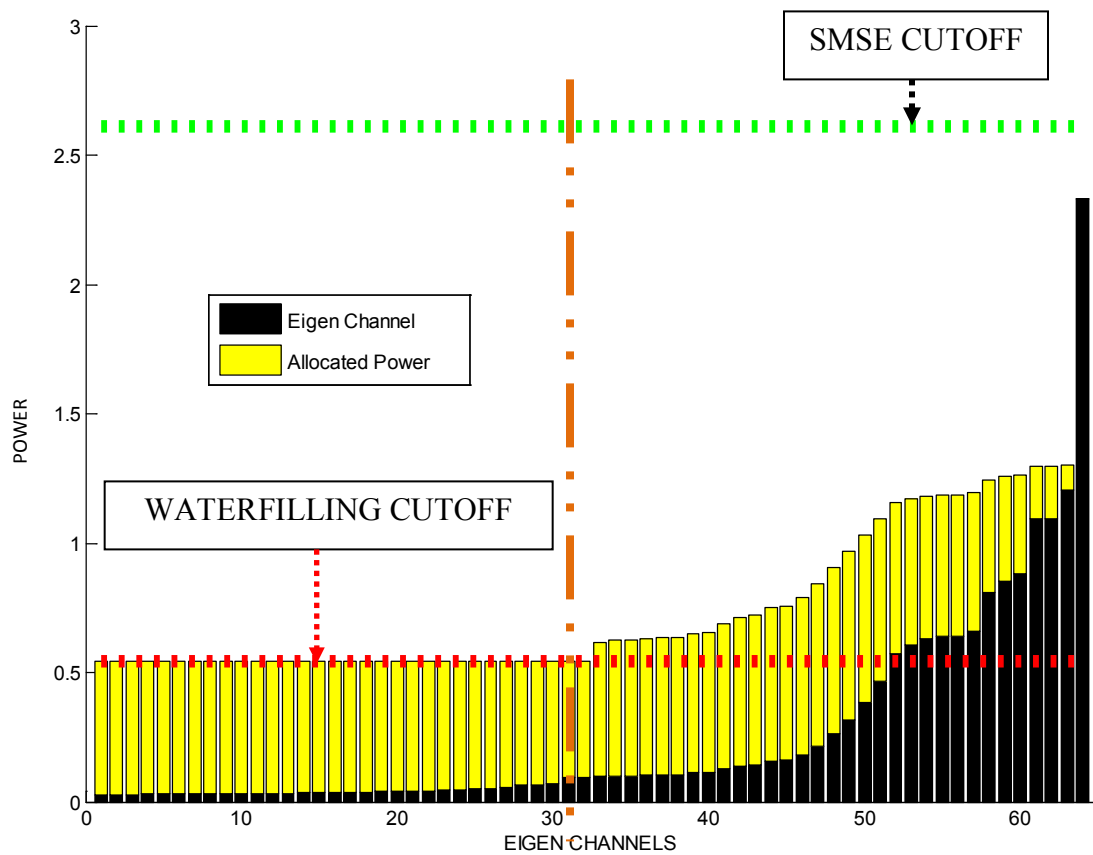


Figure 4.2: Hierarchical precoding with $R = 0.5$ for a 2×2 MIMO, 32 OFDM subcarrier system at 5dB

SIMULATION RESULTS

Figure 4.3 shows BER performance for a 2×2 MIMO, 128 subcarrier OFDM configuration. It can be seen that FR-HP performance is slightly degraded when compared to WF BER performance. At low SNR of 10dB, FR-HP with $R=0.5$ (FR-HP_{0.5}) performs better at BER 2.5×10^{-2} , while FR-HP with $R=0.8$ (FR-HP_{0.8}) has a BER of 3×10^{-2} . WF, on the other hand, has a BER of 2×10^{-2} . As the SNR increases, the BER performance of FR-HP with $R=0.8$ converges with the WF BER performance. With $R=0.5$, FR-HP causes a slight deterioration in performance at high SNR. At 30dB, WF

and FR-HP_{0.8} have a BER of 2.5×10^{-4} , while FR-HP_{0.5} has a BER of 4×10^{-4} . The reason for this performance degradation is due to the fact that SMSE minimization performs best at low SNRs (see Figure 1.9). At high SNR, the SMSE portion of FR-HP is causing degraded performance. On the other hand, FR-HP_{0.8} assigns just 20% of the total power to SMSE, therefore allowing SMSE minimization to be performed on eigen modes with the lowest SNR.

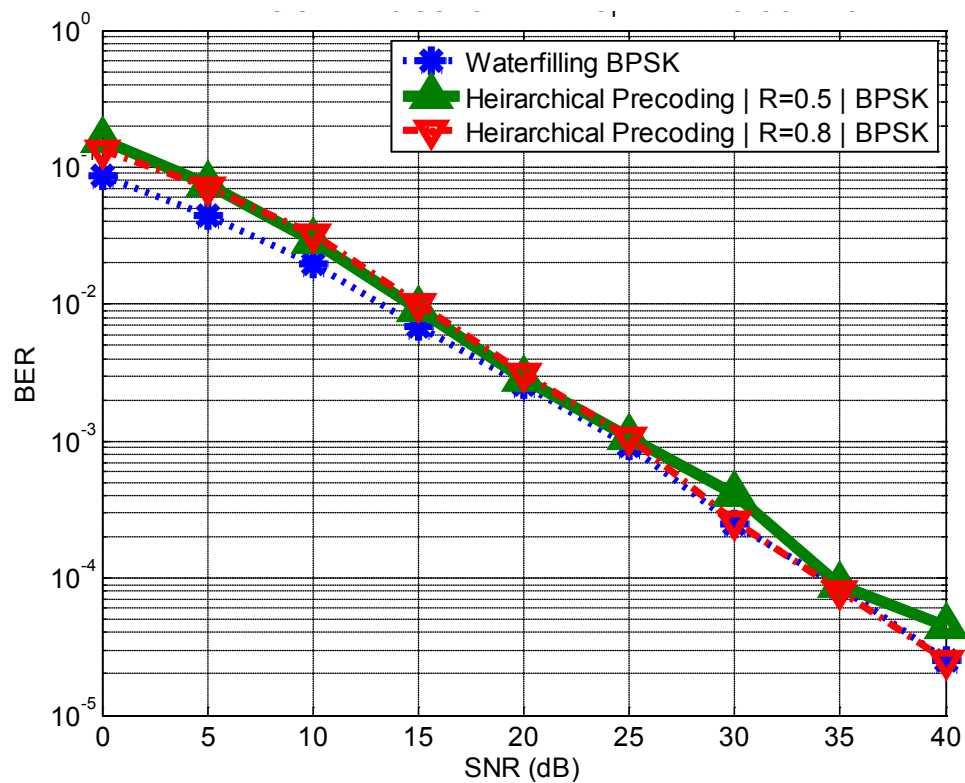


Figure 4.3: BER versus SNR comparison for a 2x2 MIMO, 128 subcarrier OFDM system with IEEE 802.16m urban macrocell channel model for BPSK constellation.

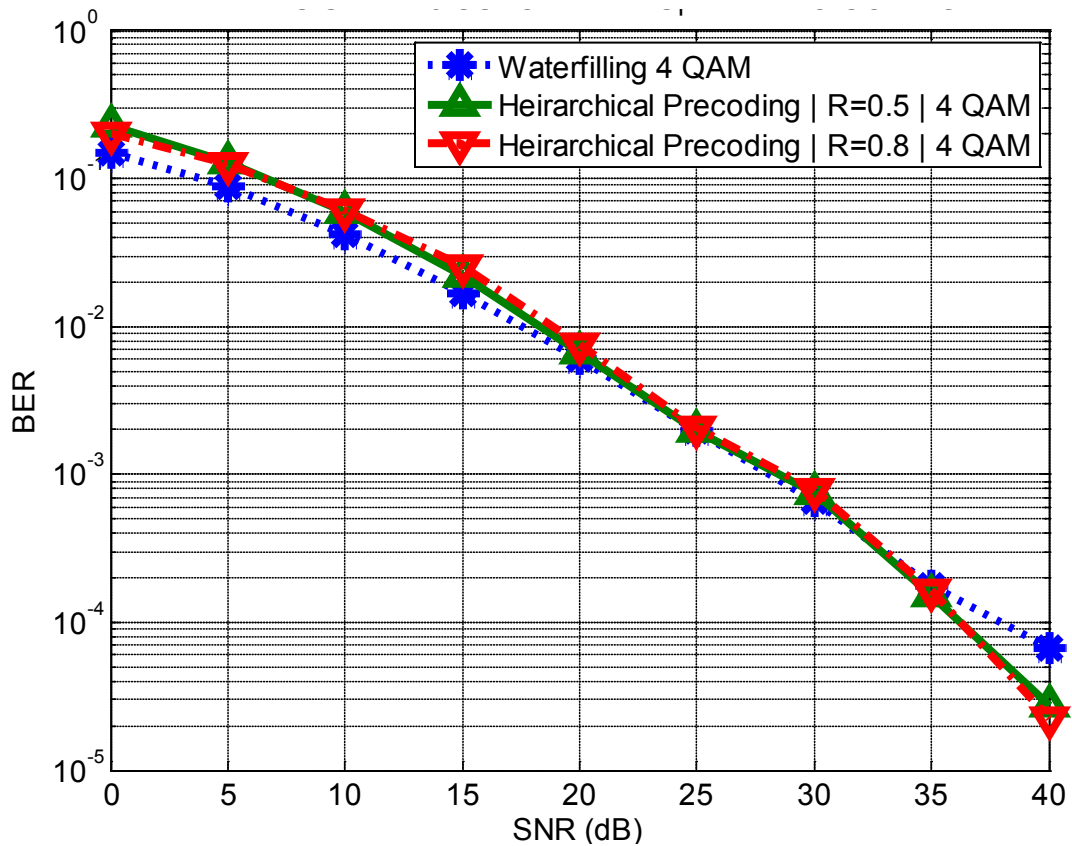


Figure 4.4: BER versus SNR comparison for a 2x2 MIMO, 128 subcarrier OFDM system with IEEE 802.16m urban macrocell channel model for 4 QAM constellation.

Figure 4.4 shows BER performance for a 2x2 MIMO, 128 subcarrier OFDM system configuration with 4-QAM constellation. As seen in Figure 4.3, FR-HP performance is worse than WF BER performance at low SNRs. At high SNRs of 20-35dB, the performance of WF and FR-HP are indistinguishable. At 40dB, FR-HP performs better than WF. For a BER of 10^{-4} , FR-HP's performance is the same as WF at an SNR lower by 2 dB than what is required for the WF algorithm.

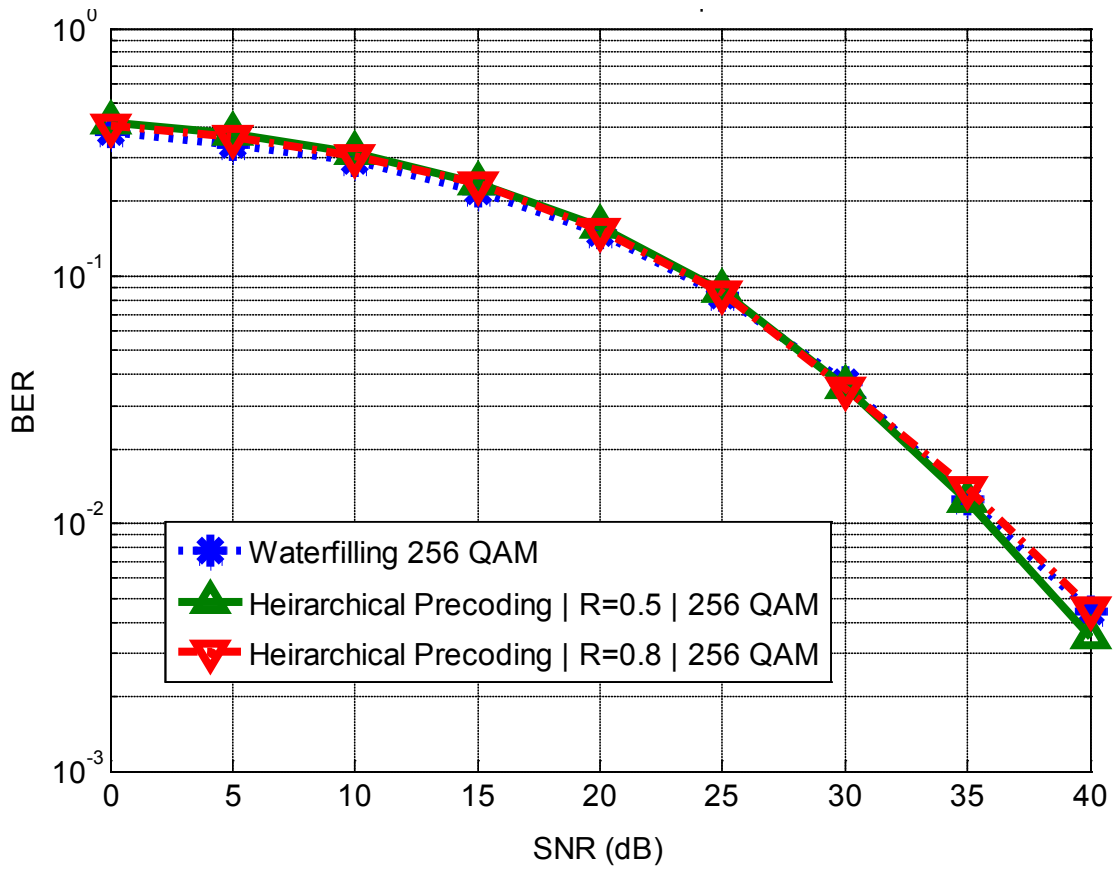


Figure 4.5: BER versus SNR comparison for a 2x2 MIMO, 128 subcarrier OFDM system with IEEE 802.16m urban macrocell channel model for 256 QAM constellation.

Figure 4.5 shows BER performance for a 2x2 MIMO, 128 subcarrier OFDM system configuration with 256-QAM constellation used for data transmission. Although the BER performance is identical for both FR-HP and WF, it can still be seen that WF is marginally better at low SNRs, followed by FR-HP_{0.8} and finally FR-HP_{0.5}.

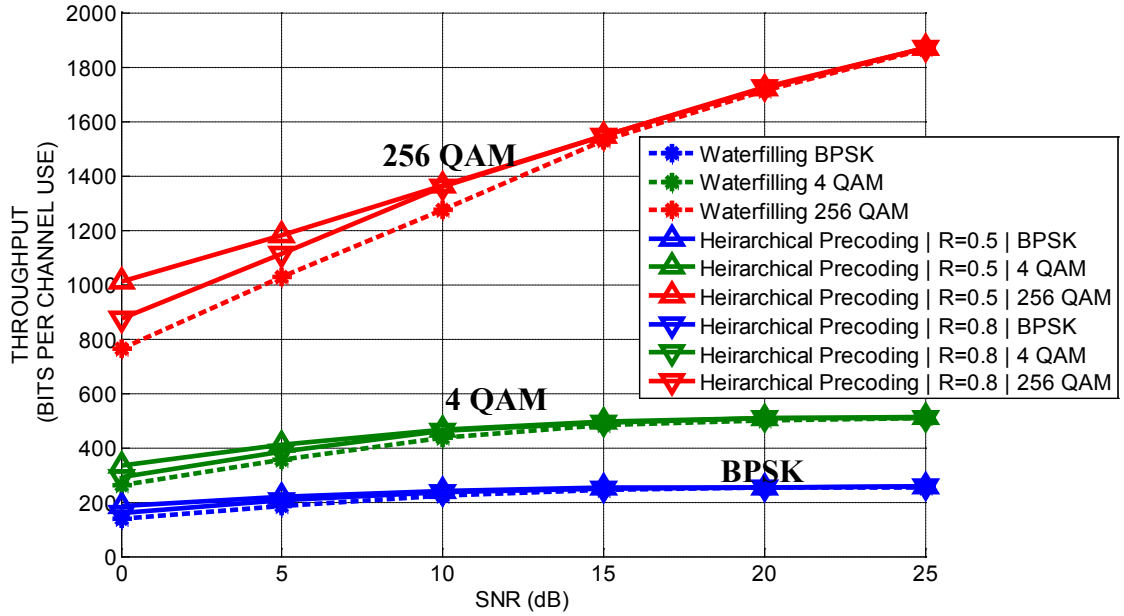


Figure 4.6: Average throughput per OFDM symbol versus SNR for a 2x2 MIMO, 128 subcarrier OFDM system with IEEE 802.16m urban macrocell channel model.

Figure 4.6 shows the throughput versus SNR plot for FR-HP_{0.5}, FR-HP_{0.8} and WF. It can be seen from the plots that at high SNRs, WF and FR-HP converge. At low SNRs, FR-HP performs significantly better than WF. The plots show that FR-HP_{0.5} performs the best, followed by FR-HP_{0.8}, and WF. The throughput gain can be defined in (4.1).

$$\text{Throughput Gain} = \frac{(\text{Throughput}_{FR-HP} - \text{Throughput}_{WF})}{\text{Throughput}_{WF}} * 100 \quad (4.1)$$

Using (4.1), the throughput gain is calculated and plotted in Figure 4.7. It can be seen that FR-HP_{0.5} performs best at 35% gain, followed by FR-HP_{0.8}.

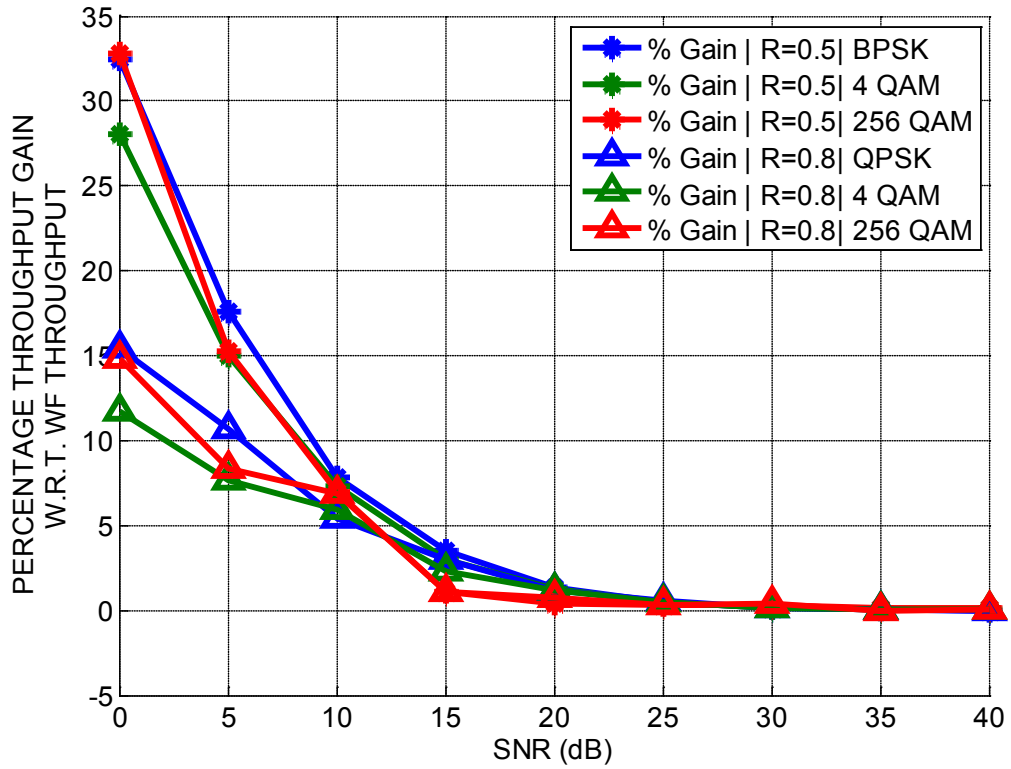


Figure 4.7: Throughput gain versus SNR for a 2x2 MIMO, 128 subcarrier OFDM system with IEEE 802.16m urban macrocell channel model.

4.1.2 CAPACITY BASED POWER ALLOCATION

Capacity based power allocation (C-HP) is an adaptive method of performing hierarchical power allocation. The ratio R is not fixed here, and changes adaptively according to changes in the channel. The capacity of the i^{th} eigen mode, C_i , is given in (4.2).

$$C_i = \log_2 \left(1 + \frac{P_i \lambda_i^2}{\sigma^2} \right) \quad (4.2)$$

For definition of each variable, refer to (1.5) (Section 1.2.3). P_i is the power allocated to the i^{th} eigen mode.

In C-HP, the eigen modes are differentiated based on their respective capacities. P_i is calculated using WF algorithm. Next, the capacity for each eigen mode is calculated using (4.2). Now, a threshold cutoff capacity value, C , is chosen. All eigen modes whose capacity is less than C are combined with the rest of the unallocated eigen modes, which were not assigned any power with WF. The power assigned to these separated eigen modes is used to perform SMSE over the remaining eigen modes.

C-HP can be understood better with the following figures. The capacity threshold, C , is taken to be 2 bits/s/Hz. The communication system is a 2X2 MIMO OFDM system with 32 subcarriers.

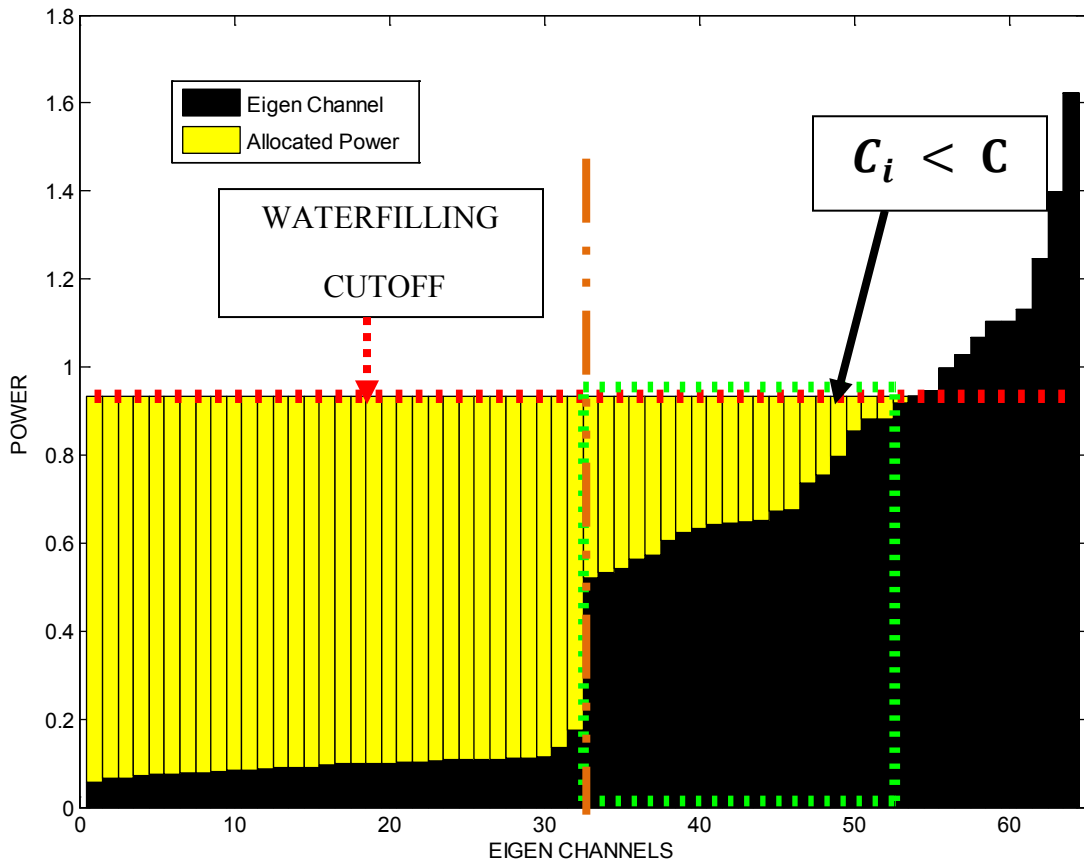


Figure 4.8: C-HP waterfilling solution

In Figure 4.8, the eigen modes marked as $C_i < C$ are subchannels whose capacity is less than the threshold C . The vertical dotted line shows the boundary such that all eigen modes to the right of the line will be precoded using SMSE algorithm. The resulting power allocation is shown in Figure 4.9.

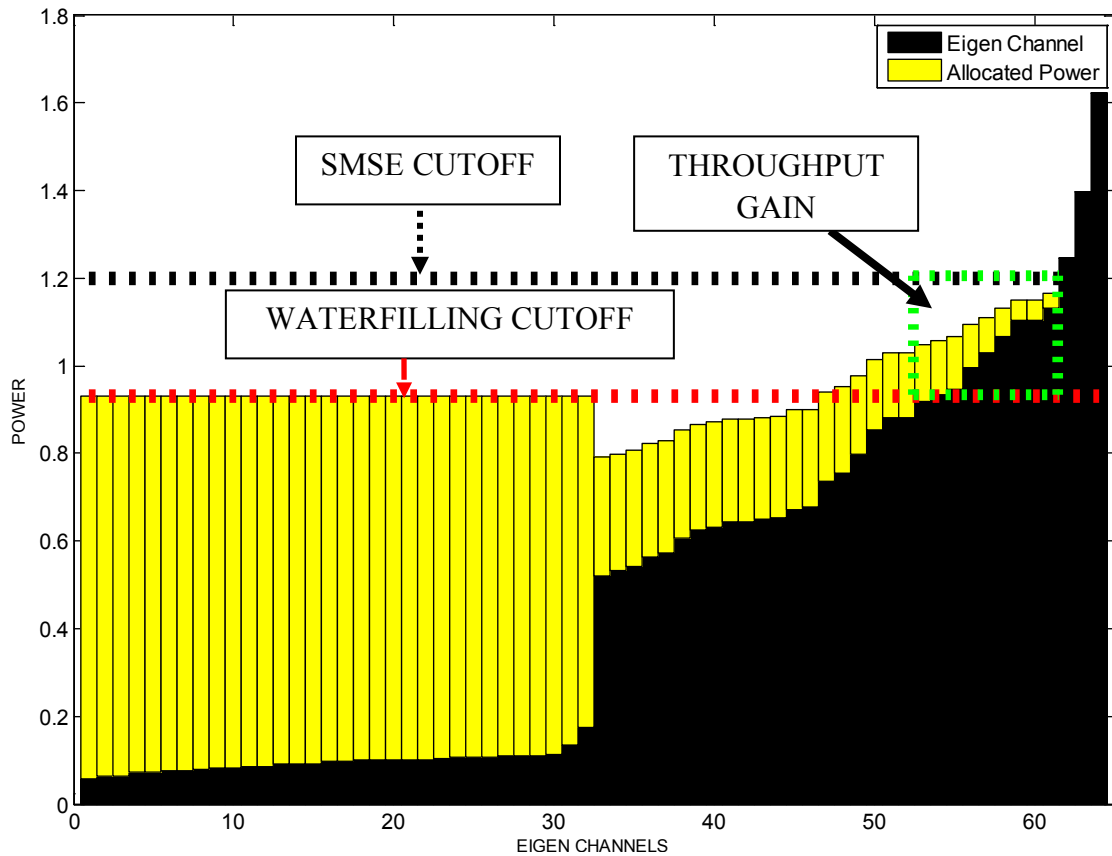


Figure 4.9: Capacity based power allocation - HP

Figure 4.9 shows a visual representation of C-HP. The WF cutoff is calculated considering $R=1$, that is, all the power is allocated for WF. Thus, if just WF was used, the first fifty two eigen modes would have been able to transmit. With C-HP, there is a gain of about ten more eigen modes for transmission, thereby increasing the overall throughput. One might argue that because these excess eigen modes are allocated less power, they will degrade the overall performance. But, as it will be shown later in the results, the performance degradation is marginal, while the throughput performance of a system with large number of OFDM subcarriers and transmit antennas (which in turn mean more

eigen modes), is significantly improved. Figure 4.10 gives the flowchart for the C-HP algorithm.

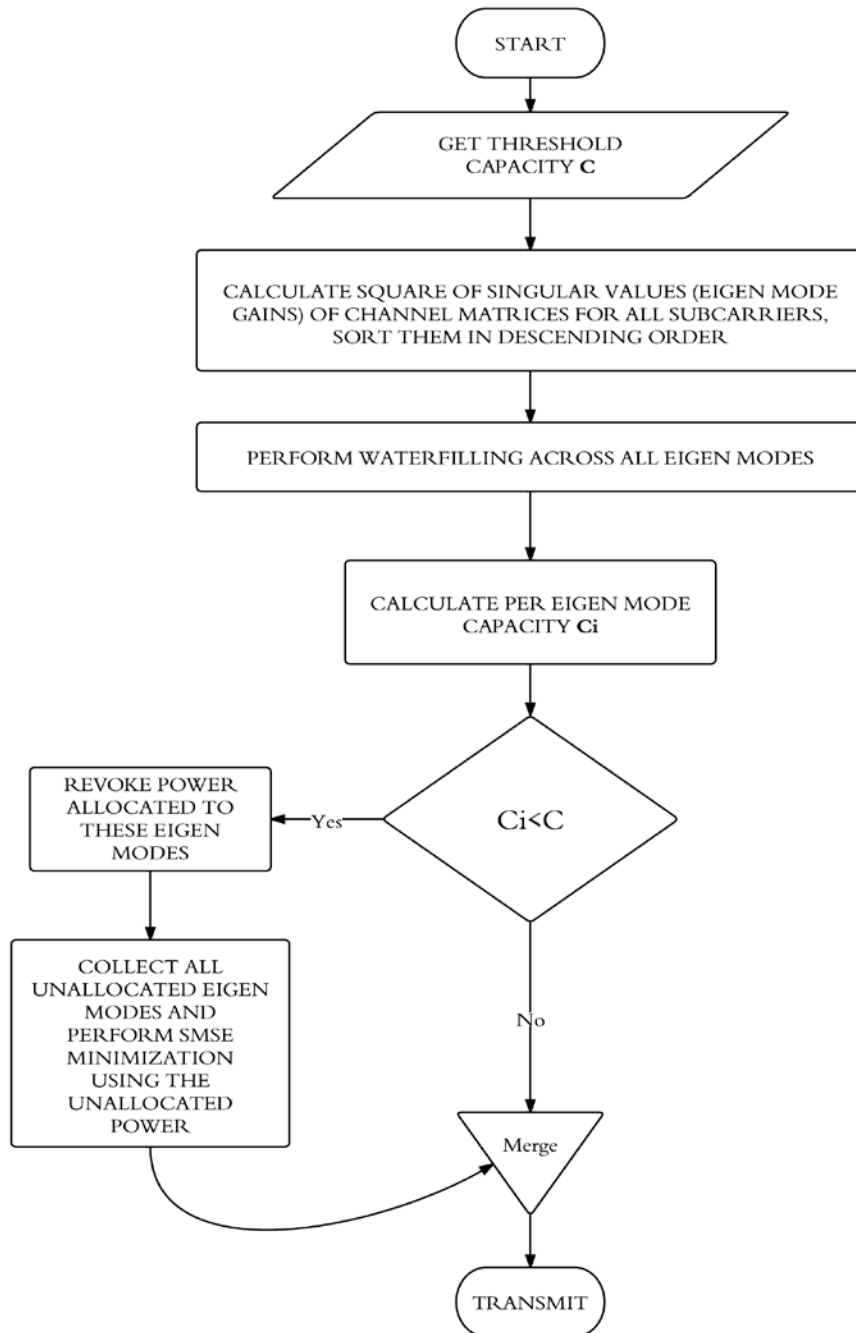


Figure 4.10: Capacity based hierarchical precoding algorithm flowchart.

SIMULATION RESULTS

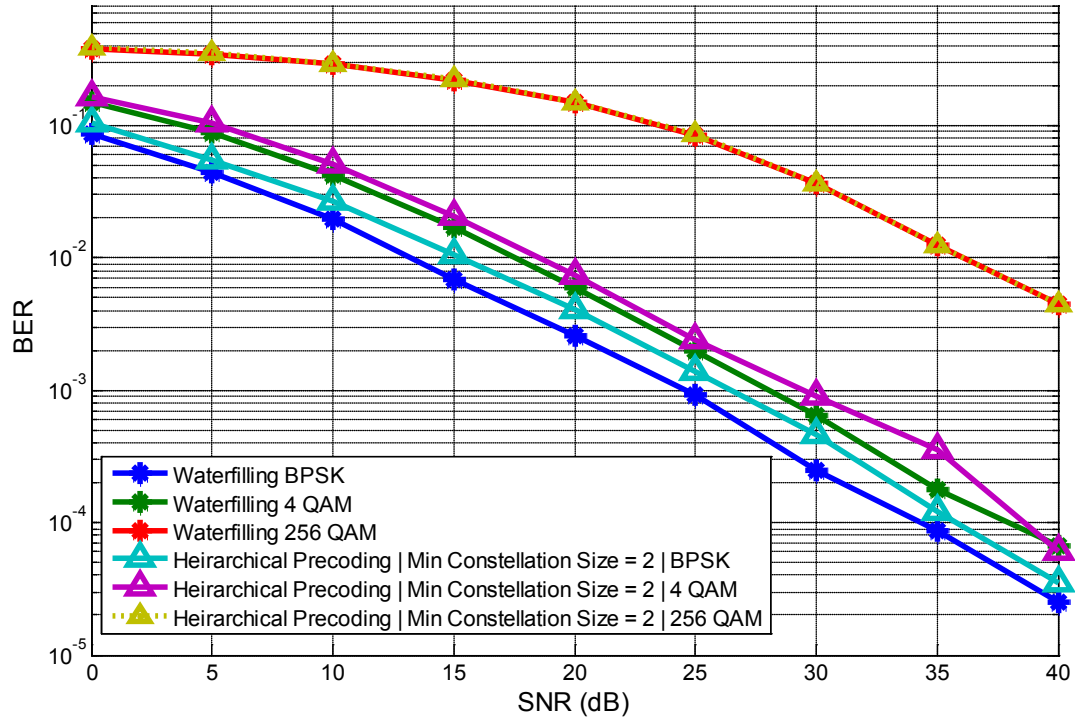


Figure 4.11: BER versus SNR for capacity based hierarchical precoding with cutoff capacity 2 bps/Hz for a 2x2 MIMO, 128 subcarrier OFDM system with IEEE 802.16m urban macrocell channel model.

Figure 4.11 shows BER Versus SNR performance for a 2x2 MIMO, 128 subcarrier OFDM system configuration. The channel model used is the urban macrocell model. C-HP with $C=2$ (C-HP₂) performs worse than WF across all SNRs. For a BER of 10^{-3} , there is a 2dB loss for a BPSK constellation, for 4-QAM, the loss is 1.5dB, while for 256-QAM, the performance is virtually indistinguishable. This implies that as the constellation size increases, WF and C-HP performance tends to converge. Figure 4.12 shows BER Versus SNR performance for C-HP with $C=4$ (C-HP₄). It can be seen that, with 4-QAM, the BER plot diverges from WF BER plot with increase in SNR. On the

other hand, the BER performance for 256-QAM constellation is identical for both WF and C-HP₄.

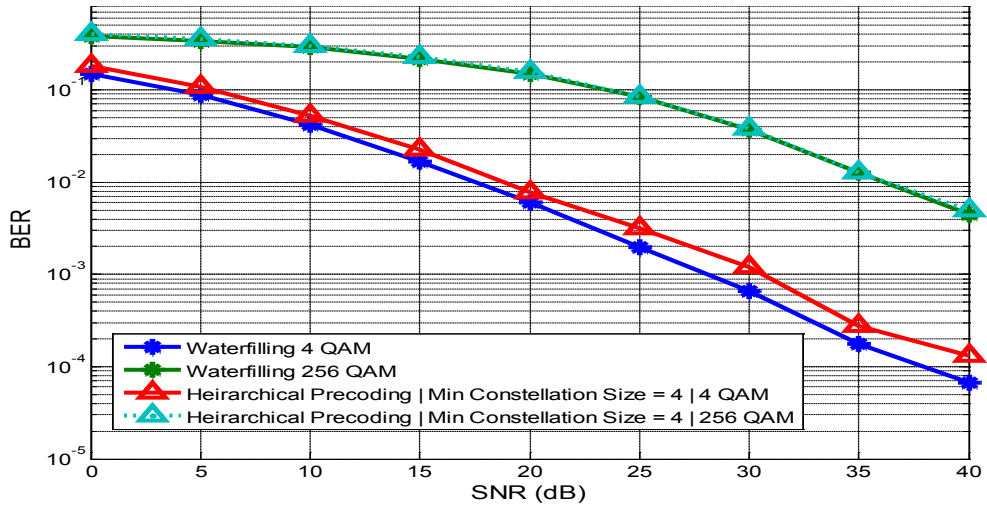


Figure 4.12: BER versus SNR for capacity based hierarchical precoding with cutoff capacity 4 bps/Hz for a 2x2 MIMO, 128 subcarrier OFDM system with IEEE 802.16m urban macrocell channel model.

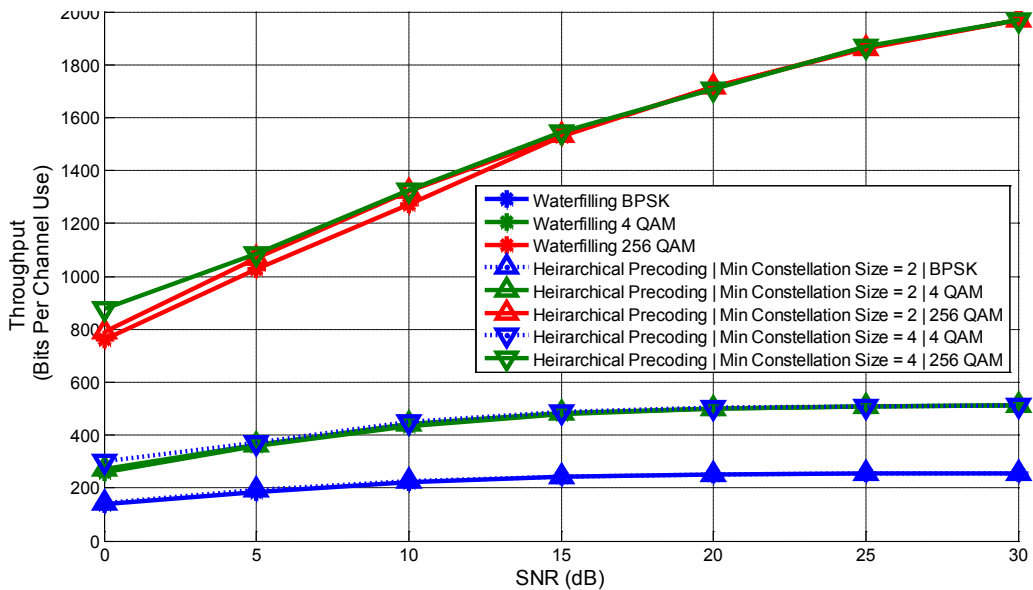


Figure 4.13: Throughput versus SNR for capacity based hierarchical precoding and WF for a 2x2 MIMO, 128 subcarrier OFDM system with IEEE 802.16m urban macrocell channel model.

Figure 4.13 gives the throughput Versus SNR plots for C-HP and comparing them to WF throughput. It can be seen that C-HP₄ performs has the best throughput performance, followed by C-HP₂, and WF. The throughput gain, as given in (4.2), is plotted in Figure 4.14. C-HP₄ performs better, providing a throughput gain of up to 16% at 0dB SNR.

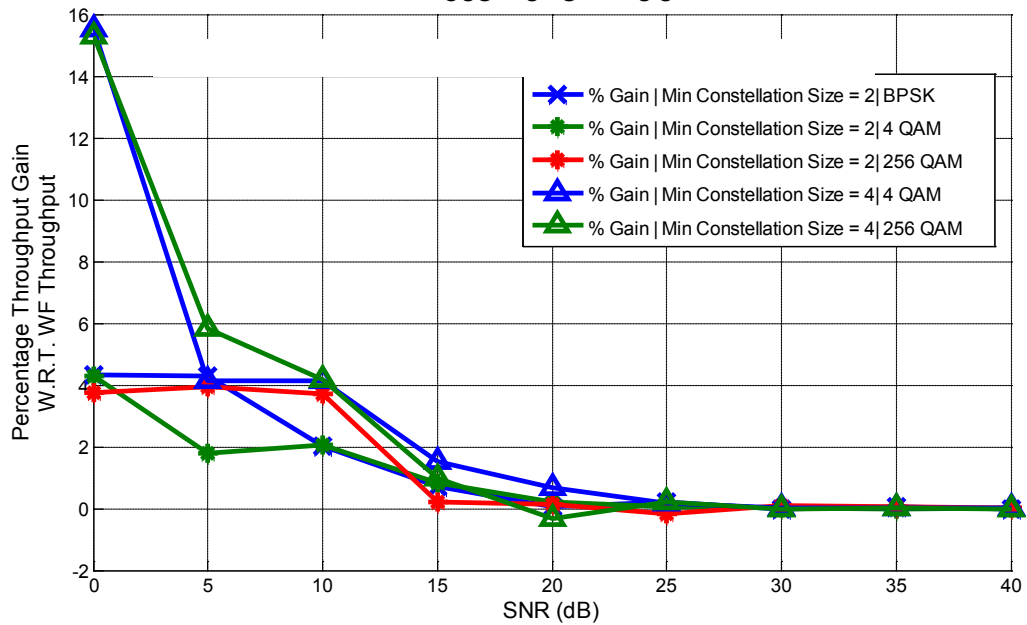


Figure 4.14: Throughput gain versus SNR for C-HP for a 2x2 MIMO, 128 subcarrier OFDM system with IEEE 802.16m urban macrocell channel model.

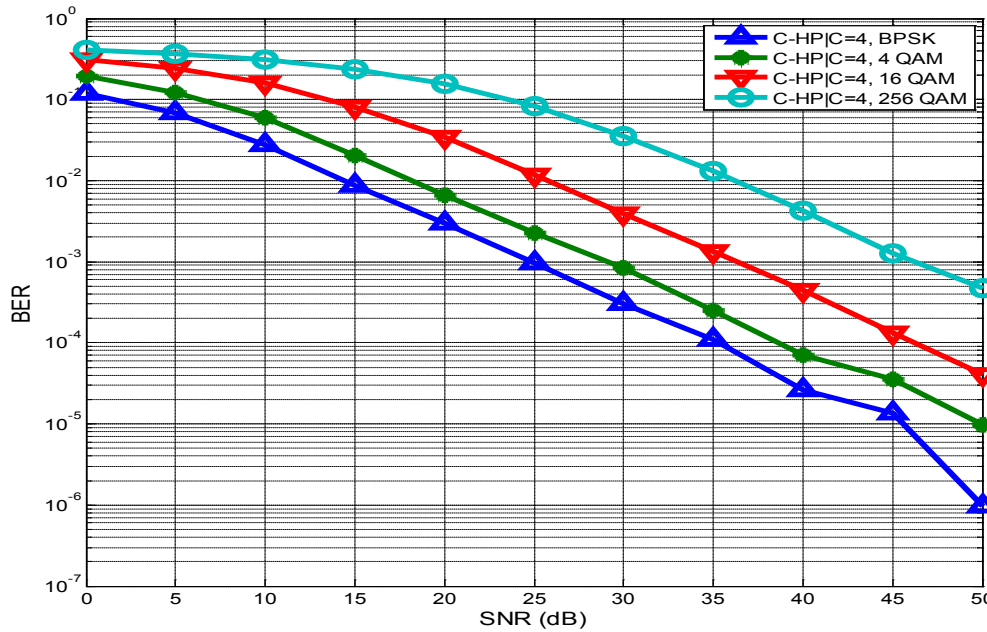


Figure 4.15: BER versus SNR for C-HP|C=4 AND MU precoding for a 2x2 MIMO, 128 subcarrier OFDM system with IEEE 802.16m urban macrocell channel model.

Figure 4.15 shows BER versus SNR curves for MU precoding with 4 users. Comparing these results with single-user (SU) cases, it can be seen that MU precoding does not cause any performance degradation, while allowing multiple users to transmit simultaneously.

Figure 4.16 show the throughput versus SNR curves for MU precoding.

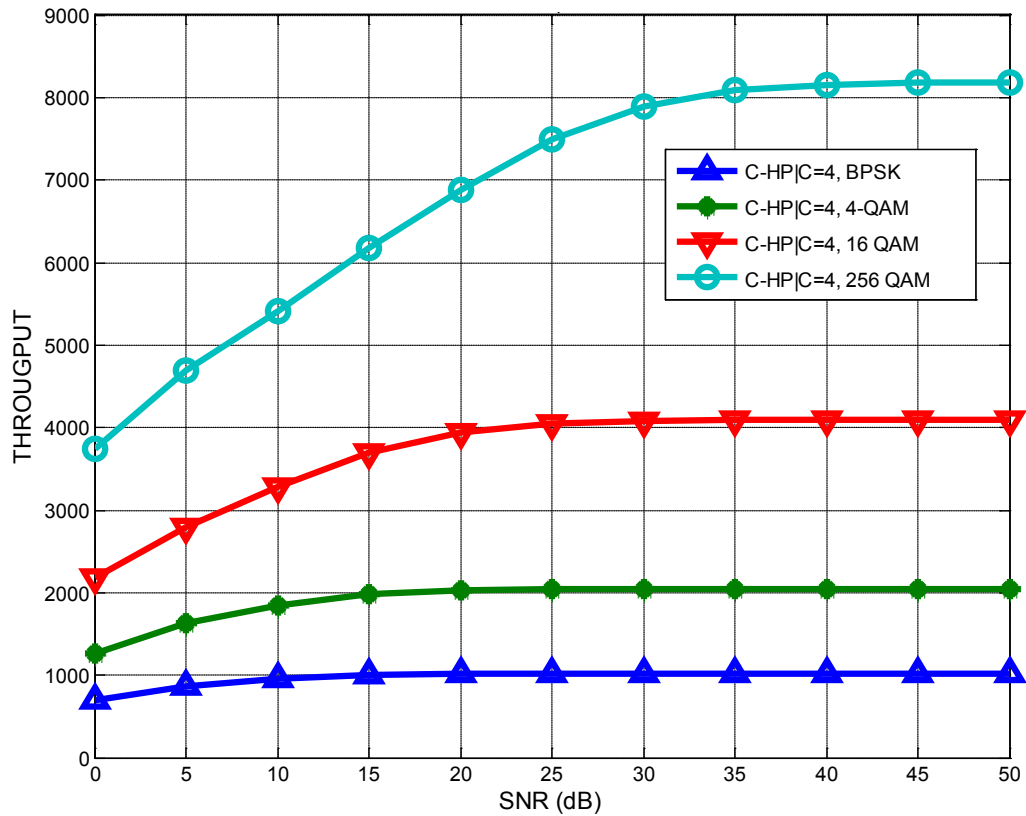


Figure 4.16: Throughput versus SNR FOR C-HP|C=4, with MU precoding for a 2x2 MIMO, 128 subcarrier OFDM system with IEEE 802.16m urban macrocell channel model.

The results for throughput and throughput gain with respect to WF using adaptive modulation are also discussed here. Figure 4.17 shows the throughput versus SNR curves for WF and HP with adaptive modulation. Figure 4.18 shows the percentage gain in throughput performance of HP over WF, when adaptive modulation is used. The results show that FR-HP, with $R=0.5$ has the worst performance, while C-HP, with $C = 1$ and $C = 2$ perform as well as WF across all SNRs.

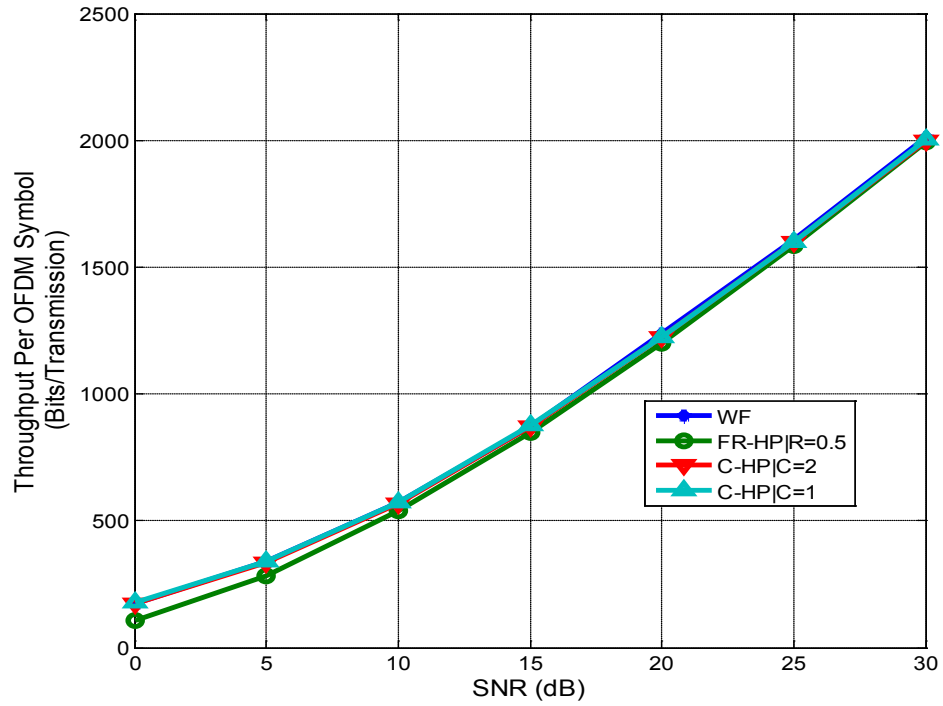


Figure 4.17: Throughput versus SNR with adaptive modulation, for a 2x2 MIMO, 128 subcarrier OFDM system with IEEE 802.16m urban macrocell channel model.

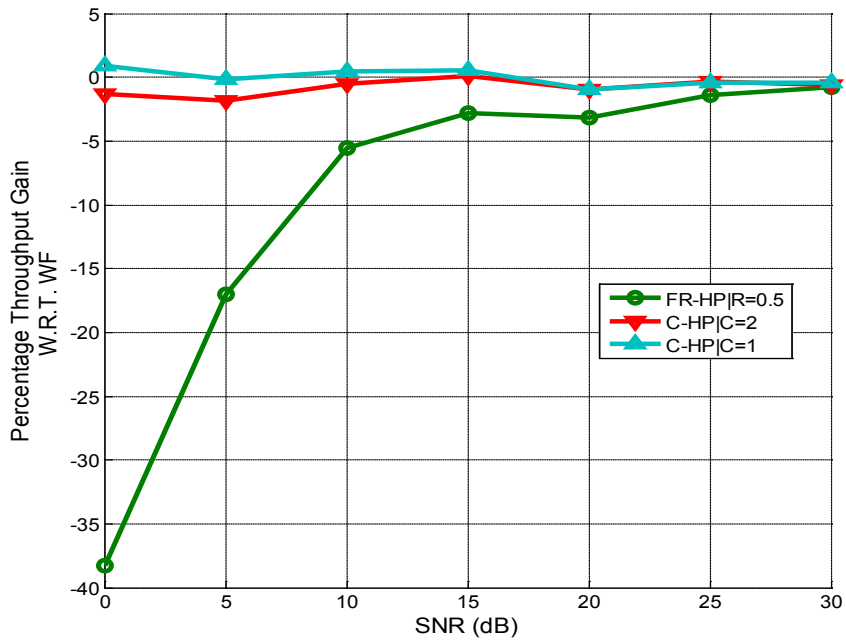


Figure 4.18: Throughput gain versus SNR with adaptive modulation for a 2x2 MIMO, 128 subcarrier OFDM system with IEEE 802.16m urban macrocell channel model.

The paper [25] gives an iterative WF algorithm, in which WF is performed with the additional constraint that the capacity of all eigen modes are greater than a chosen threshold. This allows an improvement in the per eigen mode SNR, with lesser number of eigen modes chosen to transmit. The results of iterative WF are compared with HP in the following figures. Figure 4.19 shows that, for a BER of 10^{-3} and BPSK constellation, iterative WF has an SNR gain of 8 dB over C-HP, both using the capacity threshold of 1 bps.

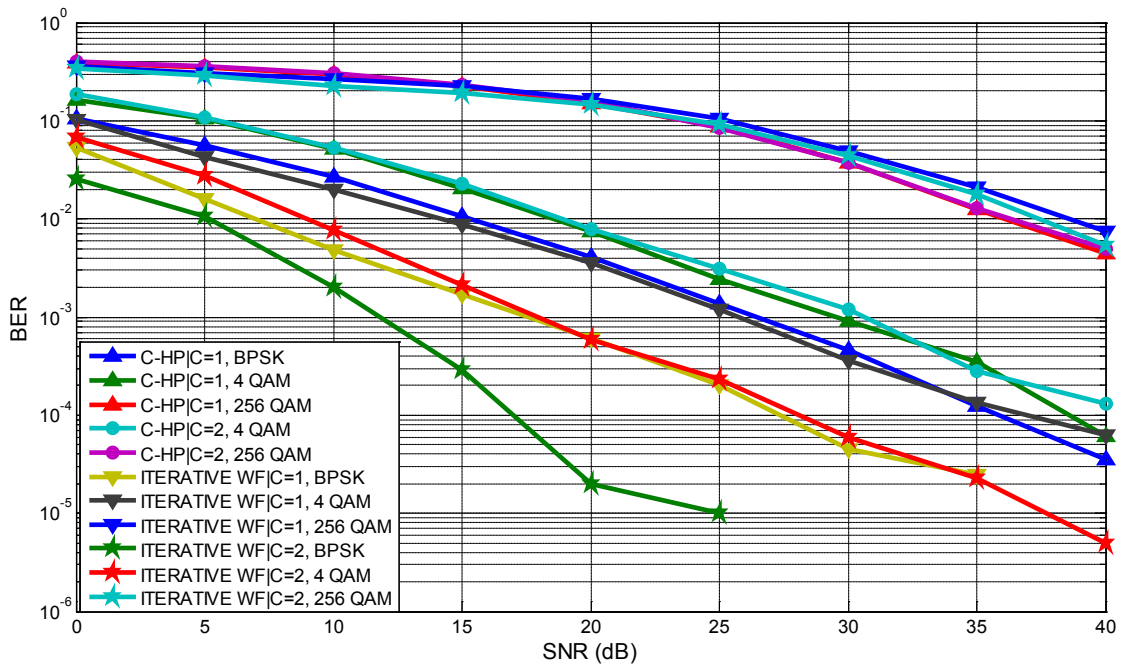


Figure 4.19: BER versus SNR comparison with iterative WF algorithm for a 2x2 MIMO, 128 subcarrier OFDM system with IEEE 802.16m urban macrocell channel model.

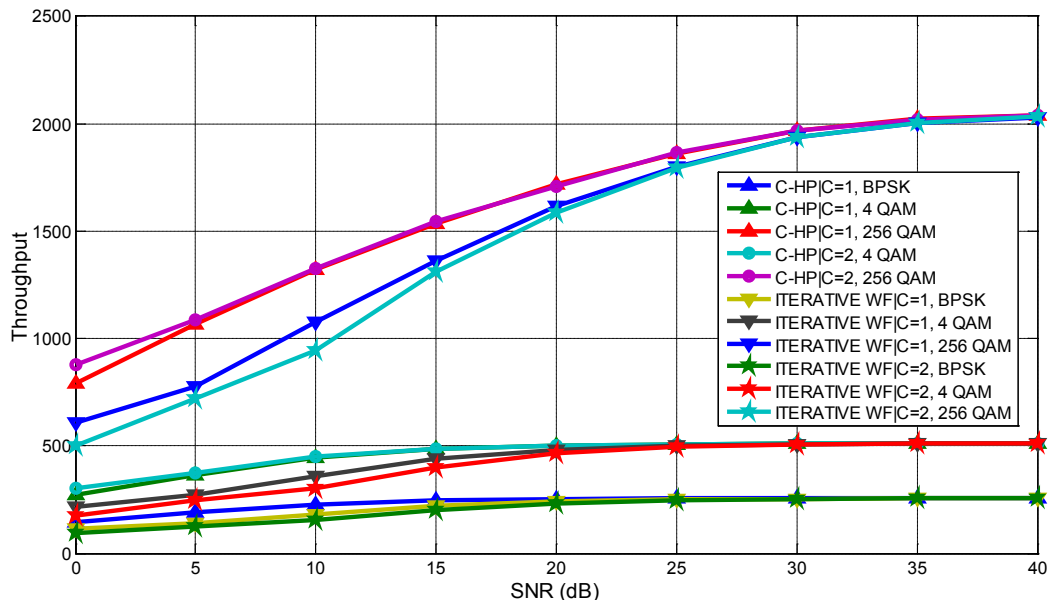


Figure 4.20: Throughput versus SNR comparison with iterative WF algorithm for a 2x2 MIMO, 128 subcarrier OFDM system with IEEE 802.16m urban macrocell channel model.

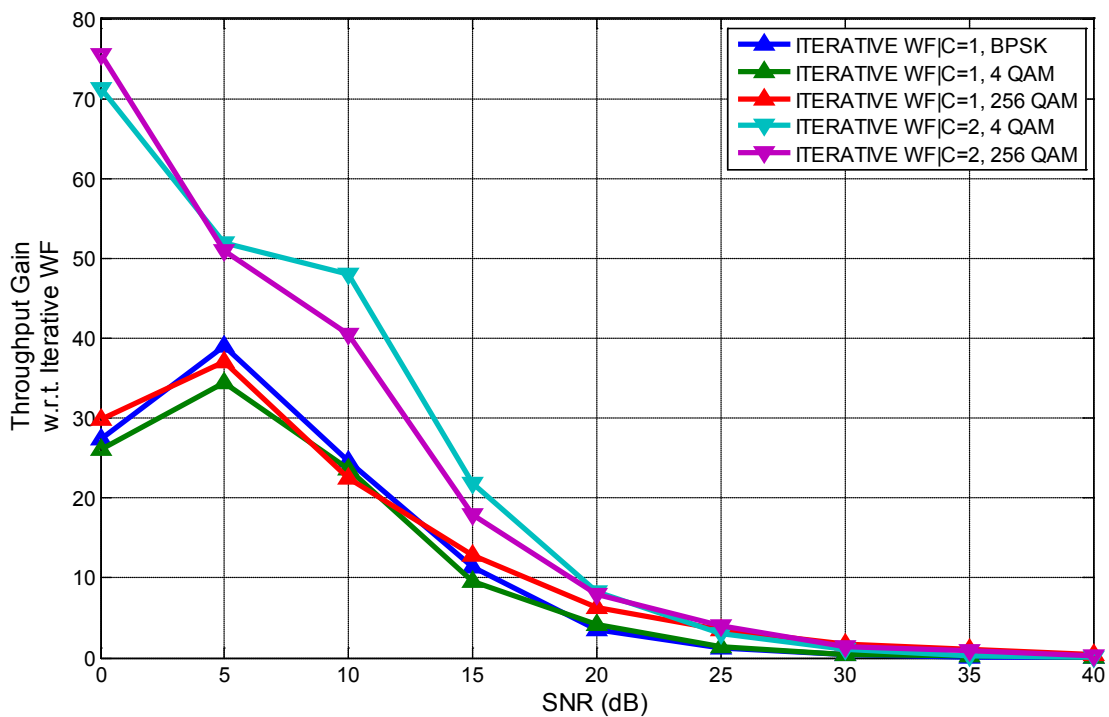


Figure 4.21: Throughput gain versus SNR with respect to iterative WF algorithm for a 2x2 MIMO, 128 subcarrier OFDM system with IEEE 802.16m urban macrocell channel model.

Figure 4.20 shows the throughput versus SNR performance comparison of HP with iterative WF. It can be seen that iterative WF has a lower throughput for a fixed constellation compared to HP. This throughput gain is quantified as a percentage in Figure 4.21.

CONCLUSION

In this chapter, HP was introduced, and its BER and throughput performance was compared with WF and with iterative WF. With fixed constellation, HP shows up to 33% increase in throughput performance with respect to WF with minimal deterioration BER performance. Two variants of HP were introduced. The first, FR-HP, allocates power hierarchically using a fixed ratio. The second, C-HP, allocates this power ratio dynamically according to the input threshold capacity. FR-HP_{0.5} shows the highest gain in throughput, followed by C-HP. The results for MU-HP are also compared with WF, and HP's allows a throughput gain with respect to WF in the MU scenario as well. The effects of adaptive modulation on HP and WF are studied as well. Finally, the performance of HP is compared with iterative WF, as given in [25]. HP performs better in terms of throughput, with the BER performance of iterative WF being better.

CHAPTER 5

ADAPTIVE EIGEN MODE REDUCTION

In this chapter, adaptive eigen mode reduction (AEMR) algorithm is introduced. In chapter 4, the simulation results for HP algorithm were discussed, and compared with WF algorithm simulation results. Figure 4.3, Figure 4.4 and Figure 4.5 show that HP's BER performance is deteriorated compared to WF. To overcome this problem, eigen modes with 'bad' channel characteristics can be removed from the precoding step in order to improve performance. This chapter first defines two ways in which an eigen mode can be termed as 'bad', followed by simulation results and discussion.

5.1 REDUCTION CRITERION

In order to classify eigen modes, a criterion needs to be defined first. All eigen modes that do not satisfy the given criterion can be termed as ‘bad’ modes, and can be removed from the precoding procedure. Two such criteria are defined here.

5.1.1 SNR CUTOFF

The simplest way of classify eigen modes is according to their respective SNR values. The eigen modes that are above a given cutoff SNR can be allowed to transmit, thereby increasing the BER performance by allowing only ‘good’ eigen modes to transmit.

The SNR of each eigen mode is calculated using (5.1).

$$SNR_{dB,i} = 10 * \log_{10} \left[P_i * \frac{\lambda_i^2}{\sigma^2} \right] \quad (5.1)$$

Here, P_i is the power allocated to the i^{th} eigen mode. If it is assumed that equal power allocation is applied, then the power allocated to the eigen modes is constant and therefore can be removed from the equation. Now, the cutoff value needs to be taken relative to the average SNR. The cutoff chosen here is such that

$$SNR_{dB,i} \geq SNR_{dB,Av} - S, \quad (5.2)$$

where, $SNR_{dB,Av}$ is the average SNR and S is the cutoff parameter. (5.2) gives the condition based on which eigen modes are chosen. This equation is illustrated more clearly with the following figure.

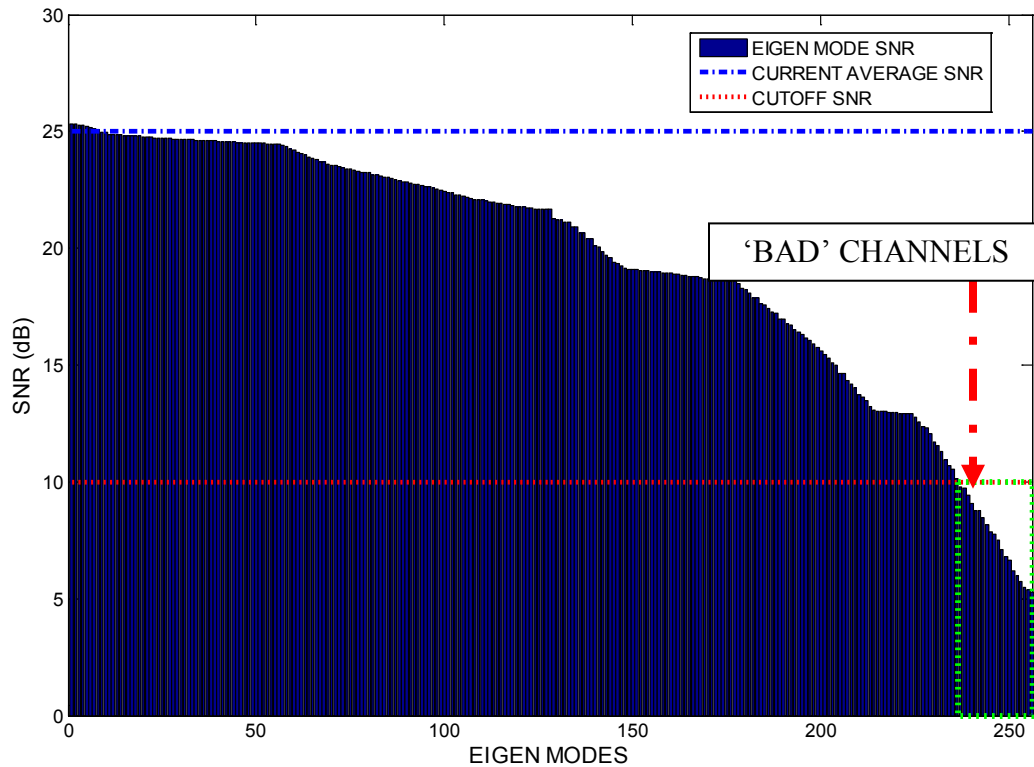


Figure 5.1: Diagrammatic representation for AEMR algorithm with $S=15$ dB, using FR-HP with $R=0.5$ and a 2×2 MIMO, 128 subcarrier OFDM system with IEEE 802.16m urban macrocell channel model.

In Figure 5.1, the instantaneous SNRs for the eigen modes of a 2×2 , 128 subcarrier MIMO OFDM system is shown. Here, S is taken as 15dB, which means all eigen modes whose SNR falls ' S ' dB below the average will be classified as 'bad' and will be prevented from transmitting by allocating them zero power.

SIMULATION RESULTS

The following results are for a 2×2 MIMO, 128 subcarrier OFDM system configuration. The channel model used is the urban macrocell channel model.

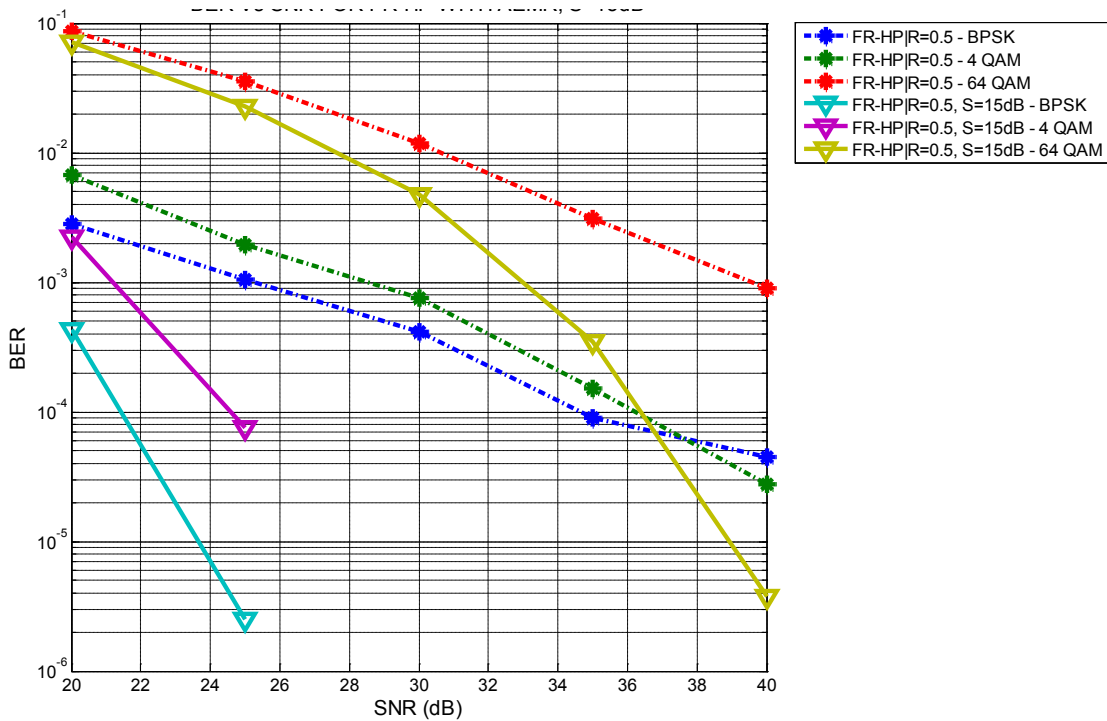


Figure 5.2: BER versus SNR for FR-HP_{0.5} with AEMR_{S=15dB} for a 2x2 MIMO, 128 subcarrier OFDM system with IEEE 802.16m urban macrocell channel model.

Figure 5.2 shows the gain provided by AEMR with $S=15\text{dB}$, for FR-HP_{0.5}. For a BER of 10^{-3} , the SNR gain for 64 QAM is 7dB, while for 4 QAM, the SNR gain is 8dB. Figure 5.3 shows throughput versus SNR curves for BPSK, 4 QAM and 64 QAM. It can be seen that FR-HP_{0.5} with AEMR_{S=15dB} performs slightly worse than FR-HP_{0.5} with no eigen reduction. Thus, using AEMR_{S=15dB} allows improves the BER performance at the cost of reduced throughput performance. Comparing Figure 1.8 and Figure 5.2, for a BER threshold of 10^{-4} , FR-HP_{0.5} with AEMR_{S=15dB} allows an SNR gain of 15.5dB.

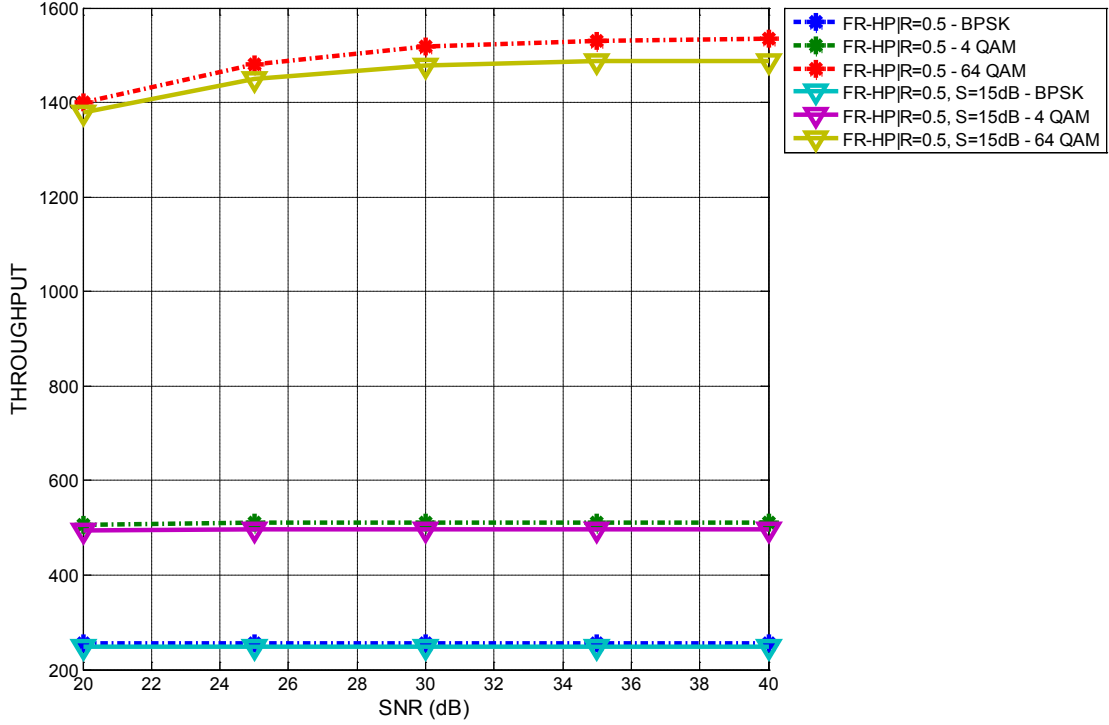


Figure 5.3: Throughput versus SNR for FR-HP_{0.5} with AEMR_{S=15dB} for a 2x2 MIMO, 128 subcarrier OFDM system with IEEE 802.16m urban macrocell channel model.

5.1.2 BER BASED CUTOFF

In Chapter 2, a theoretical BER equation for M-QAM constellations is given. The results shown in Figure 1.17 show that the theoretical BER equation approximates the actual simulated BER curve well. The theoretical BER equation is given in (5.3).

$$P(e) \cong \frac{4(\sqrt{M} - 1)}{\sqrt{M}} * \frac{1}{\log_2 M} \sum_{i=1}^{\sqrt{M}/2} Q \left\{ (2i - 1) * \sqrt{3 * \frac{P_i \lambda_i^2}{(M - 1) \sigma^2}} \right\} \quad (5.3)$$

The BER based cutoff for AEMR is calculated using the equation given above. A threshold BER value, BER_{Th}, is chosen. All eigen modes whose BER value is less than

the $BERT_h$ are allowed to transmit, and the rest are not considered when performing precoding.

SIMULATION RESULTS

The following results are for a 2x2 MIMO, 128 subcarrier OFDM system configuration and $BERT_h=10^{-2}$.

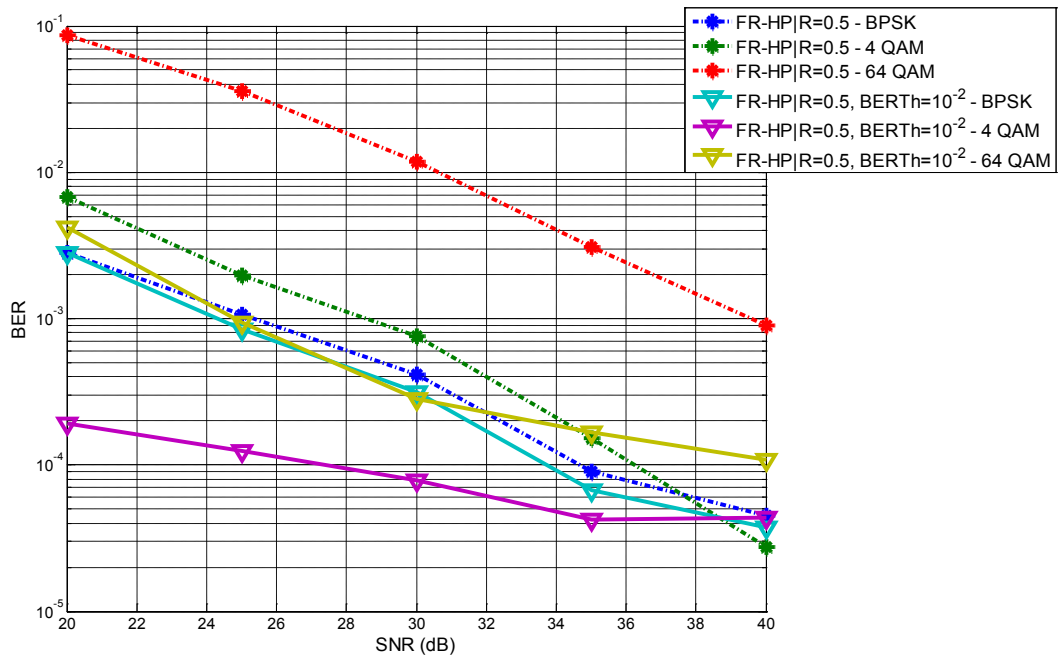


Figure 5.4: BER Versus SNR FOR FR-HP WITH $AEMR_{BERT_h=10^{-2}}$ for a 2x2 MIMO, 128 subcarrier OFDM system with IEEE 802.16m urban macrocell channel model.

Figure 5.4 shows the BER Versus SNR plots for FR-HP_{0.5} with AEMR implemented. It can be seen that the BER values are less than $BERT_h$ for all constellations. Thus, it can be deduced that the BER performance of AEMR with $BERT_h=10^{-2}$ is significantly better than AEMR with SNR Cutoff of 15dB. Throughput curves for AEMR with $BERT_h=10^{-2}$

are given in Figure 5.5. The performance is degraded at low SNRs, and improves as the SNR increases. At 30dB, the throughput difference between FR-HP_{0.5} and FR-HP_{0.5} with AEMR_{S=15dB} for 256-QAM is 450 bits, or 56.25 256-QAM symbols, per channel use. This difference reduces to 65 bits, or 8.125 256-QAM symbols, per channel use.

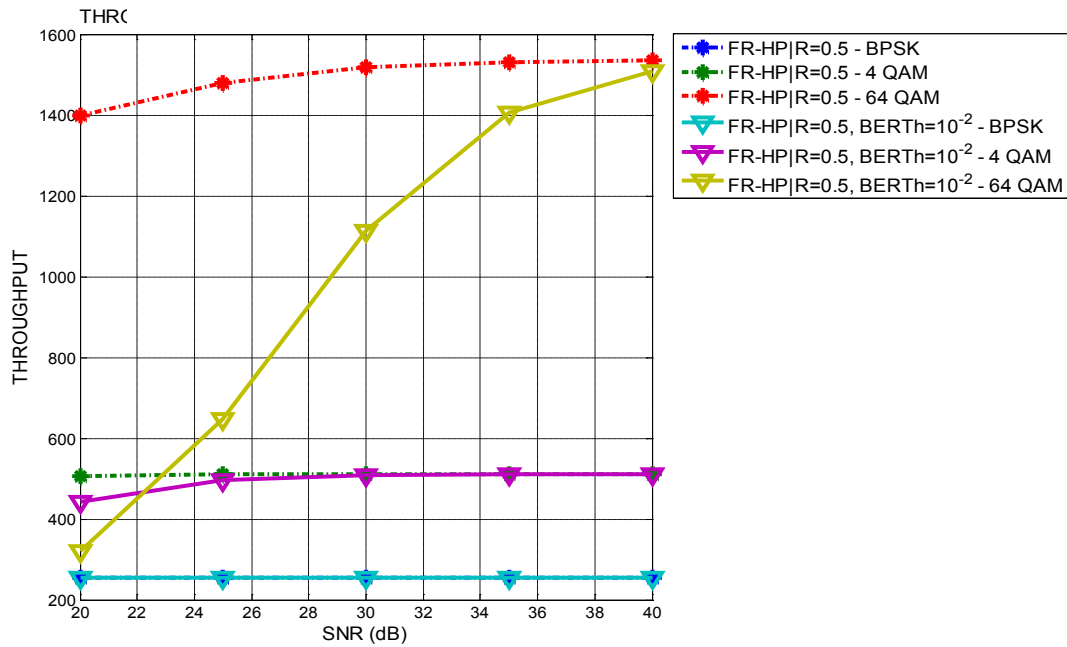


Figure 5.5: Throughput versus SNR for FR-HP_{0.5} and AEMR_{BERTH=10⁻²} for a 2x2 MIMO, 128 subcarrier OFDM system with IEEE 802.16m urban macrocell channel model.

Figure 5.6 and Figure 5.7 show the BER performance and throughput performance, respectively, for C-HP₂ with AEMR with BERTH = 10⁻².

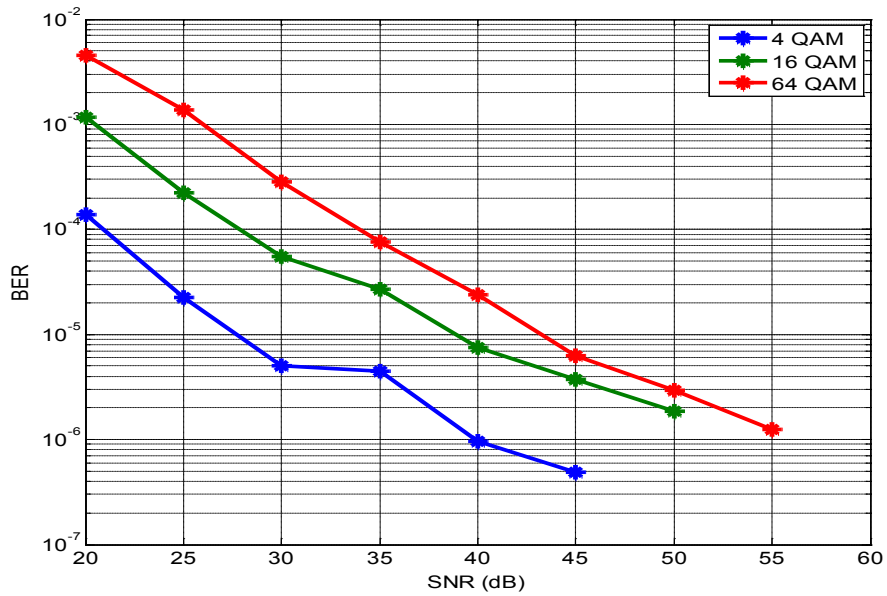


Figure 5.6: BER Versus SNR FOR C-HP₂ WITH $AEMR_{BERth=10^{-2}}$ for a 2x2 MIMO, 128 subcarrier OFDM system with IEEE 802.16m urban macrocell channel model.

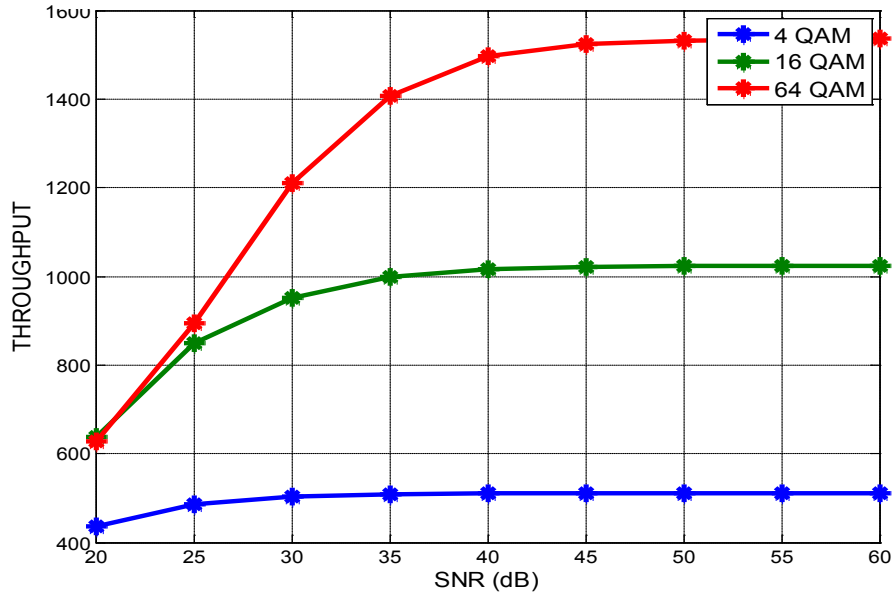


Figure 5.7: Throughput versus SNR for C-HP₂ with $AEMR_{BERth=10^{-2}}$ for a 2x2 MIMO, 128 subcarrier OFDM system with IEEE 802.16m urban macrocell channel model.

CONCLUSION

AEMR provides a BER performance versus throughput trade-off. AEMR using SNR cutoff of 15 dB has a lower throughput loss when compared to AEMR using BER cutoff of 10^{-3} , both being compared with WF throughput. AEMR provides the option to trade-off throughput performance to improve the BER performance. AEMR can be used in conjunction with HP in order to offset the BER performance degradation that is inherent to HP.

CHAPTER 6

FEEDBACK REDUCTION

In the previous chapters, it is assumed that the transmitter has perfect channel knowledge, and it can perform accurate precoding according to channel conditions. Perfect channel knowledge at the transmitter produces the best results because the precoding algorithm can perfectly compensate for the channel at the transmitter. This perfect channel knowledge at the transmitter requires feedback from the receiver. This implies that, for perfect channel knowledge at the transmitter the receiver would have to send a channel feedback to the transmitter for every symbol transmitted.

6.1 FEEDBACK REDUCTION IN TIME

Feedback can be reduced if the channel is assumed to be correlated in time. In chapter 3.4, it was shown how doppler shift causes time correlation in the channel. The correlation in time can be used to reduce the channel information feedback. If f_d is the doppler shift, coherence time, which is the time for which the channel remains highly correlated, can be approximated as given in (6.1).

$$\text{Coherence Time} = T_c \approx \frac{1}{f_d} \quad (6.1)$$

Let F_s be the signal bandwidth and N_{OFDM} be the number of OFDM symbols. The bandwidth of each OFDM subcarrier is given in (6.2).

$$F_{Sub} = \frac{F_s}{N_{OFDM}} \quad (6.2)$$

In the time domain, all the subcarriers in an OFDM symbol are superimposed and transmitted simultaneously. A cyclic prefix is added to the OFDM symbol to mitigate inter symbol interference (ISI) due to multipath channel (See Section 2.3). The OFDM symbol duration is given in (6.3).

$$T_{OFDM} = \frac{1}{F_{Sub}} = \frac{N_{OFDM}}{F_s} \quad (6.3)$$

The number of OFDM symbols per coherence time, N_C , can be calculated in (6.4).

$$N_C = \frac{T_C}{T_{OFDM}} = \frac{F_s}{f_d * N_{OFDM}} \quad (6.4)$$

For N_C symbols, the channel will remain highly correlated. Using (3.5) and setting $\Delta t = 1/f_d$, (6.5) is formulated as follows.

$$\rho(\Delta t) = J_0(2\pi f_d \Delta t) = J_0\left(2\pi f_d * \frac{1}{f_d}\right) = J_0(2\pi) = 0.2203 \quad (6.5)$$

Thus, for a coherence time of $T_c \approx \frac{1}{f_d}$, the channel is 22.03% correlated.

From (3.5) it can be deduced that channel autocorrelation is a function of f_d and Δt . If Δt is made a function of f_d , the autocorrelation function can become independent of doppler shift.

Let $\Delta t = \frac{K}{f_d}$, where, K is a real number, such that $\in R(0, \infty)$. Substituting in (3.5), (6.6) is formed.

$$\rho(\Delta t) = J_0(2\pi f_d \Delta t) = J_0\left(2\pi f_d * \frac{K}{f_d}\right) = J_0(2\pi K) \quad (6.6)$$

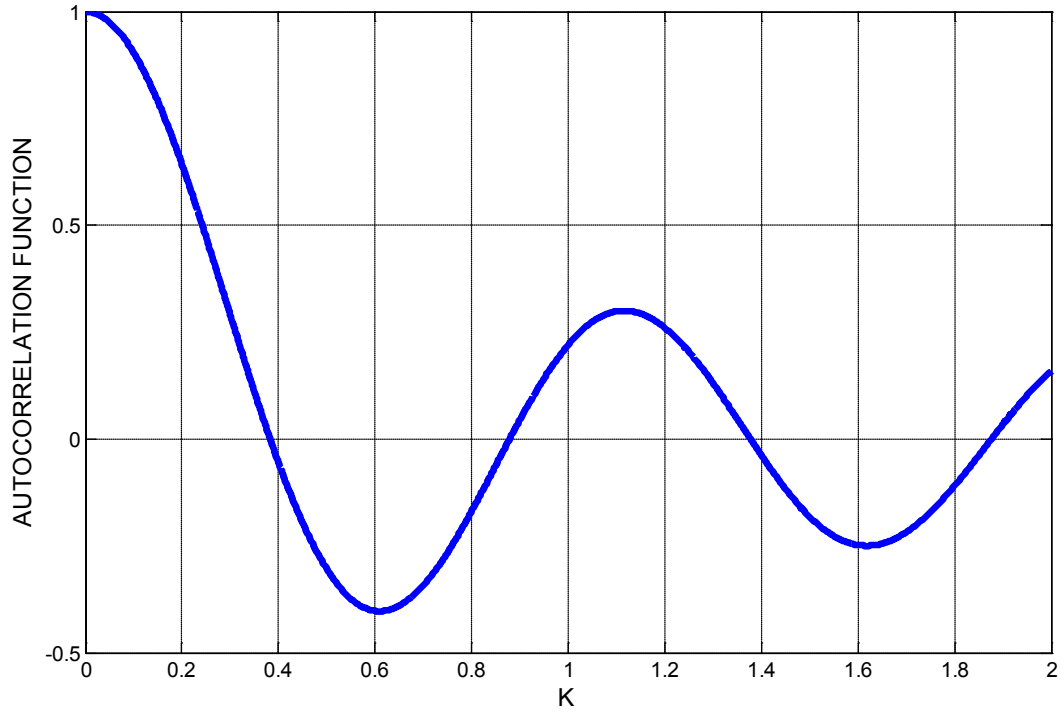


Figure 6.1: Doppler shift autocorrelation function versus K

For perfect channel state information at the transmitter (CSIT), the receiver needs to feedback channel state information (CSI) for each OFDM symbol transmission, that is, every, T_{OFDM} seconds. With feedback reduction, this feedback time changes to multiples of T_{OFDM} . If $N_{FEEDBACK}$ is defined as the number of symbols after which CSI is fed back to the transmitter, then, using (6.4) and (6.6), $N_{FEEDBACK}$ can be defined as given in (6.7).

$$N_{FEEDBACK} = \left\lfloor K * \frac{F_s}{f_d * N_{OFDM}} \right\rfloor \quad (6.7)$$

The operation $[*]$ denotes the floor value function. The value of K can be varied in order to vary the feedback reduction factor, $N_{FEEDBACK}$.

SIMULATION RESULTS

The following simulations are done for a 2x2 MIMO, 128 subcarrier OFDM system configuration. The channel model used here is the urban macrocell channel model. Signal bandwidth is 1MHz, doppler shift is 10Hz, and N_C is calculated as follows.

$$N_C = \frac{F_s}{f_d * N_{OFDM}} = \frac{10^6}{10 * 128} = 781.2500$$

The following results are obtained by varying K to obtain $N_{FEEDBACK}$.

1. $K=0.01 \rightarrow N_{FEEDBACK} = 7$ OFDM Symbols ($\rho(\Delta t) = 0.2203$)
2. $K=0.1 \rightarrow N_{FEEDBACK} = 78$ OFDM Symbols ($\rho(\Delta t) = 0.9037$)
3. $K=1 \rightarrow N_{FEEDBACK} = 781$ OFDM Symbols ($\rho(\Delta t) = 0.9990$)

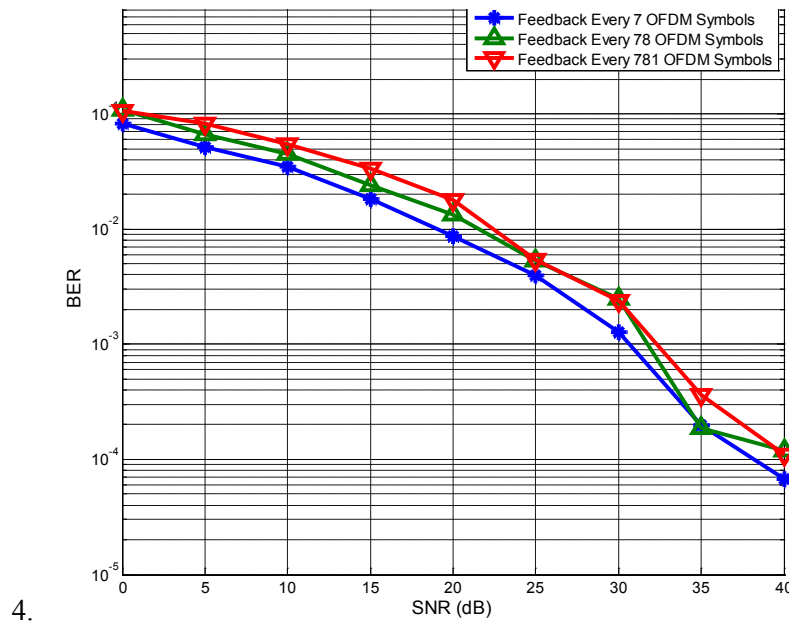


Figure 6.2: BER versus SNR performance comparison with WF algorithm for a 2x2 MIMO, 128 subcarrier OFDM system with IEEE 802.16m urban macrocell channel model, using QPSK constellation.

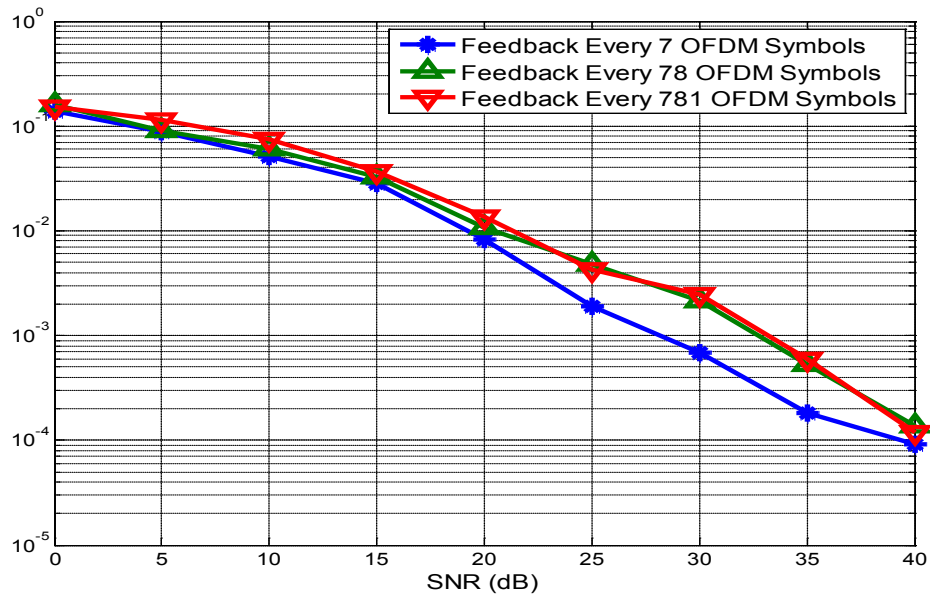


Figure 6.3: BER versus SNR performance comparison with WF algorithm for a 2x2 MIMO, 128 subcarrier OFDM system with IEEE 802.16m urban macrocell channel model, using 4 QAM constellation.

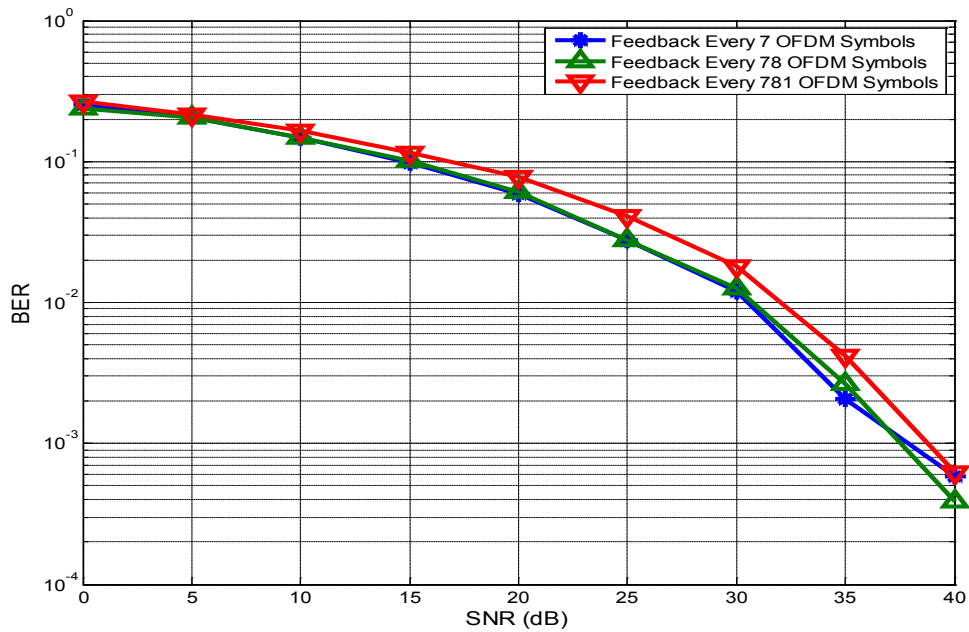


Figure 6.4: BER versus SNR performance comparison with WF algorithm for a 2x2 MIMO, 128 subcarrier OFDM system with IEEE 802.16m urban macrocell channel model, using 16 QAM constellation.

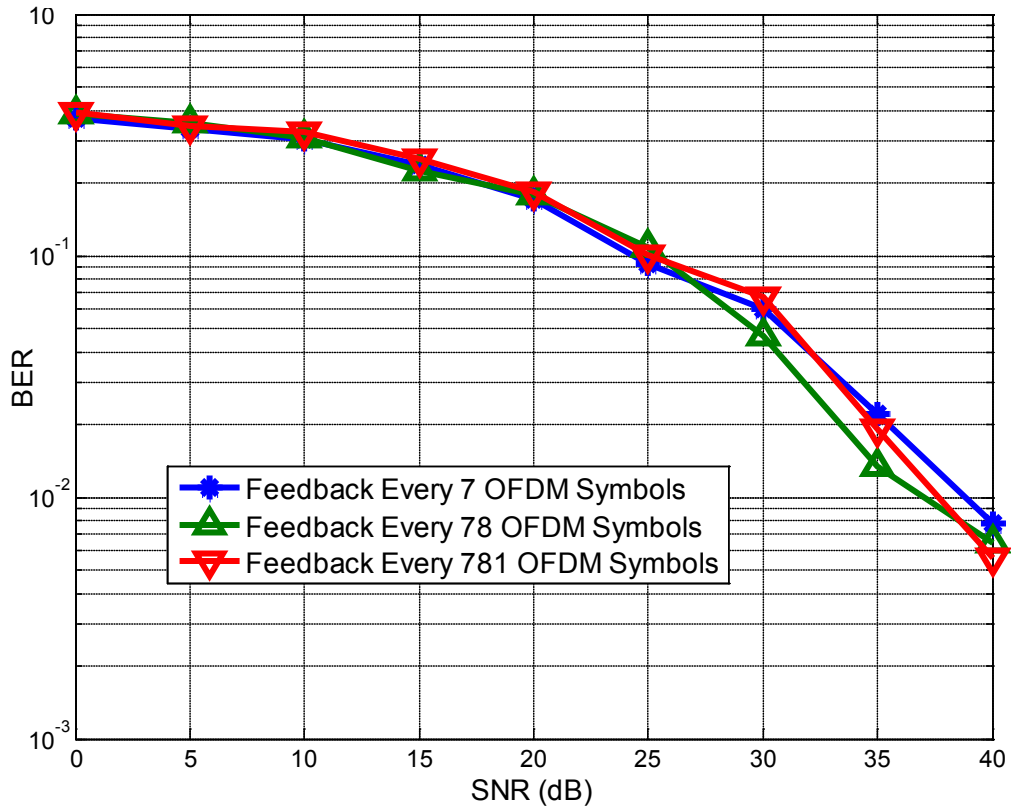


Figure 6.5: BER versus SNR performance comparison with WF algorithm for a 2x2 MIMO, 128 subcarrier OFDM system with IEEE 802.16m urban macrocell channel model, using 256 QAM constellation.

Figure 6.2, Figure 6.3, Figure 6.4 and Figure 6.5 illustrate the BER Versus SNR performance of a reduced feedback system, for constellations QPSK, 4 QAM, 16 QAM and 256 QAM, respectively. For BPSK, $K = 0.01$ performs the best, with an SNR gain of 5dB over $K = 1$ case for a BER of 10^{-3} . This difference in performance for varying values of K , however, reduces as the constellation size increases. For 256 QAM, the BER plots for the three cases are indistinguishable up to 25 dB.

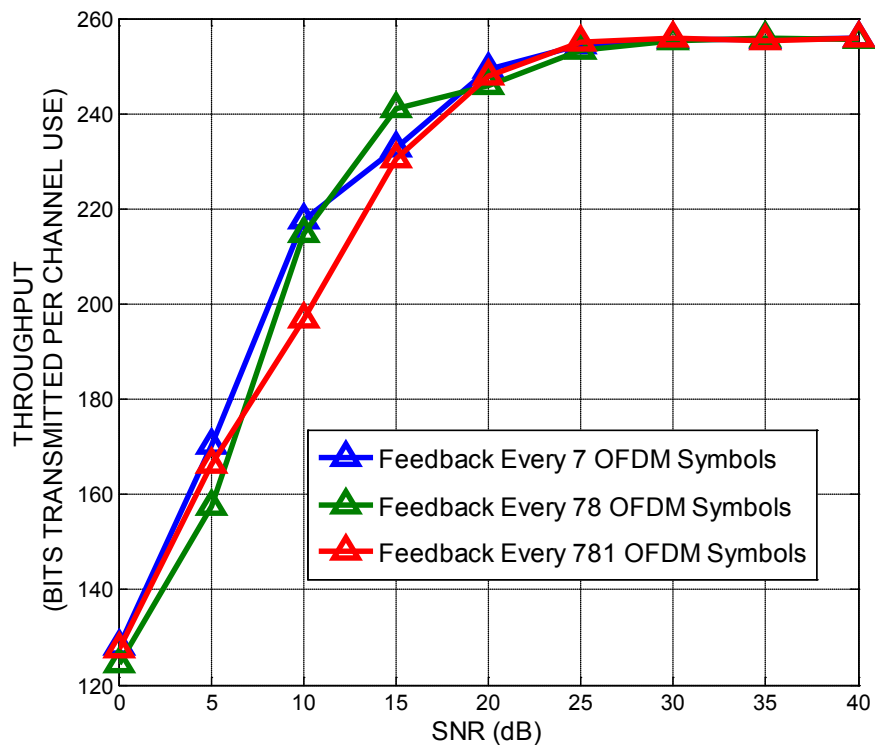


Figure 6.6: Throughput versus SNR performance comparison with WF algorithm for a 2x2 MIMO, 128 subcarrier OFDM system with IEEE 802.16m urban macrocell channel model, using BPSK constellation.

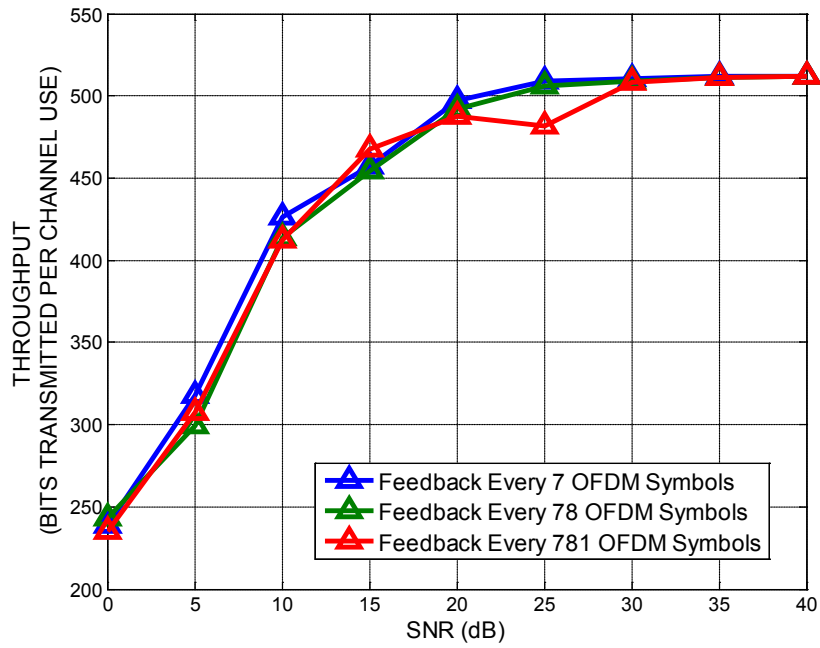


Figure 6.7: Throughput versus SNR performance comparison with WF algorithm for a 2x2 MIMO, 128 subcarrier OFDM system with IEEE 802.16m urban macrocell channel model, using 4 QAM constellation.

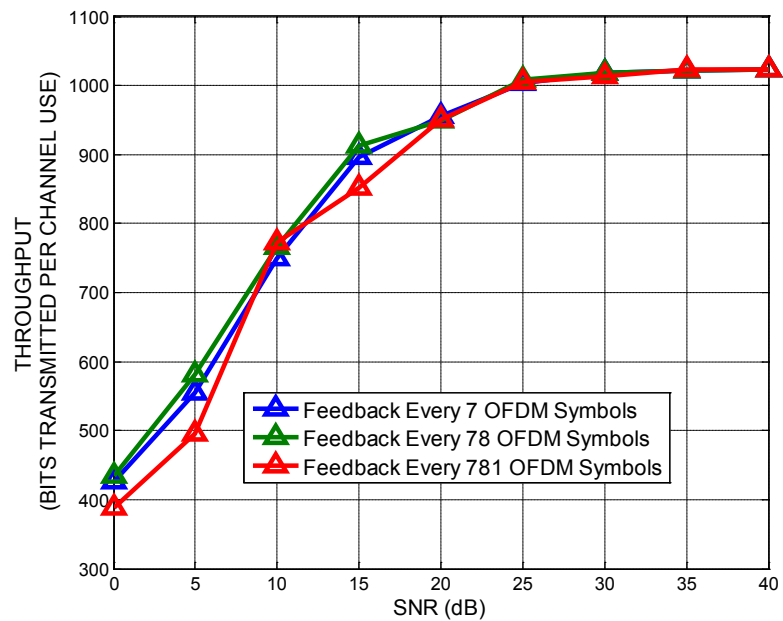


Figure 6.8: Throughput versus SNR performance comparison with WF algorithm for a 2x2 MIMO, 128 subcarrier OFDM system with IEEE 802.16m urban macrocell channel model, using 16 QAM constellation.

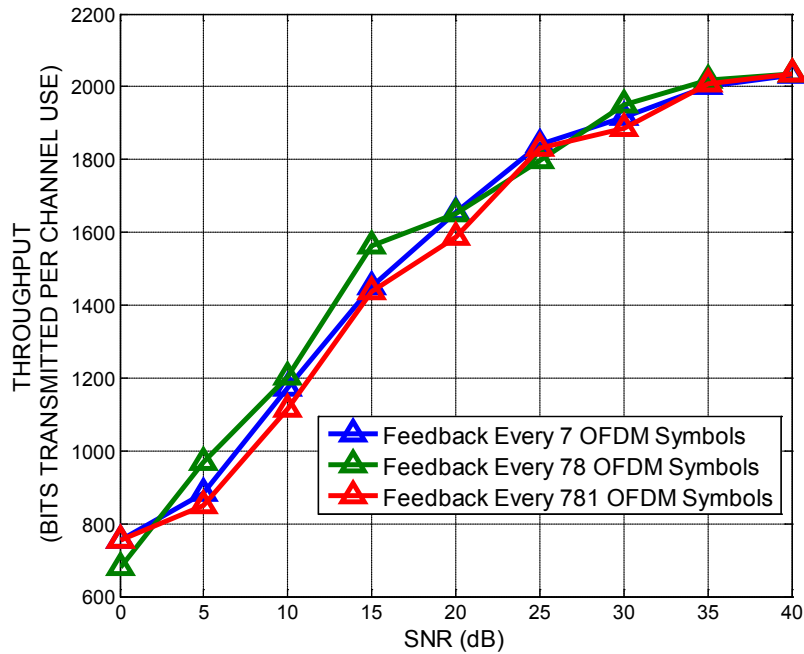


Figure 6.9: Throughput versus SNR performance comparison with WF algorithm for a 2x2 MIMO, 128 subcarrier OFDM system with IEEE 802.16m urban macrocell channel model, using 256 QAM constellation.

Figure 6.6, Figure 6.7, Figure 6.8 and Figure 6.9 show the throughput versus SNR plots for feedback reduction with constellations QPSK, 4 QAM, 16 QAM and 256 QAM, respectively. The best throughput results are for $K=0.01$, and the throughput performance deteriorates as K increases. For BPSK, the difference between throughput for $K = 0.01$ and $K=1$ is 20 bits, or 20 QPSK symbols, per channel use at 10 dB SNR. For 256 QAM and at 10dB SNR, the difference is a 100 bits, or 12.5 256-QAM symbols, per channel use.

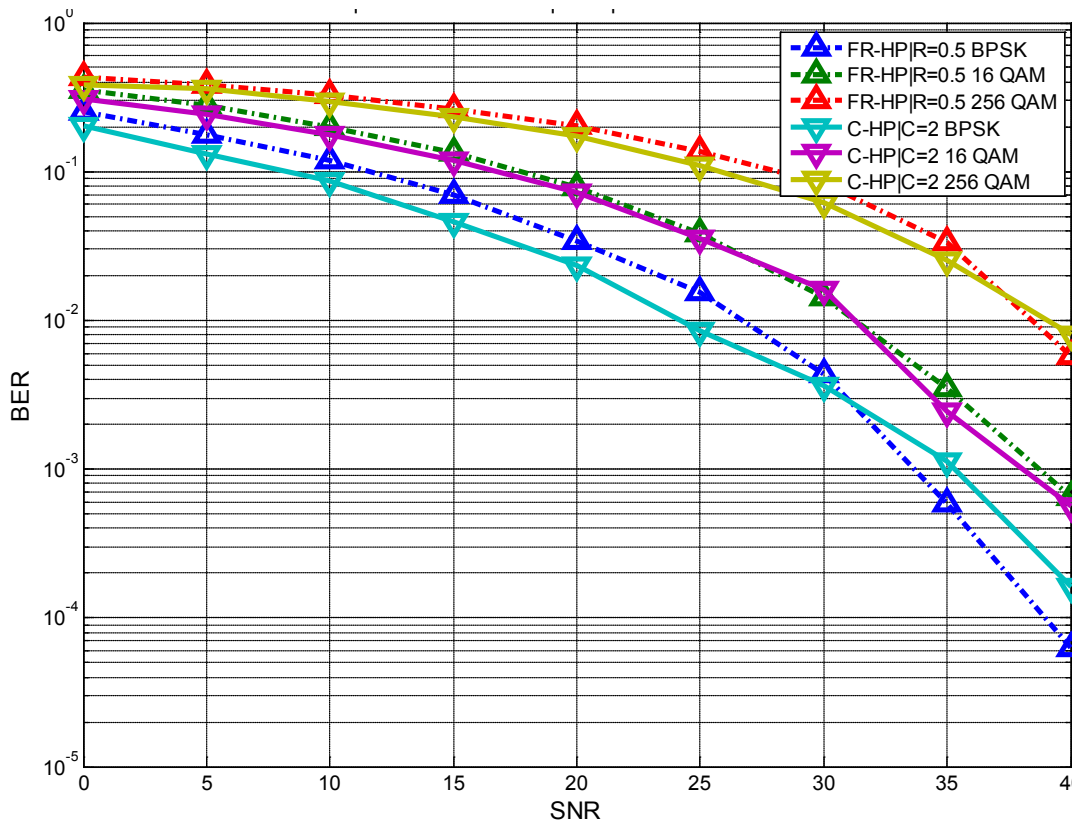


Figure 6.10: BER Versus SNR comparison for feedback reduction for $K = 0.1$ and doppler shift of 10 Hz with FR-HP_{0.5} and C-HP₂ for a 2x2 MIMO, 128 subcarrier OFDM system with IEEE 802.16m urban macrocell channel model.

Figure 6.10 shows BER versus SNR performance for FR-HP_{0.5} and C-HP₂, with $K=0.1$. It can be seen that C-HP₂ performs better than FR-HP_{0.5} for 256 QAM across all SNRs. At low SNRs of up to 15 dB, C-HP₂ performs better than FR-HP_{0.5} for BPSK and 16 QAM. Figure 6.11 shows the throughput versus SNR plots for FR-HP_{0.5} and C-HP₂, with $K=0.1$. Till 15dB, it can be seen that FR-HP_{0.5} performs better across all constellations, beyond which C-HP₂ starts performing better.

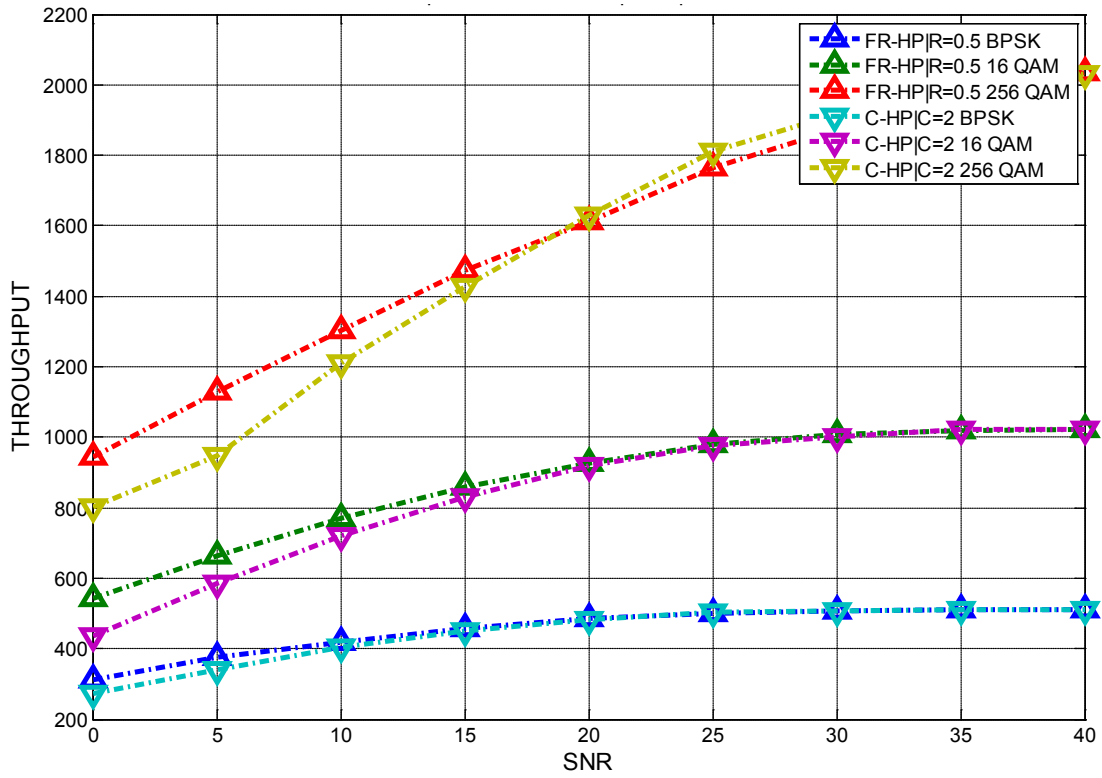


Figure 6.11: Throughput versus SNR comparison for feedback reduction for $K = 0.1$ and doppler shift of 10 Hz with FR-HP_{0.5} and C-HP₂ for a 2x2 MIMO, 128 subcarrier OFDM system with IEEE 802.16m urban macrocell channel model.

6.2 FEEDBACK REDUCTION IN

FREQUENCY DOMAIN

Figure 3.19 shows channel correlation in frequency. This correlation can be used to reduce feedback in the frequency domain. The coherence bandwidth is defined as the channel bandwidth over which the channel frequency response remains correlated. Coherence bandwidth is given in (6.8).

$$B_C \approx \frac{1}{\tau_{Max}} \quad (6.8)$$

Here, τ_{Max} is the maximum excess delay.

Maximum excess delay is the time at which the last tap in a multipath channel is received, relative to the first tap. Number of OFDM subcarriers per coherence bandwidth is given in (6.9).

$$N_{C,F} = \frac{N_{OFDM}}{F_S} \cdot B_C \quad (6.9)$$

In order to reduce feedback, OFDM subcarriers are put together in groups, such that each group has highly correlated gain. Each group is represented by the first subcarrier in that group, and precoding is performed on all the subcarriers in the group based on the first subcarrier. In order to group subcarriers together, a feedback reduction factor, G , is defined here, $G \in R[0, \infty)$.

If $N_{Feedback,F}$ is the number of OFDM subcarriers grouped together, the relation between $N_{Feedback,F}$ and G is defined in (6.10).

$$N_{Feedback,F} = \lfloor N_{C,F} \cdot G \rfloor = \left\lfloor \frac{N_{OFDM}}{F_S} \cdot B_C \cdot G \right\rfloor \quad (6.10)$$

Note that $N_{Feedback,F} \leq N_{OFDM}$, because the maximum group size would be the whole OFDM symbol, that is, the first subcarrier of the OFDM symbol would represent the whole OFDM symbol. This implies that $G \leq F_S/B_C$.

SIMULATION RESULTS

The following simulations are done for a 2x2 MIMO, 128 subcarrier OFDM system configuration. The channel model used here is the urban macrocell channel model, whose maximum excess delay is $\tau_{Max} = 1845 \cdot 10^{-9}$ s which implies $B_C = 5.42 \cdot 10^5$ Hz. Signal bandwidth is 1MHz, doppler shift is 10Hz, and $N_{C,F}$ is calculated as follows.

$$N_{C,F} = \frac{N_{OFDM}}{F_S} \cdot B_C = 128 \cdot 5.42 \cdot \frac{10^5}{10^6} = 69.37$$

The following results are obtained by varying G to obtain $N_{Feedback,F}$.

1. $G=5.765 \cdot 10^{-2} \rightarrow N_{Feedback,F} = 4$ OFDM Subcarriers
2. $G=2.306 \cdot 10^{-1} \rightarrow N_{Feedback,F} = 16$ OFDM Subcarriers
3. $G=0.9255 \rightarrow N_{Feedback,F} = 64$ OFDM Subcarriers

The values of K show feedback reduction in time as defined in (6.7). By combining feedback reduction in time and frequency domain, the overall feedback requirements can

be reduced considerably. For example, $K=0.01$ and $N_{Feedback,F} = 4$ implies that, in one OFDM symbol, just 32 subcarriers' channel state information is fed back to the transmitter; while over time, a feedback is sent to the transmitter every 7 OFDM symbols. For perfect channel knowledge at the receiver, $128 \cdot 7 = 896$ feedbacks need to be transmitted. For the reduced feedback case, however, only $\frac{128}{4} \cdot 1 = 32$ feedbacks are transmitted. That is a feedback reduction of $\left(\frac{896-32}{896}\right) \cdot 100 = 96.43\%$. The results show that this reduction in feedback has minimal effect on the performance of the system.

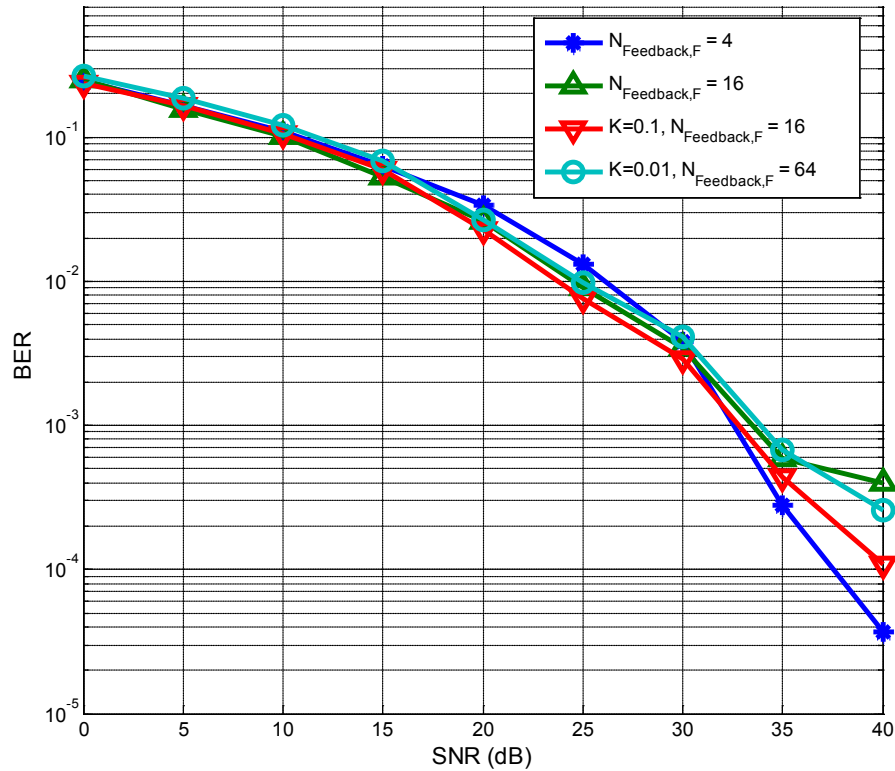


Figure 6.12: BER Versus SNR for feedback reduction for $K = 0.1$ and doppler shift of 10 Hz with FR-HP_{0.5} for a 2x2 MIMO, 128 subcarrier OFDM system with IEEE 802.16m urban macrocell channel model, using 4 QAM constellation.

Figure 6.12 shows BER versus SNR plots for 4 QAM constellation using FR-HP_{0.5}. It can be seen that for SNR values of up to 20 dB, the BER performance for all the reduced feedback cases is the same. For a BER of 10^{-3} , $N_{Feedback,F} = 4$ needs 32.5 dB, $N_{Feedback,F} = 16$ needs 33.5 dB, $K = 0.1, N_{Feedback,F} = 16$ requires 32.8 dB, and $K = 0.01, N_{Feedback,F} = 64$ needs 33.9 dB. Although the difference between the four plots is small, it can be seen that $N_{Feedback,F} = 4$ has the best BER performance.

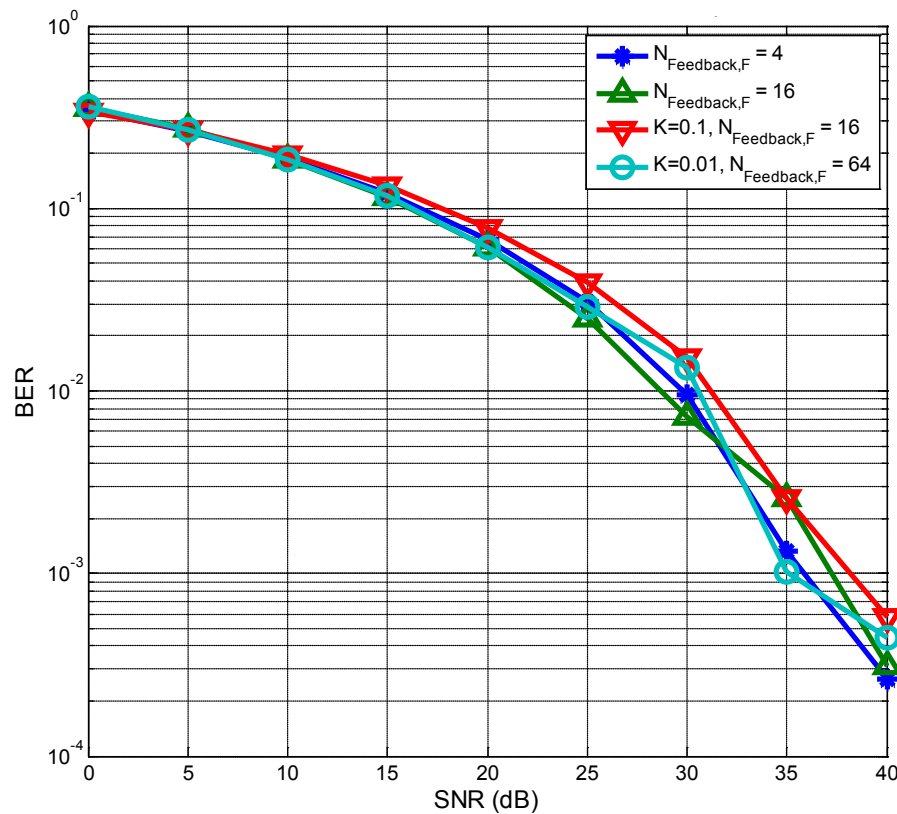


Figure 6.13: BER Versus SNR for feedback reduction for $K = 0.1$ and doppler shift of 10 Hz with FR-HP_{0.5} for a 2x2 MIMO, 128 subcarrier OFDM system with IEEE 802.16m urban macrocell channel model, using 16 QAM constellation.

Figure 6.13 shows the BER versus SNR plots for feedback reduction for 16 QAM constellation and FR-HP_{0.5} precoding. For a BER of 10^{-3} , $N_{Feedback,F} = 4$ requires 35.85 dB, $N_{Feedback,F} = 16$ requires 37.23 dB, $K = 0.1, N_{Feedback,F} = 16$ needs 38.16 dB, while $K = 0.01, N_{Feedback,F} = 64$ needs 35.1 dB, which is the best performer of the four, with an SNR gain of 3.06 dB over $N_{Feedback,F} = 16$.

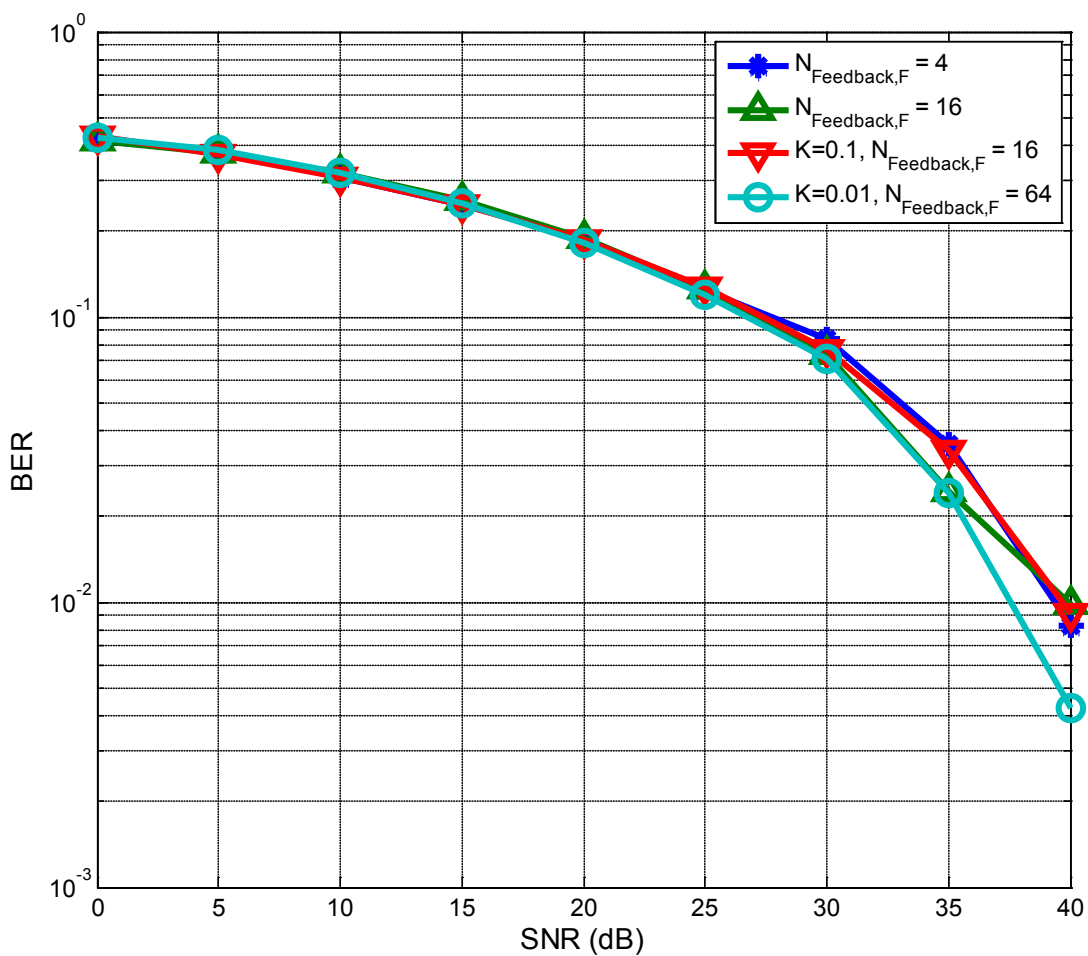


Figure 6.14: BER Versus SNR for feedback reduction for $K = 0.1$ and doppler shift of 10 Hz with FR-HP_{0.5} for a 2x2 MIMO, 128 subcarrier OFDM system with IEEE 802.16m urban macrocell channel model, using 256 QAM constellation.

Figure 6.14 shows the BER versus SNR plots for FR-HP_{0.5} with feedback reduction and 256 QAM constellation. For a BER of 10^{-2} , $K = 0.01$, $N_{Feedback, F} = 64$ performs the best, requiring 37.5 dB, and $N_{Feedback, F} = 16$ has the worst performance, requiring 40 dB.

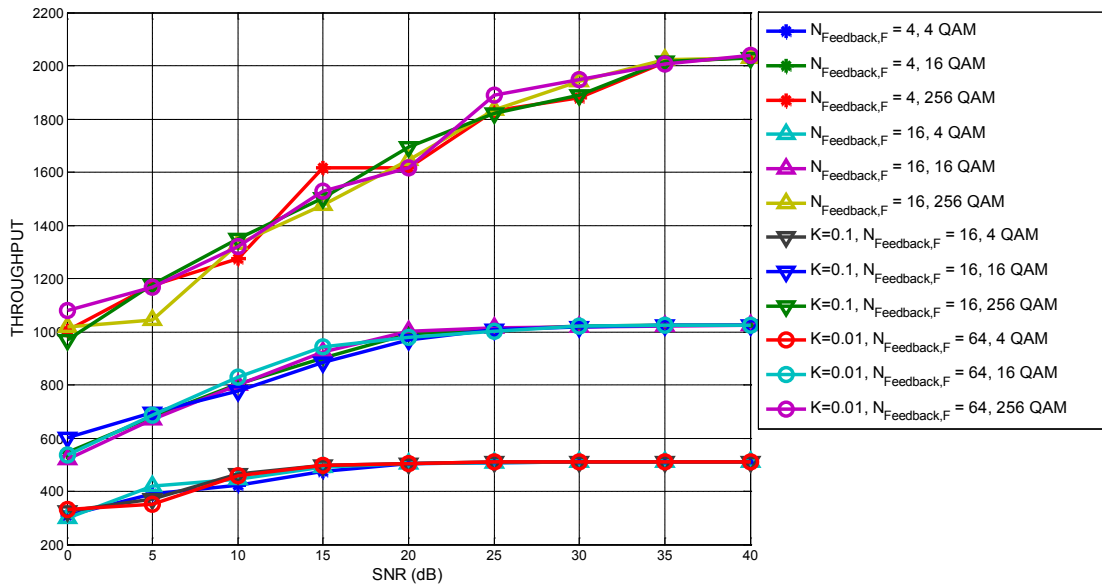


Figure 6.15: Throughput versus SNR for feedback reduction for $K = 0.1$ and doppler shift of 10 Hz with FR-HP_{0.5} for a 2x2 MIMO, 128 subcarrier OFDM system with IEEE 802.16m urban macrocell channel model.

Figure 6.15 shows the throughput versus SNR plots for FR-HP_{0.5} precoding with feedback reduction. At 15 dB and 4 QAM constellation, $N_{Feedback, F} = 4$ has a throughput of 425 bits per channel use, $N_{Feedback, F} = 16$ has a throughput of 445 bits per channel use, $K = 0.1$, $N_{Feedback, F} = 16$ has a throughput of 465 bits per channel use, while $K = 0.01$, $N_{Feedback, F} = 64$ has a throughput of 457 bits per channel use. For 16 QAM constellation, $K = 0.1$, $N_{Feedback, F} = 16$ performs the worst at 775 bits per channel use,

while $K = 0.01$, $N_{Feedback, F} = 64$ has the best performance, with a throughput of 830 bits per channel use.

CHAPTER 7

SCHEDULING

In this chapter, user scheduling will be discussed. Figure 1.14 shows the capacity CDF plots for a frequency correlated channel, versus a frequency independent channel. Due to uncorrelated subcarrier gains, the average capacity per subcarrier per channel use is close to the average subcarrier gain taken over multiple channel uses. This causes the capacity values to have a small variance. On the other hand, if the per subcarrier gains are correlated, the variance will be higher because all the subcarriers at any given time will have similar gain. Figure 1.15 shows the effect of greedy scheduling on the average capacity values, for different user set sizes. Here, the user with the highest capacity for a given subcarrier is allowed to transmit on that particular subcarrier. This technique of user scheduling is known as orthogonal frequency division multiple access (OFDMA) as

multiple users are allowed to transmit simultaneously over different subcarriers. As the subcarriers in an OFDM symbol are orthogonal to each other, there is no inter-user interference. Another multiple access method, as discussed in chapter 2, is multiuser precoding. In this scheme, users are assigned orthogonal spatial channels, instead of orthogonal subcarriers. In this scheme, multiple users can transmit on the same frequency, and the users are made orthogonal using precoding as described in chapter 2.

Figure 1.15 uses capacity as a criterion to choose the best user. Other such criteria have been studied in literature. In [8], different criteria have been defined, and are described as follows.

7.1 SCHEDULING CRITERIA

In this section, several user scheduling criteria are described. The following notation is used.

H_k is the k^{th} subcarrier MIMO Channel, A^H is HERMITIAN[A].

I. MaxMIMOCapc

Here, we find the MIMO capacity per user, and allow the user with maximum MIMO capacity to transmit.

$$k = \arg \max_{k=1,2,\dots,K} \left\{ \log_2 \left(\det \left(I_{M_R} + \frac{SNR}{N_T} * H_k H_k^H \right) \right) \right\}. \quad (7.1)$$

II. Max SNR

This criterion is similar to the Maximum SNR criteria of SISO systems.

$$\text{MIMO Channel Power} = \text{trace}(H_k H_k^H) \cdot \quad (7.2)$$

The user with the Maximum Channel Power is chosen.

III. Minimum Eigen Spread

This criterion checks for channel matrix orthogonality. A matrix is said to be more orthogonal if its eigen spread is smaller. An orthogonal channel matrix implies linearity, which means that the channel will affect all frequency components the same way.

IV. Minimum Singular Value

This criterion finds the user channel with the maximum value for the minimum singular value.

The above criteria are used in conjunction with one of the scheduling algorithms, namely, ORR, Greedy and PF, to choose which users would be allowed to transmit. For OFDMA, the procedure is simple. First, the scheduling parameter is calculated for each subcarrier and each user. Then users are selected according to the scheduling algorithm being used. Each user gets to communicate over just one subcarrier at any given time.

For multiuser precoding, however, multiple users transmit on the same frequency. Therefore, after calculating the scheduling parameter for each user, the best ‘N’ users need to be chosen from a larger set of users. ‘N’ is the maximum users that can communicate at any given time over the same frequency. If the number of antennas per user is N_R and the number of transmit antennas at the base station (BS) are M_T , then

$$N = \left\lfloor \frac{M_T}{N_R} \right\rfloor, M_T > N_R. \quad (7.3)$$

Once N users have been selected using one of the criteria and using a scheduling algorithm, multiuser precoding can be performed. Here, another problem arises. The users can first be selected and then orthogonalized, that is, users are scheduled before orthogonalization, or users are first orthogonalized and then scheduling is done, that is, orthogonalization before scheduling. Both these scenarios are studied here through simulation results.

In a realistic channel model, the channel is correlated in time. This implies that a user that has a ‘good’ channel will have a good channel for some period of time. This causes a fairness issue, where a user with a good channel could be selected to communicate multiple times consecutively, thereby being unfair to the other users. On the other hand, if users are allowed to transmit in RR fashion, that is, one after another, there will be no multi-user gain seen in performance. This point is illustrated in the Figure 7.1. In the figure, the CDF plots for a 4x4 MIMO channel using waterfilling algorithm, with an SNR of 10dB, is shown. The green curves are CDF curves for capacity values for each user, that is, each user has one green CDF curve. The mean capacity CDF curve is shown as a thick red curve, while the user with the least and highest mean capacity are shown as thin red and black curves. The total number of users is 100. The figure (a) shows the CDF plots for users’ channels that are uncorrelated in time. It can be seen that all the users’ capacity CDF curves are close to the mean capacity curve. This implies that the mean capacity of each user, at any given SNR, is more or less constant. The figure (b) shows capacity CDF curves for a time correlated channel, with a doppler shift of 50 Hz. Here it

can be seen that the CDF plots of the users, shown in green, are more spread out, thereby causing one user to have a very good channel throughout, whose CDF curve is shown in black. The user with the least mean capacity will have a bad channel, and therefore, would not be able to use the channel to communicate much if users are scheduled using the greedy algorithm. Therefore, scheduling algorithms such as ORR and PF gain significance because they allow relatively high fairness amongst users.

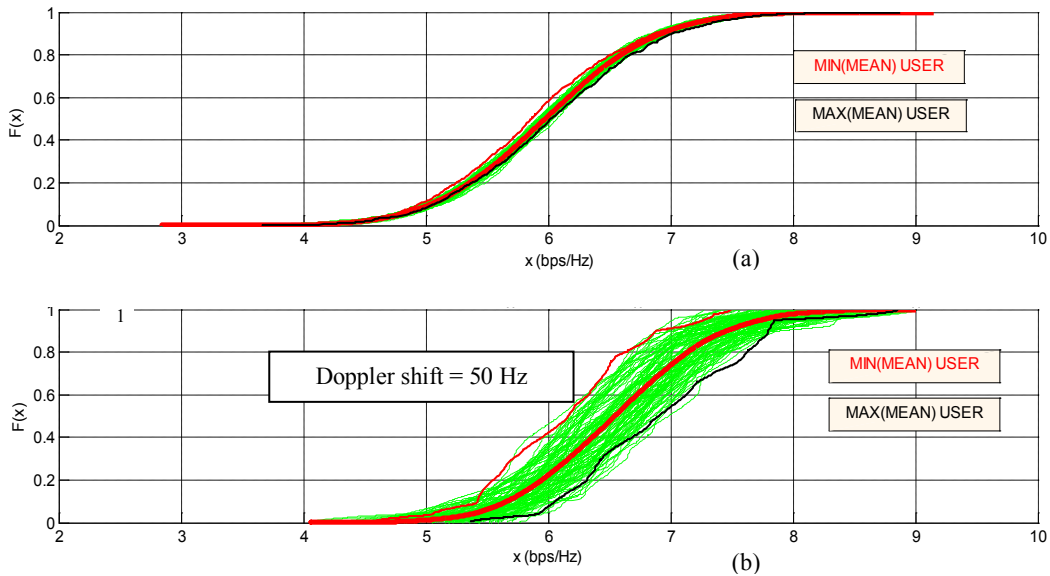


Figure 7.1: Capacity CDF plot for time uncorrelated (a) and time correlated (b) channels, with round robin scheduling for a 2x2 MIMO, 128 subcarrier OFDM system with IEEE 802.16m urban macrocell channel model.

7.2 USER SELECTION FAIRNESS

The user scheduling criterion and scheduling algorithms need to be fair in their selection of users, such that all users get to transmit over a period of time. Allowing best user to transmit all the time will produce optimal performance, but this would be unfair to other

users whose channel is highly attenuated. In order to visually gauge how fair a user selection procedure is, the probability density functions (PDFs) for various combinations of scheduling criteria and scheduling algorithms are shown below. The channel model is a 2x2 MIMO, 128 subcarrier OFDMA system, with user scheduling performed on a per subcarrier basis. The channel model used is the urban macrocell channel model. A doppler shift of 350 Hz is assumed. The channel is assumed to be spatially correlated, with transmitter antenna spacing of 4 wavelengths and the receiver antenna spacing of 0.5 wavelengths. A sampling frequency of 1 MHz is assumed.

Using (6.1), the number of OFDM symbols transmitted per coherence time, N_C , is calculated to be 22.3214. The number of observations taken for the PDF data is a multiple of N_C . For instance, for 100 coherence times, the number of OFDM symbols considered part of the observations would be $\lceil N_C * 100 \rceil = 2232$ OFDM symbols. By taking different multiples of N_C as observations, the effect of time correlation on user scheduling can be studied. Total number of users is 5. For fair scheduling, the probability of a user being selected should be equal. This means, for 5 users, each user should have a probability of selection of $1/5 = 0.2$. Deviation from this value would mean that the given scheduling criterion and algorithm are not fair. In the following figures, PDFs are calculated using channel instances over 10 coherence times, and 100 coherence times. Asymptotically, all scheduling algorithms would be fair, assuming that the channel is fading, and the coherence time of the channel is small relative to the time over which channel data is collected and scheduling is done based on the collected data. The reason is that, over a period of time much longer than the coherence time, each user's channel

would have varied enough such that all users would have an equal chance of being selected during scheduling. In the short term, however, it is unlikely that the channel of all users would be able to vary enough such that all users could get a chance to transmit. Therefore, the short term PDFs (that is, 10 coherence times) are shown along with long term PDFs (that is, 100 coherence times) in order to gauge the fairness performance of a scheduling algorithm in both scenarios.

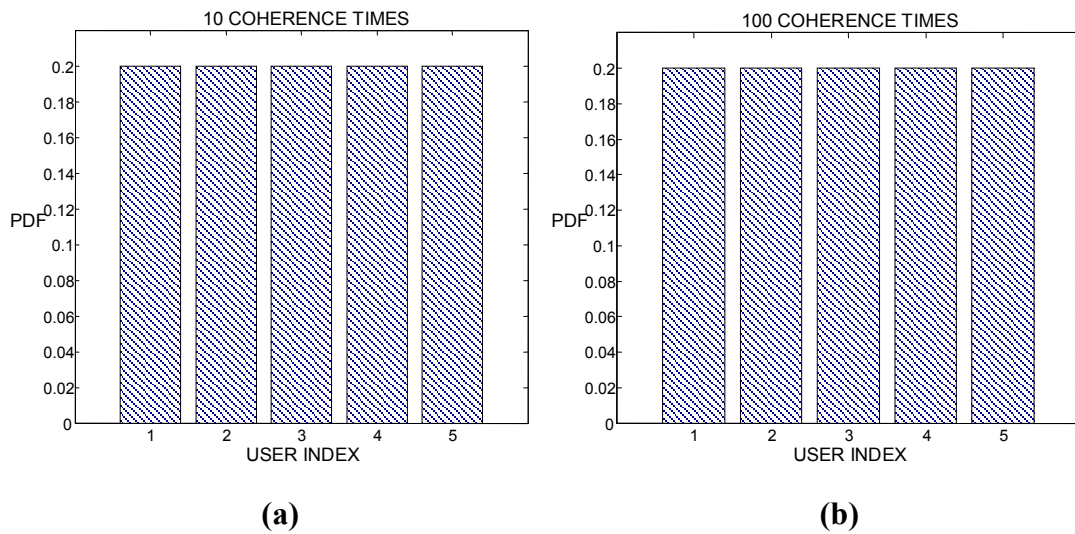
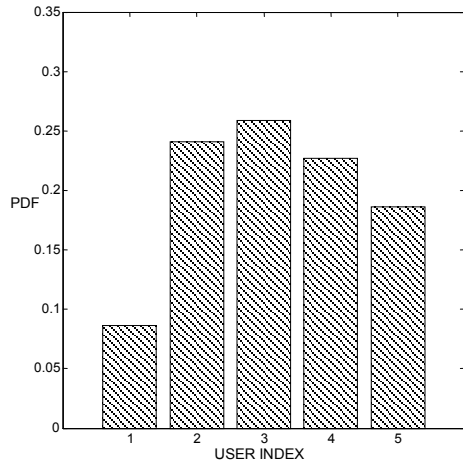


Figure 7.2: PDF for user scheduling using ORR scheduling algorithm and MaxMIMOCapc scheduling criterion, with 10 coherence times (a) and 100 coherence times (b) considered.

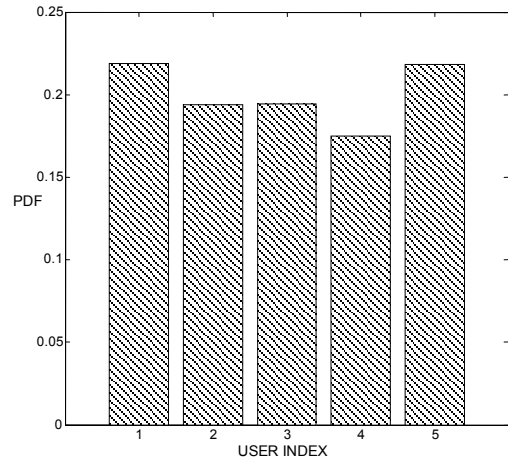
Figure 7.2 shows the PDF plots for ORR scheduling with MaxMIMOCapc criterion. It can be seen that both short term and long term PDFs quickly converge, thereby being fair even in the short term. Comparing this result with Figure 7.3 and Figure 7.4, it can be seen that although the long term PDFs are close to being fair, in the short term, one user is allowed to transmit more often than others. For example, for Greedy scheduling, user 1 is allowed to transmit less than 10% of the 10 coherence times taken into consideration. In

PF scheduling, it is user 3 that is left out, and has been scheduled just 10% of the time. In the short term, the difference in probability of being selected between the most scheduled and the least scheduled user for Greedy scheduling is 17.26%, and for PF scheduling this difference is 17.70%. In the long term, this difference has reduced to 4.4% and 3.7%, respectively.

Figure 7.5 and Figure 7.8 show the PDF for ORR scheduling for MaxMinSV and MaxSNR criteria, respectively. The PDFs show that ORR has perfect fairness for these scheduling criteria as well. In the short term for MaxMinSV criterion, the difference in probability of being selected between the most scheduled and the least scheduled user for Greedy scheduling is 10.5%, and for PF scheduling this difference is 7.3%. In the long term, this difference has reduced to 5.8% and 4.8%, respectively. In the short term for MaxSNR, the difference in probability of being selected between the most scheduled and the least scheduled user for Greedy scheduling is a whopping 25.04%, and for PF scheduling this difference is 17.71%. In the long term, this difference has reduced to 4.6% and 4.3%, respectively.

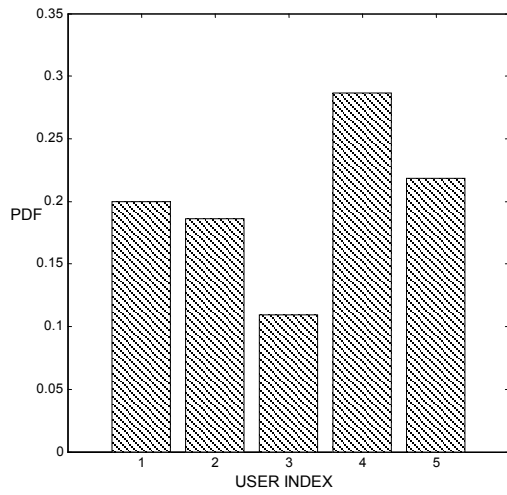


(a)

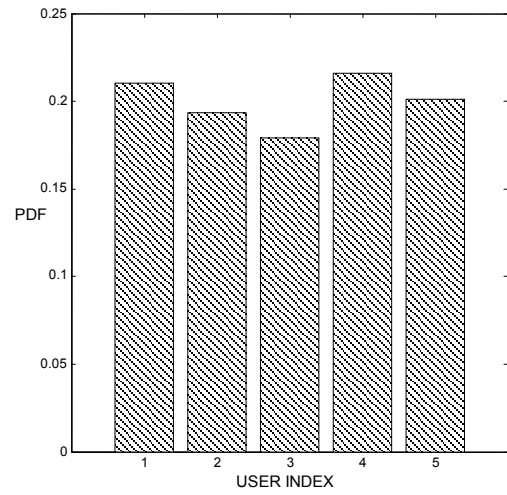


(b)

Figure 7.3: PDF for user scheduling using greedy scheduling algorithm and MaxMIMOCapc scheduling criterion, with 10 coherence times (a) and 100 coherence times (b) considered.

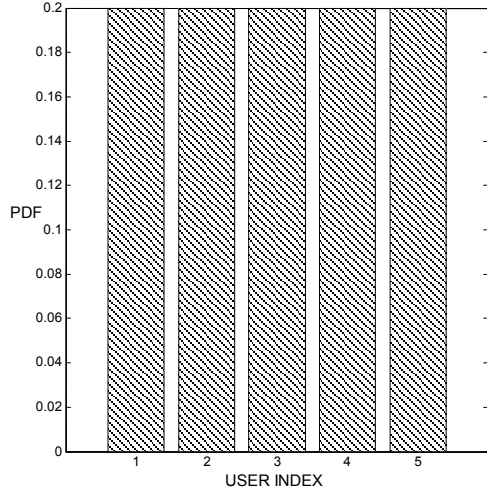


(a)

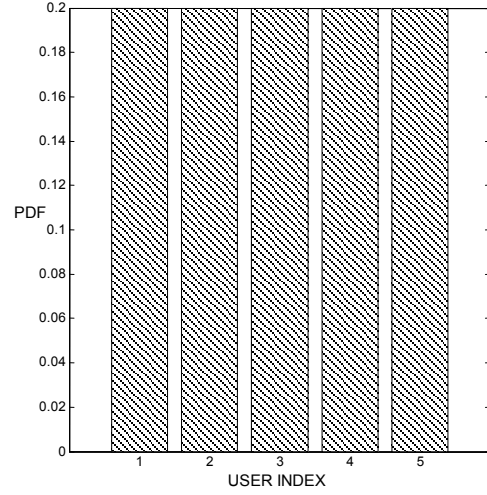


(b)

Figure 7.4: PDF for user scheduling using PF scheduling algorithm and MaxMIMOCapc scheduling criterion with 10 coherence times (a) and 100 coherence times (b) considered.

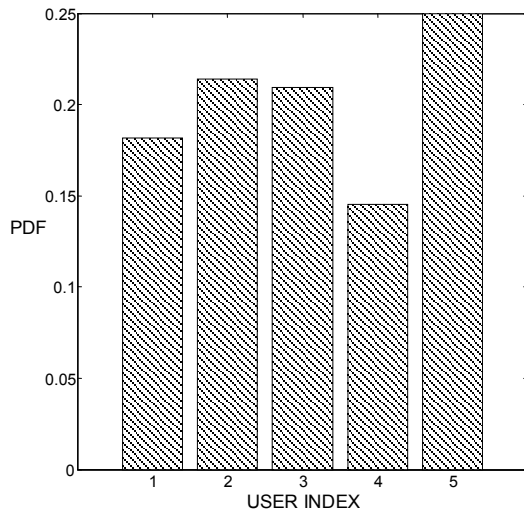


(a)

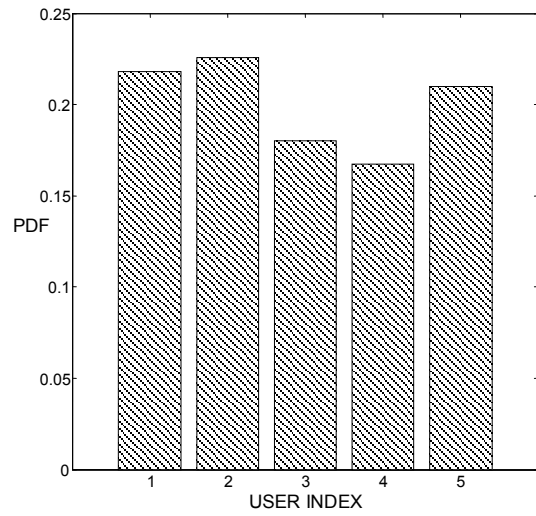


(b)

Figure 7.5: PDF for user scheduling using ORR scheduling algorithm and MaxMinSV scheduling criterion with 10 coherence times (a) and 100 coherence times (b) considered.



(a)



(b)

Figure 7.6: PDF for user scheduling using greedy scheduling algorithm and MaxMinSV scheduling criterion with 10 coherence times (a) and 100 coherence times (b) considered.

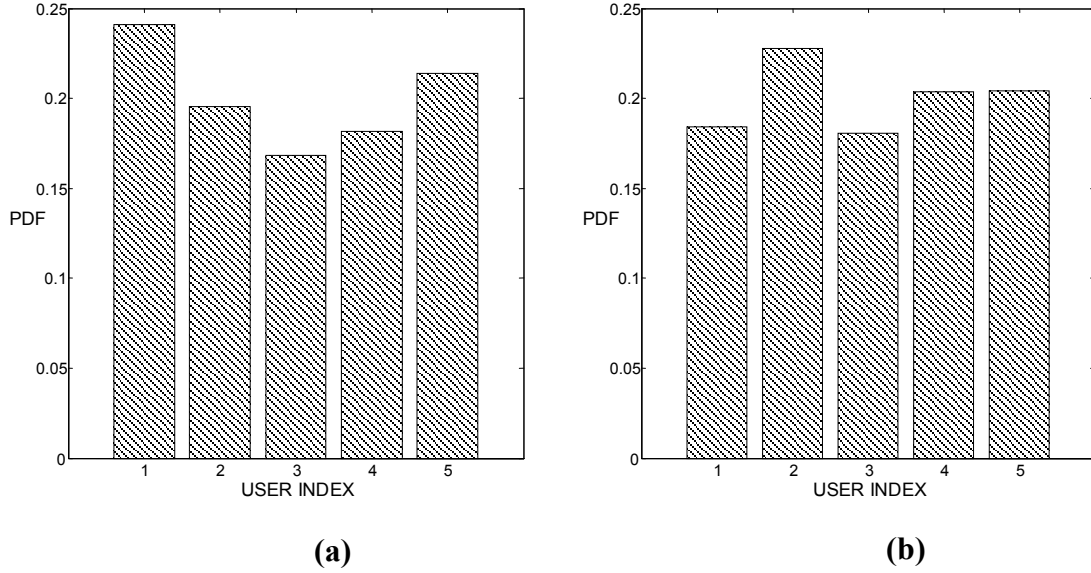


Figure 7.7: PDF for user scheduling using PF scheduling algorithm and MaxMinSV scheduling criterion with 10 coherence times (a) and 100 coherence times (b) considered.

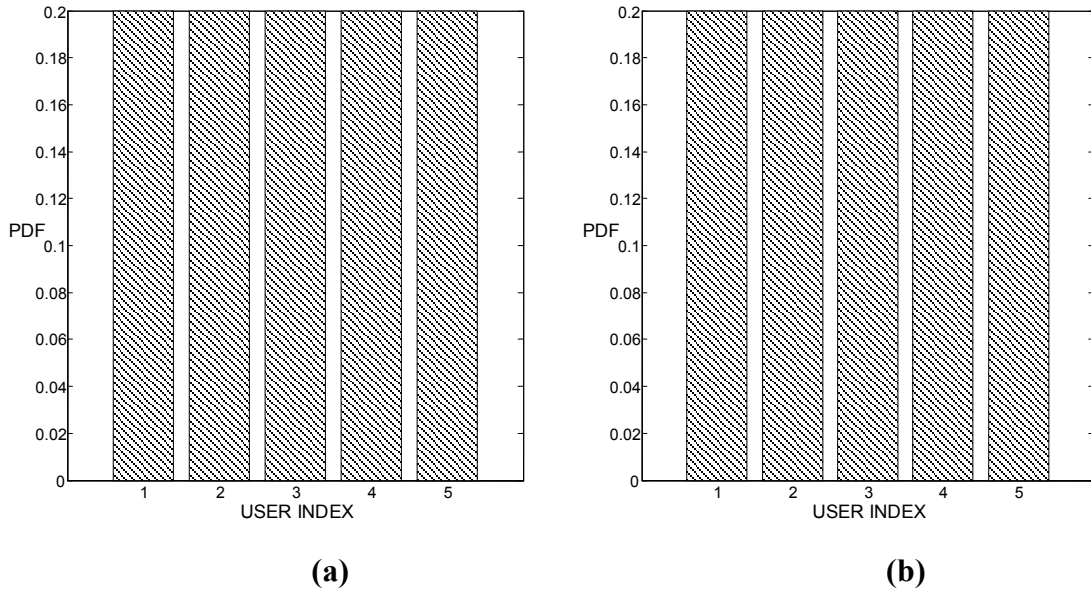
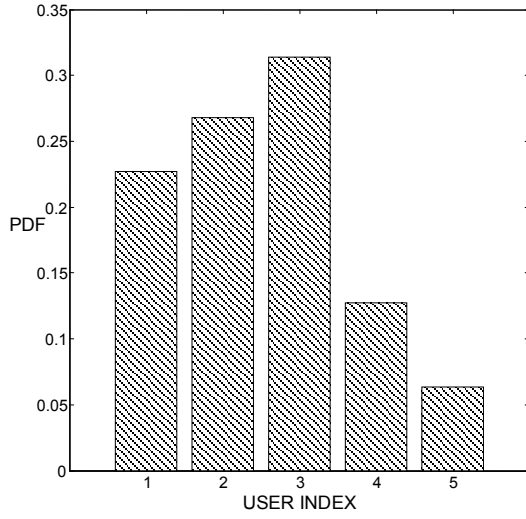
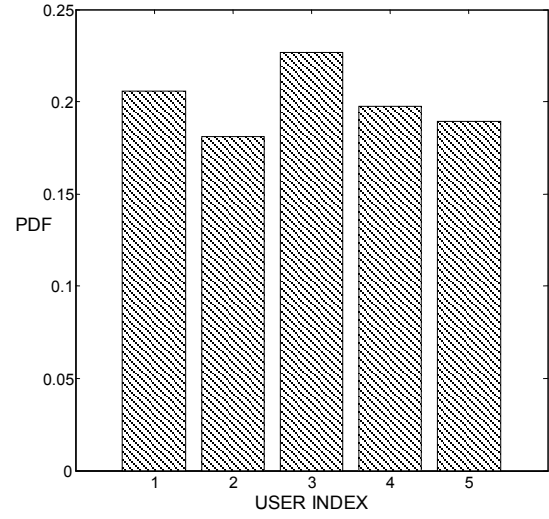


Figure 7.8: PDF for user scheduling using ORR scheduling algorithm and MaxSNR scheduling criterion with 10 coherence times (a) and 100 coherence times (b) considered.

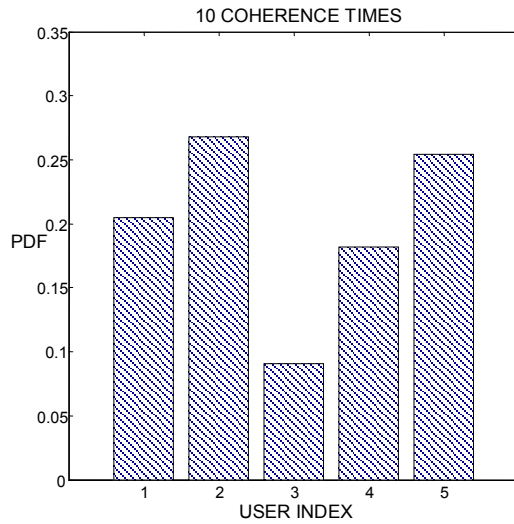


(a)

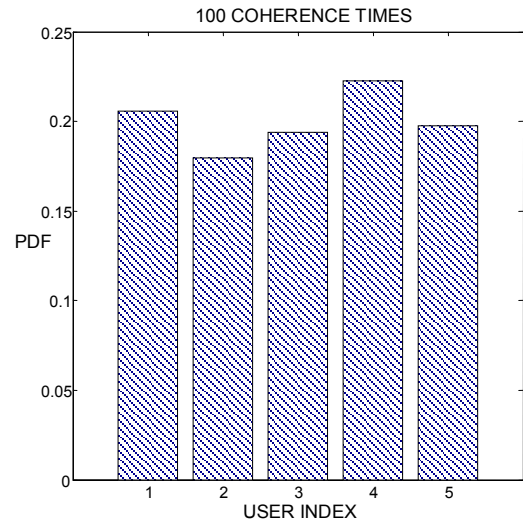


(b)

Figure 7.9: PDF for user scheduling using greedy scheduling algorithm and MaxSNR scheduling criterion with 10 coherence times (a) and 100 coherence times (b) considered.



(a)



(b)

Figure 7.10: PDF for user scheduling using PF scheduling algorithm and MaxSNR scheduling criterion with 10 coherence times (a) and 100 coherence times (b) considered.

SIMULATION RESULTS

The following results are for a 2x2 MIMO, 128 subcarrier OFDMA system configuration with user scheduling. The total number of users is chosen to be 5. The channel model used is the urban macrocell channel model. Input symbol rate is taken to be 10^6 symbols/s, and the sampling rate is 1 MHz. The channel is assumed to be spatially correlated, with transmitter antenna spacing of 4 wavelengths and the receiver antenna spacing of 0.5 wavelengths. The channels are assumed to be correlated in time, and the doppler shift is taken to be 350Hz.

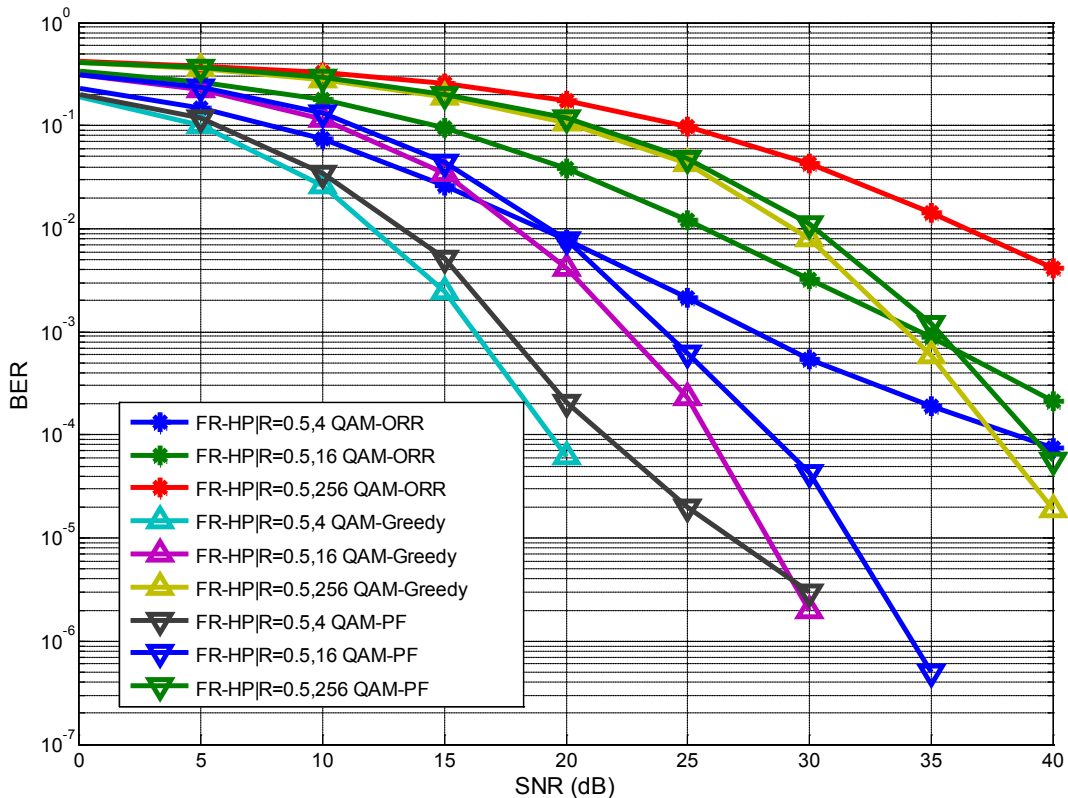


Figure 7.11: BER versus SNR for FR-HP_{0.5} with user scheduling with 5 users and MaxMIMOCapc scheduling criterion, for a 2x2 MIMO, 128 subcarrier OFDM system with IEEE 802.16m urban macrocell channel model.

Figure 7.11 shows the BER Versus SNR performance of MaxMIMOCapc criterion for FR-HP_{0.5} precoding with ORR, Greedy and PF scheduling, respectively. It can be seen from the plots that Greedy scheduling produces the best results for MaxMIMOCapc criterion. For 4-QAM constellation, SNR required for a BER of 10^{-3} is as follows. ORR requires 27.75 dB, Greedy requires 16.25 dB, while PF requires 17.5 dB. It can be seen that Greedy performs the best amongst all the scheduling algorithms, closely followed by PF.

Figure 7.12 shows BER Versus SNR performance for C-HP₂ precoding. Greedy scheduling performs the best, although PF scheduling BER performance is very close to it.

For a BER of 10^{-3} and 4 QAM constellation, ORR requires 30dB SNR, Greedy requires 17.4dB, while PF scheduling requires 17.9dB.

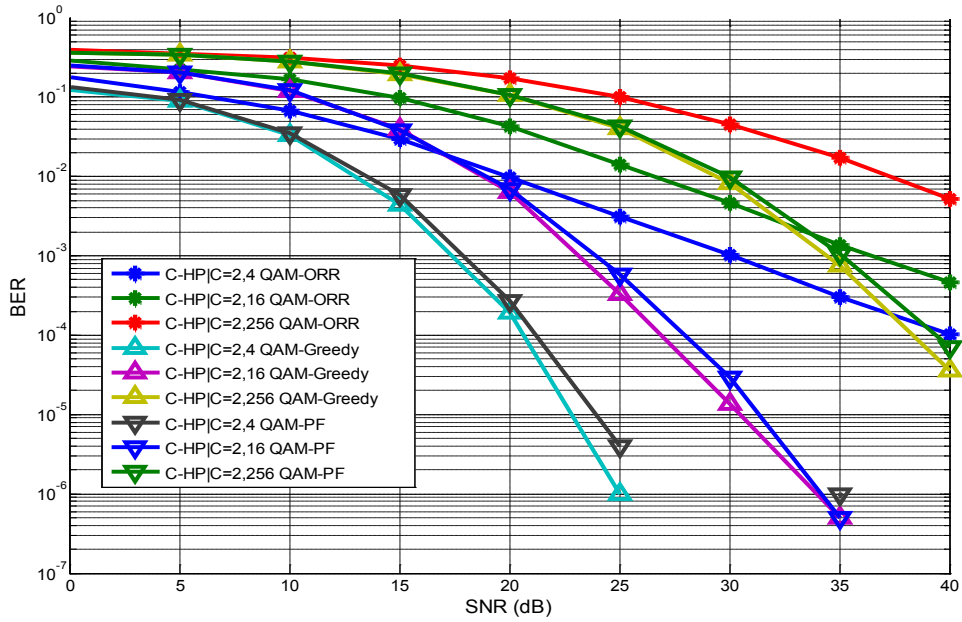


Figure 7.12: BER versus SNR for C-HP₂ with user scheduling with 5 users and MaxMIMOCapc scheduling criterion, for a 2x2 MIMO, 128 subcarrier OFDM system with IEEE 802.16m urban macrocell channel model.

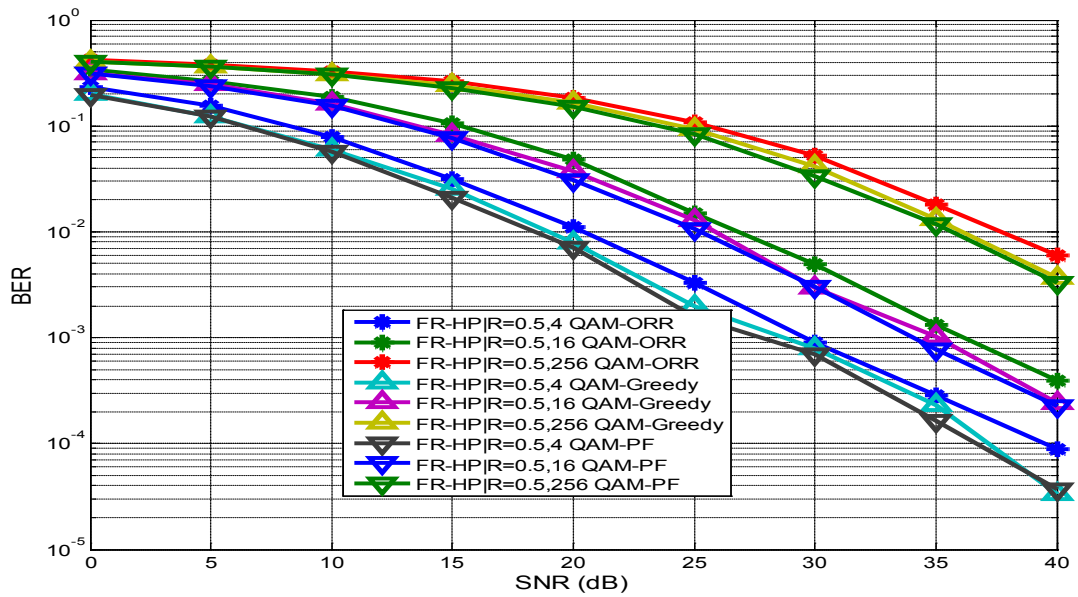


Figure 7.13: BER versus SNR for FR-HP_{0.5} with user scheduling with 5 users and MaxSNR scheduling criterion, for a 2x2 MIMO, 128 subcarrier OFDM system with IEEE 802.16m urban macrocell channel model.

Figure 7.13 shows the BER Versus SNR performance for the scheduling criterion MaxSNR, for FR-HP_{0.5} precoding. It can be seen that PF algorithm performs the best for all constellations. For a BER of 10⁻³ and constellation 5-QAM, there is an SNR gain of 2.5 dB over ORR. It's the same case in Figure 7.14, where C-HP₂ precoding is used. It can be seen that PF performs as well as Greedy scheduling across all SNRs. Figure 7.14 shows BER Versus SNR curves for C-HP₂ precoding. Here, too PF performs better than the rest of the scheduling algorithms.

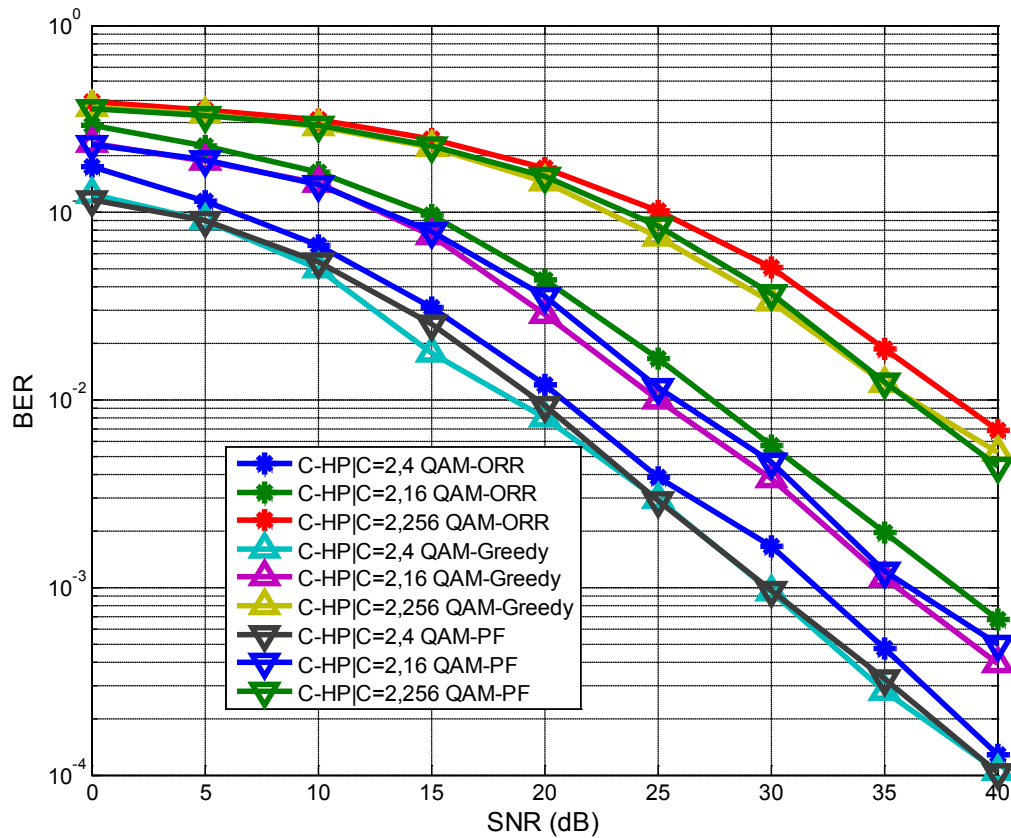


Figure 7.14: BER versus SNR for C-HP₂ with user scheduling with 5 users and MaxSNR scheduling criterion, for a 2x2 MIMO, 128 subcarrier OFDM system with IEEE 802.16m urban macrocell channel model.

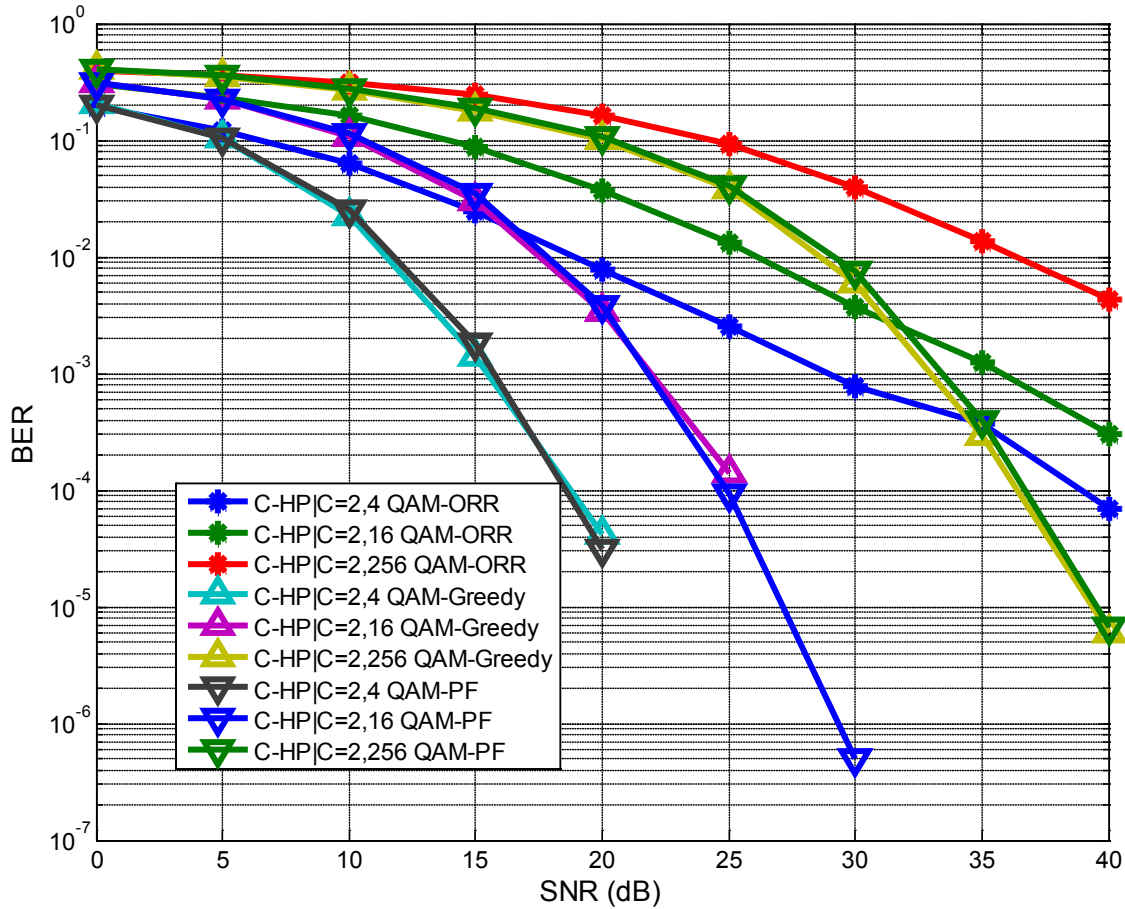


Figure 7.15: BER versus SNR for C-HP₂ with user scheduling with 5 users and MaxMinSV scheduling criterion, for a 2x2 MIMO, 128 subcarrier OFDM system with IEEE 802.16m urban macrocell channel model.

Figure 7.15 shows BER Versus SNR performance for C-HP₂ precoding and scheduling criterion MaxMinSV. It can be seen that Greedy and PF scheduling are virtually identical across all SNRs. ORR performance is the worst amongst the scheduling algorithm. Figure 7.16 shows BER Versus SNR performance for FR-HP_{0.5} for MaxMinSV scheduling criterion. Here, too, PF and Greedy perform the best.

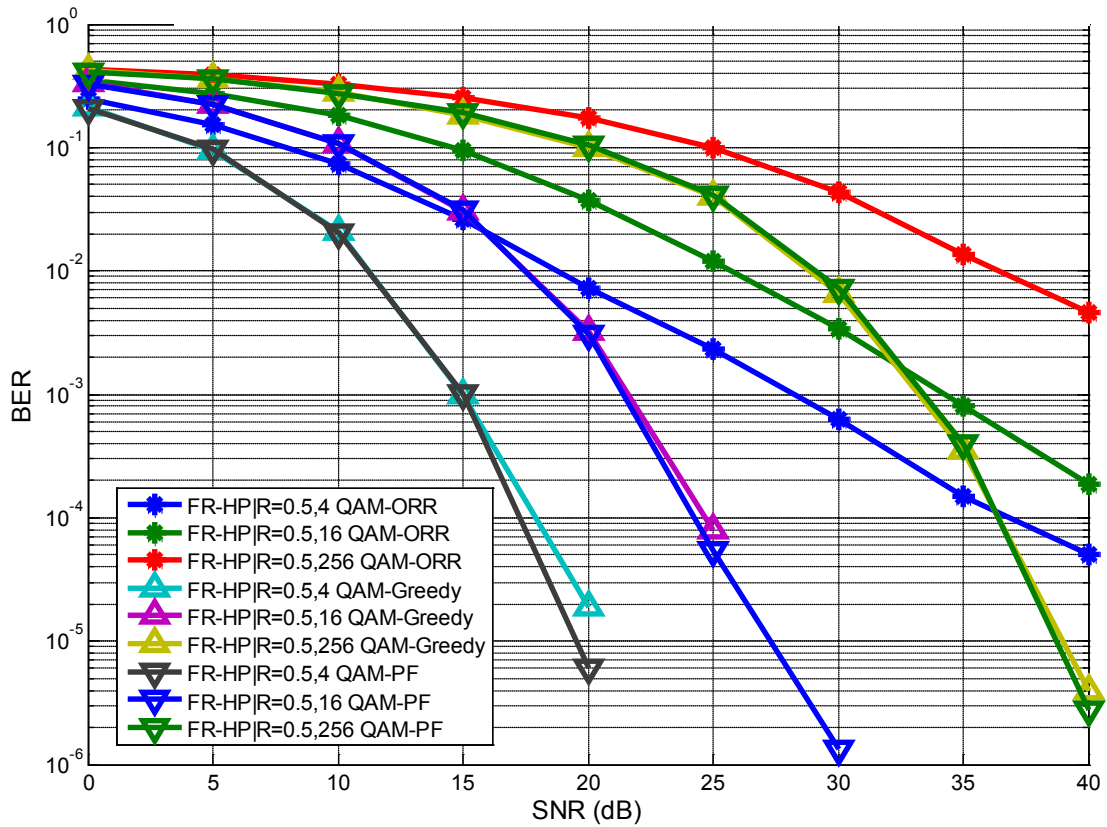


Figure 7.16: BER versus SNR for FR-HP_{0.5} with user scheduling with 5 users and MaxMinSV scheduling criterion, for a 2x2 MIMO, 128 subcarrier OFDM system with IEEE 802.16m urban macrocell channel model.

Figure 7.17 and Figure 7.18 show the BER versus SNR performance curves for FR-HP_{0.5} and C-HP₂, respectively. ORR performance is the worst, while PF and Greedy scheduling perform virtually identically across all SNRs.

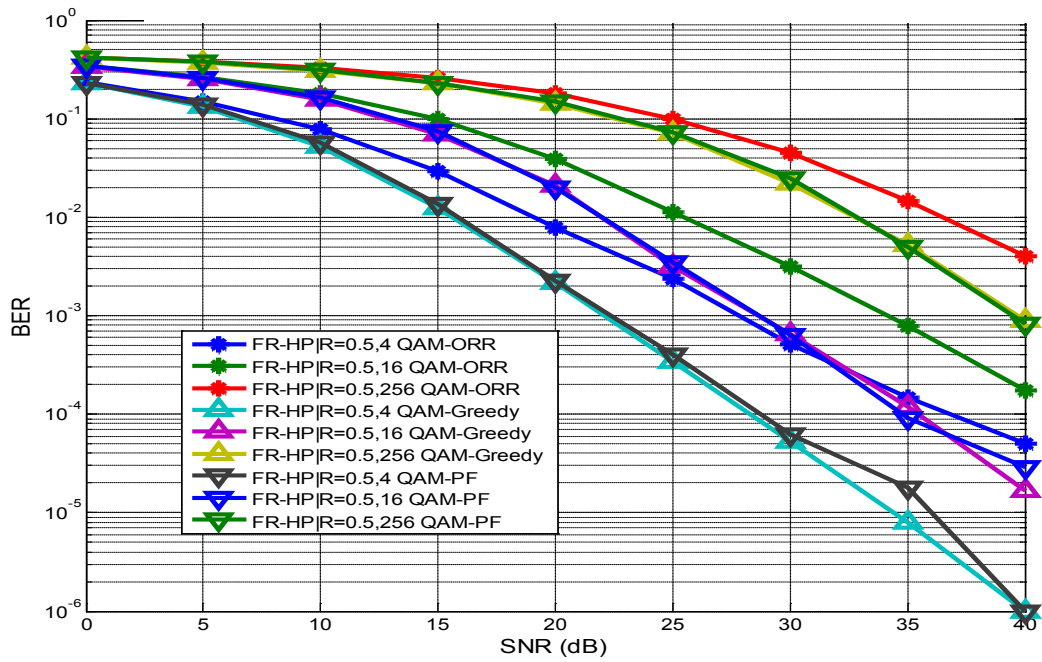


Figure 7.17: BER versus SNR for FR-HP_{0.5} with user scheduling with 5 users and MinES scheduling criterion, for a 2x2 MIMO, 128 subcarrier OFDM system with IEEE 802.16m urban macrocell channel model.

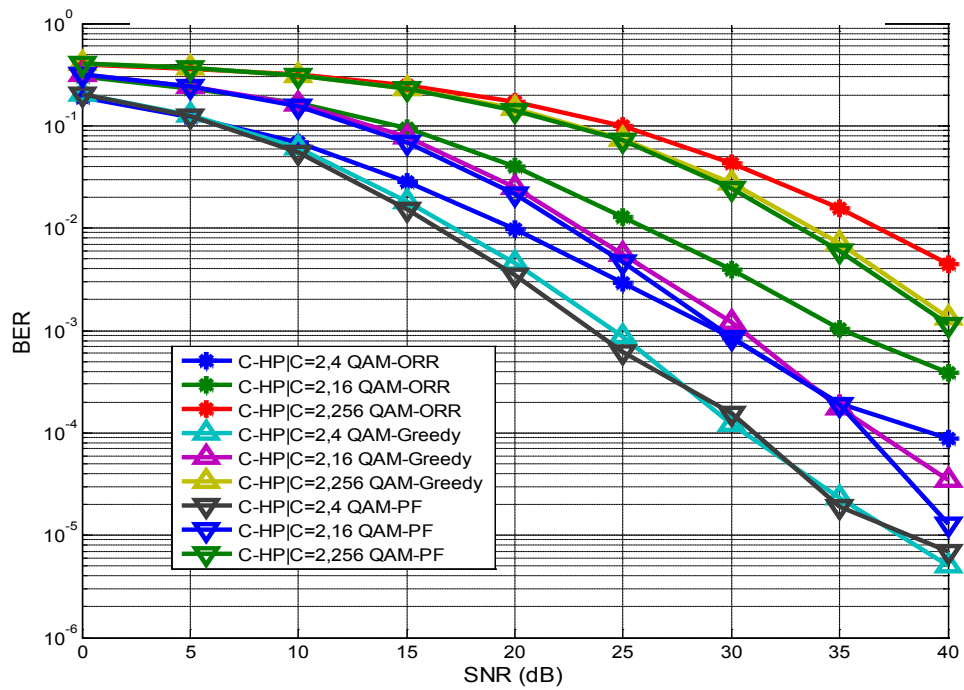


Figure 7.18: BER versus SNR for C-HP₂ with user scheduling with 5 users and MinES scheduling criterion, for a 2x2 MIMO, 128 subcarrier OFDM system with IEEE 802.16m urban macrocell channel model.

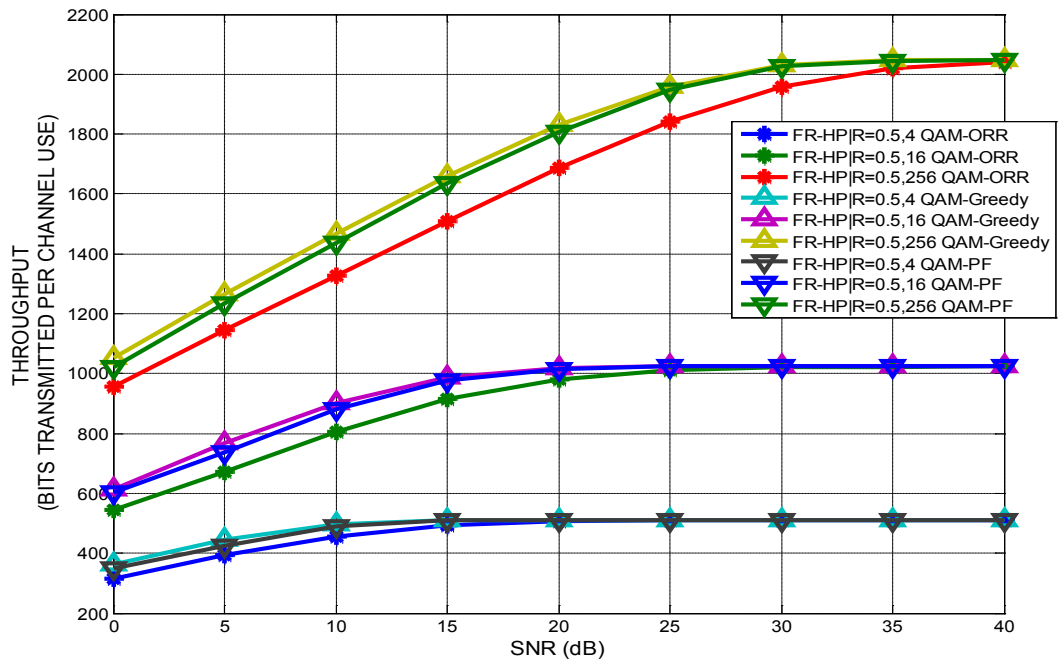


Figure 7.19: Throughput versus SNR for FR-HP_{0.5} with user scheduling with 5 users and MaxMIMOCapc scheduling criterion, for a 2x2 MIMO, 128 subcarrier OFDM system with IEEE 802.16m urban macrocell channel model.

Figure 7.19 and Figure 7.20 show throughput versus SNR curves for FR-HP_{0.5} and C-HP₂, respectively, for MaxMIMOCapc criterion. For FR-HP_{0.5}, ORR performs the worst. For 256 QAM at 10 dB, the throughput difference between ORR and Greedy is about 139 bits/channel use. This gap, however, reduces as SNR increases, and is virtually non-existent for 4-QAM and 16-QAM beyond 20dB. For C-HP₂, the throughput difference between ORR and Greedy for 256 QAM at 10dB is 179 bits/channel use.

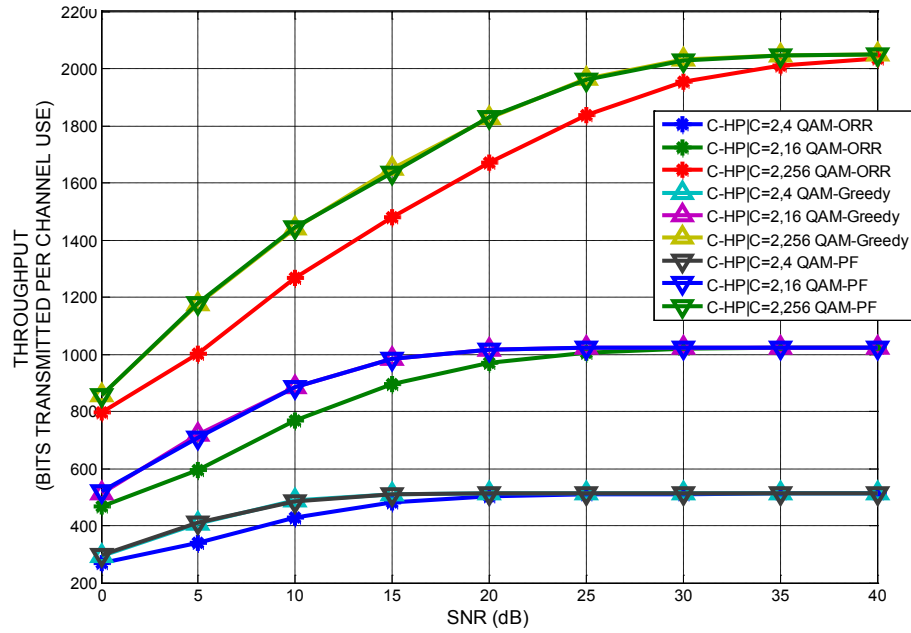


Figure 7.20: Throughput versus SNR for C-HP₂ with user scheduling with 5 users and MaxMIMOCap scheduling criterion, for a 2x2 MIMO, 128 subcarrier OFDM system with IEEE 802.16m urban macrocell channel model.

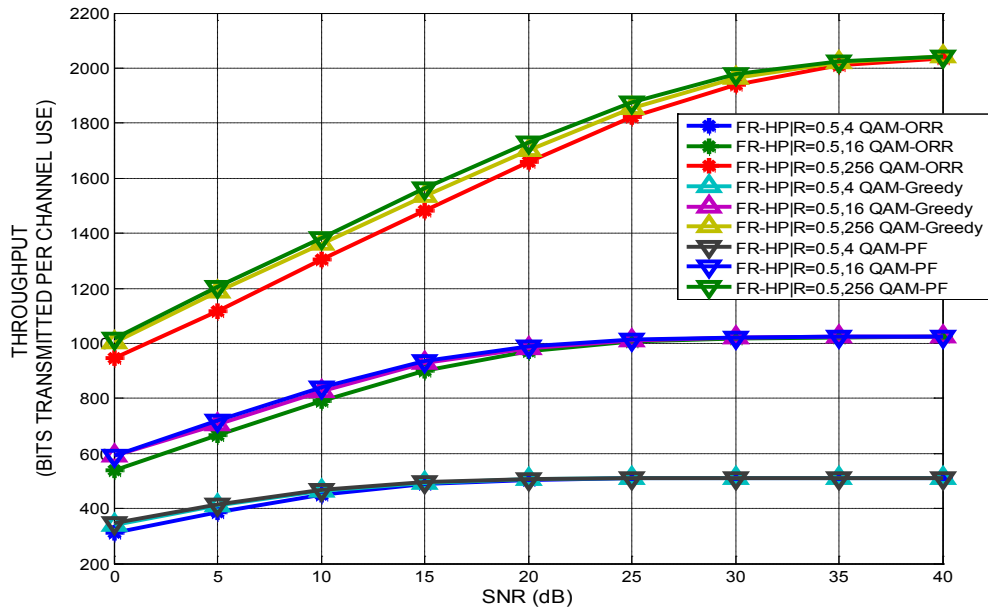


Figure 7.21: Throughput versus SNR for FR-HP_{0.5} with user scheduling with 5 users and MaxSNR scheduling criterion, for a 2x2 MIMO, 128 subcarrier OFDM system with IEEE 802.16m urban macrocell channel model.

shows throughput versus SNR curves for FR-HP_{0.5} for MaxSNR criterion. Here, PF performs the best, with an SNR gain of 2.5 dB for a throughput of 1200 bits/channel use between ORR and PF scheduling algorithms, for 256 QAM constellation. This gain reduces as the SNR increases, but PF performance is the best across all SNRs. Figure 7.22 shows throughput versus SNR curves for C-HP₂. Here, Greedy scheduling performs better, although marginally better than PF, across all SNRs.

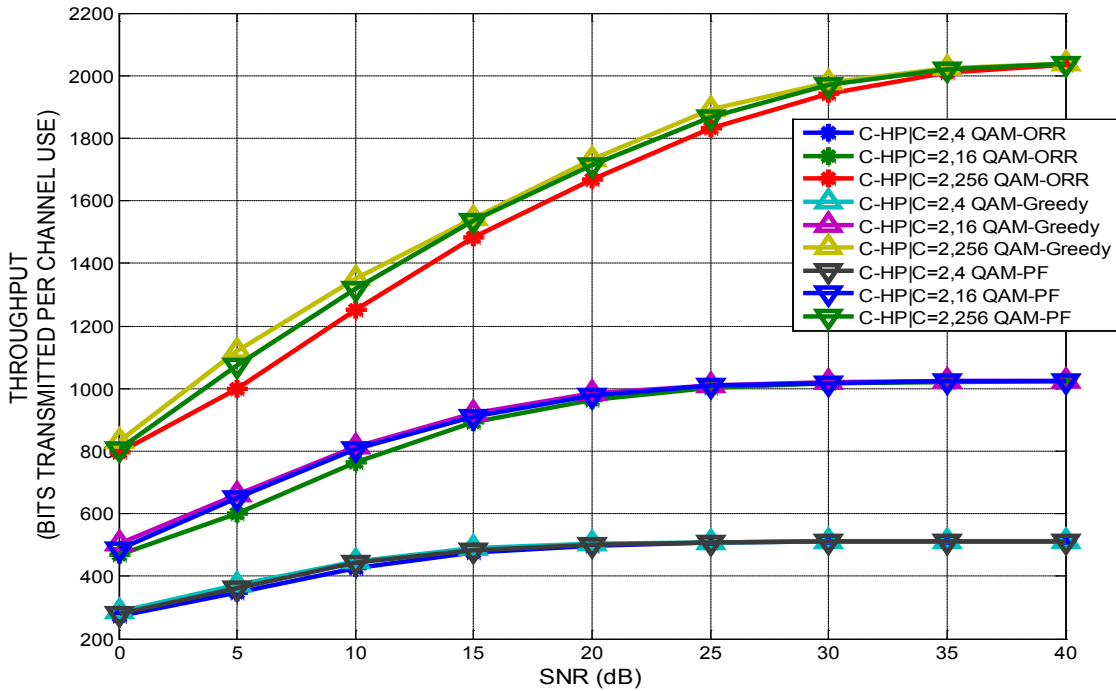


Figure 7.22: Throughput versus SNR for C-HP₂ with user scheduling with 5 users and MaxSNR scheduling criterion, for a 2x2 MIMO, 128 subcarrier OFDM system with IEEE 802.16m urban macrocell channel model.

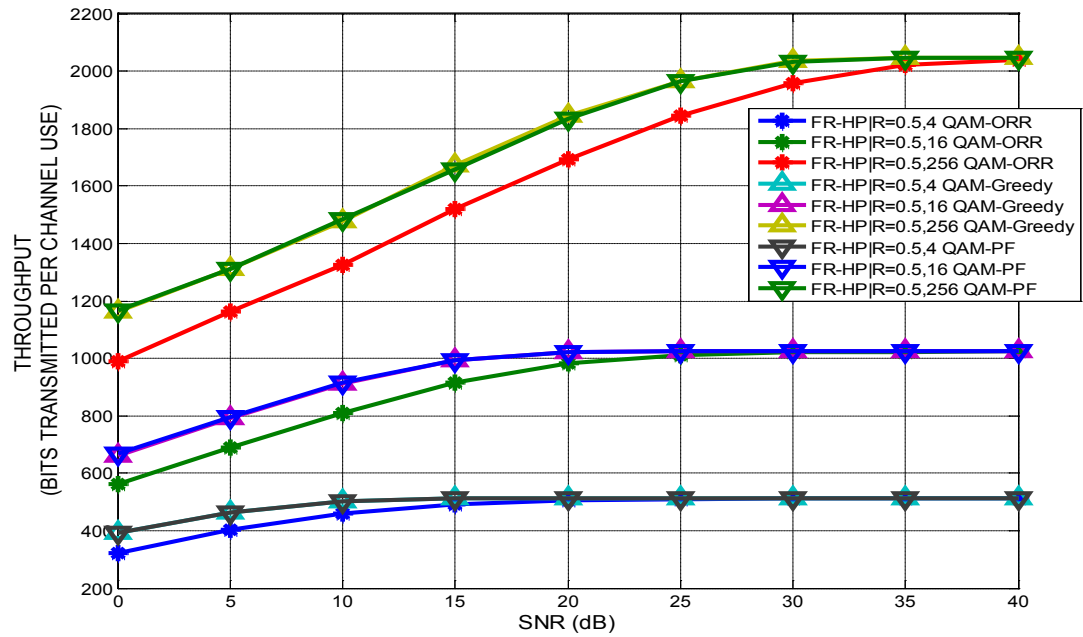


Figure 7.23: Throughput versus SNR for FR-HP_{0.5} with user scheduling with 5 users and MaxMinSV scheduling criterion, for a 2x2 MIMO, 128 subcarrier OFDM system with IEEE 802.16m urban macrocell channel model.

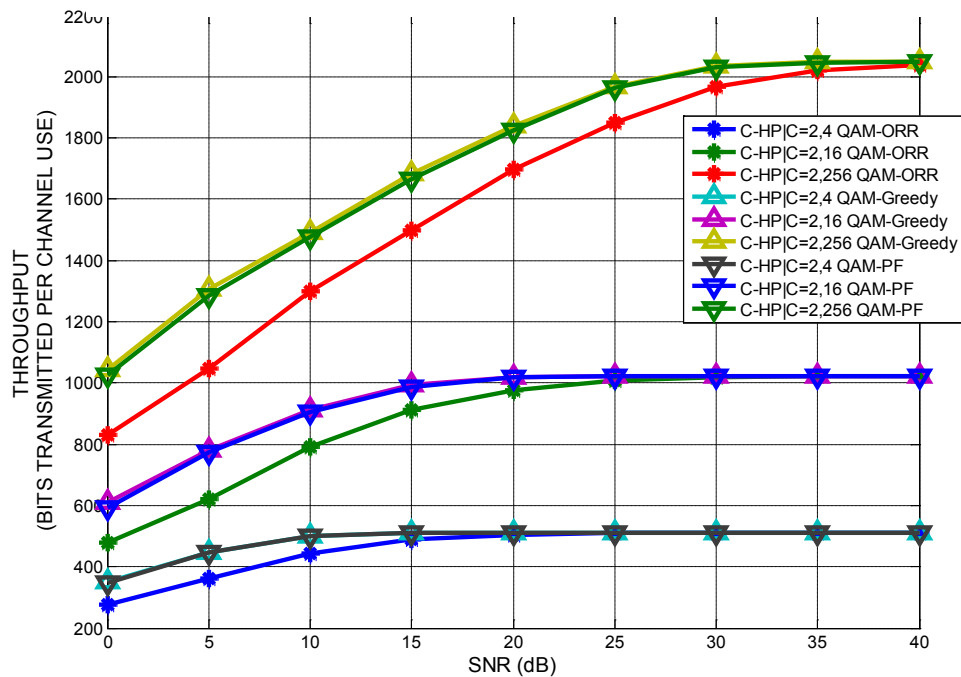


Figure 7.24: Throughput versus SNR for C-HP₂ with user scheduling with 5 users and MaxMinSV scheduling criterion, for a 2x2 MIMO, 128 subcarrier OFDM system with IEEE 802.16m urban macrocell channel model.

Figure 7.23 shows throughput versus SNR curves for MaxMinSV criterion, with FR-HP_{0.5} precoding. Here, PF and Greedy have the best performance, while ORR lags behind. At 10dB, the throughput gain for 256 QAM for PF over ORR scheduling is 180 bits/channel use. This gain, however, reduces as the SNR increases. Figure 7.24 shows throughput versus SNR performance for C-HP₂ precoding. ORR throughput performance is low compared to PF and Greedy, which are virtually identical.

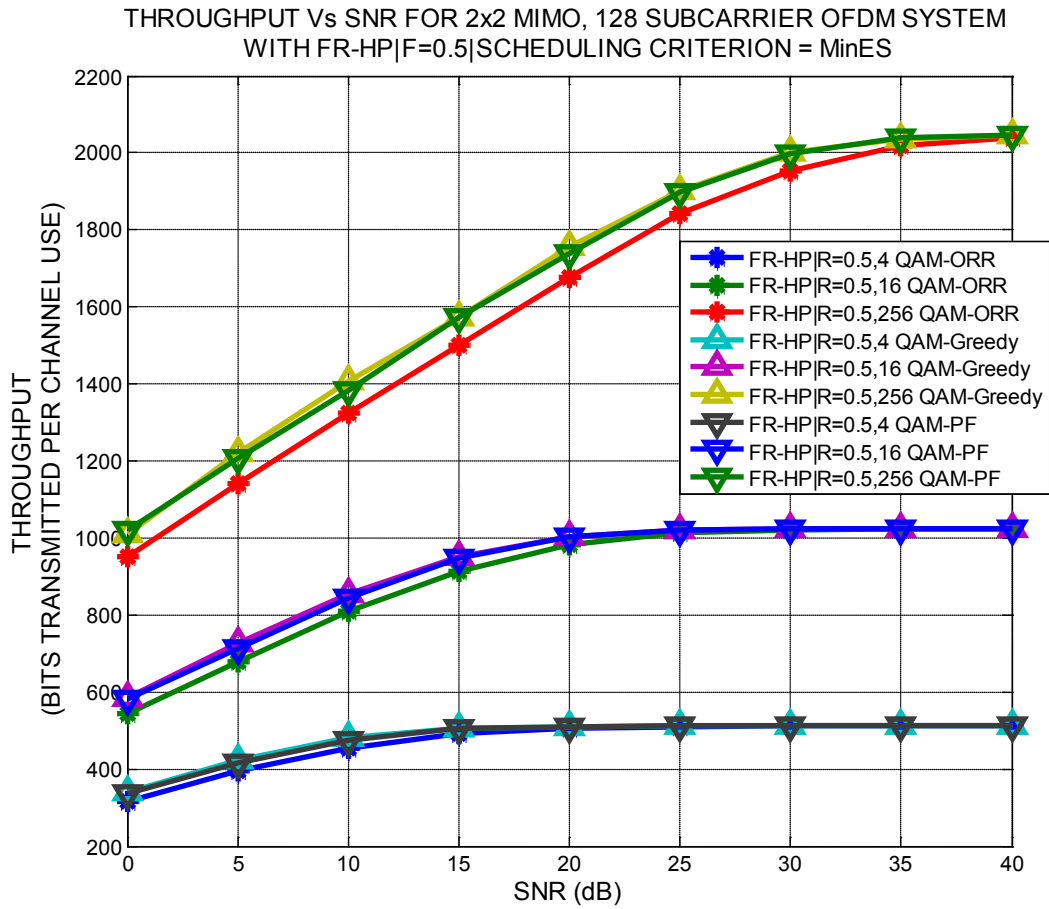


Figure 7.25: Throughput versus SNR for FR-HP_{0.5} with user scheduling with 5 users and MinES scheduling criterion, for a 2x2 MIMO, 128 subcarrier OFDM system with IEEE 802.16m urban macrocell channel model.

Figure 7.25 shows throughput versus SNR performance for FR-HP_{0.5} for user scheduling criterion MinES. Greedy scheduling performs marginally better than PF scheduling algorithm, and significantly better than ORR scheduling. Figure 7.26 shows throughput curves for C-HP₂. PF scheduling performs marginally better in this case compared to Greedy scheduling.

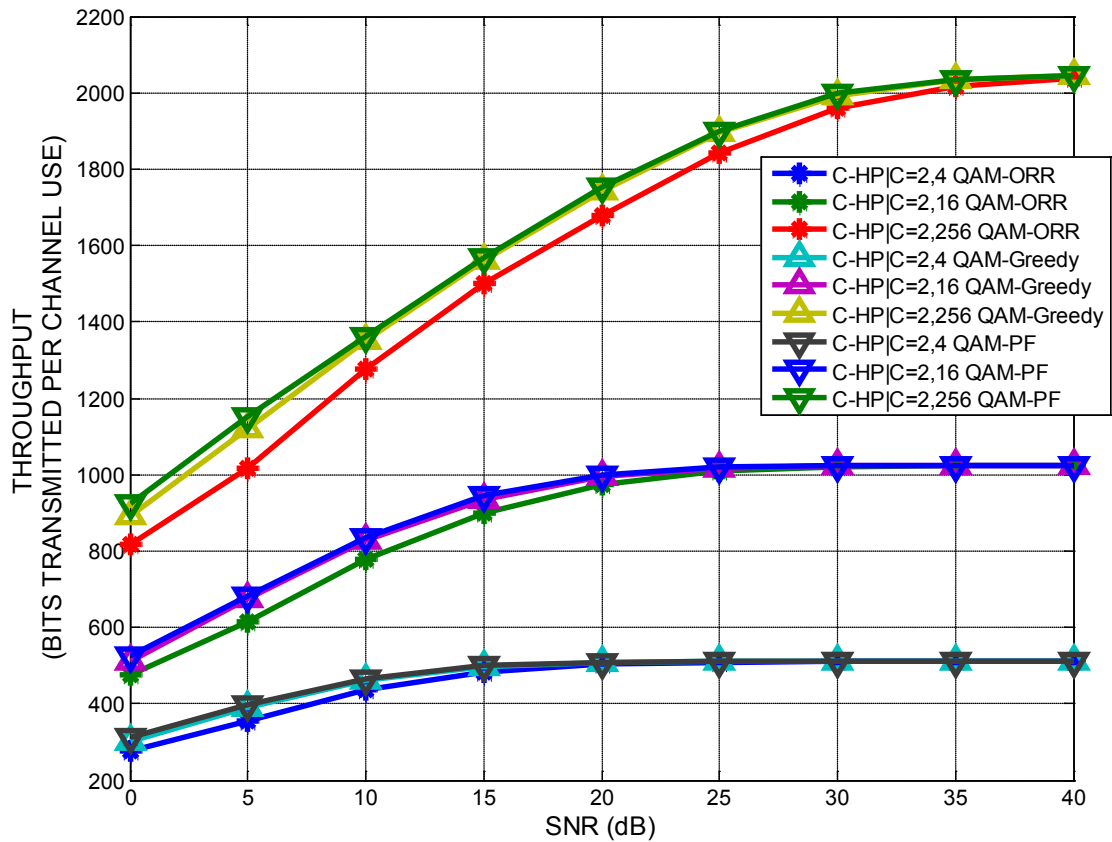


Figure 7.26: Throughput versus SNR for C-HP₂ with user scheduling with 5 users and MinES scheduling criterion, for a 2x2 MIMO, 128 subcarrier OFDM system with IEEE 802.16m urban macrocell channel model.

From the above results in figure 7.26 it can be inferred that MaxMinSV performs the best for both FR-HP and C-HP. Also, PF scheduling performance is similar to Greedy scheduling. Due to PF scheduling algorithm's inherent user fairness, the combination of MaxMinSV and PF scheduling will produce the best results.

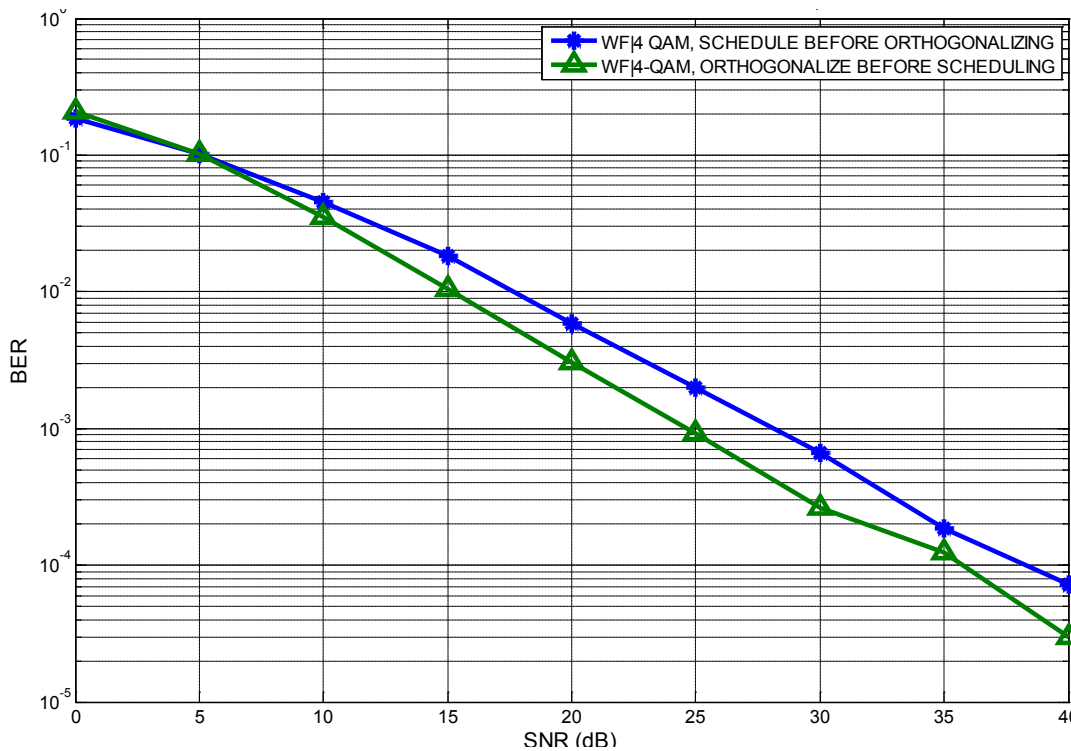


Figure 7.27: BER versus SNR for MU scheduling using WF precoding with MaxMinSV scheduling criterion and greedy scheduling algorithm. 4 users are chosen from a set of 16, for a 2x2 MIMO, 128 subcarrier OFDM system with IEEE 802.16m urban macrocell channel model.

Figure 7.27 shows the BER versus SNR plot for MU scheduling using MaxMinSV criterion and Greedy scheduling algorithm. It can be seen that scheduling the users before orthogonalizing them performs not as well as orthogonalization before scheduling. For a BER of 10^{-3} , there is a gain of 4 dB if users are first orthogonalized and then scheduled. A similar result can be seen in figure 7.28, which shows BER versus SNR curves for FR-HP_{0.5} using MaxMinSV as the scheduling criterion and Greedy scheduling. Figure 7.29 shows the throughput versus SNR curves.

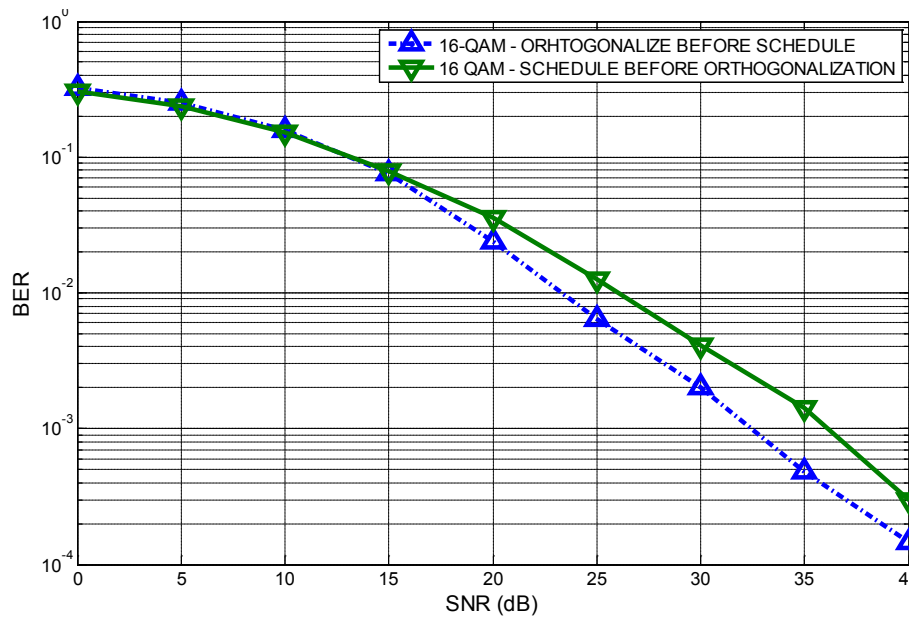


Figure 7.28: BER versus SNR for MU scheduling using WF precoding and 16 QAM constellation with MaxMinSV scheduling criterion and greedy scheduling algorithm. 4 users are chosen from a set of 16, for a 2x2 MIMO, 128 subcarrier OFDM system with IEEE 802.16m urban macrocell channel model.

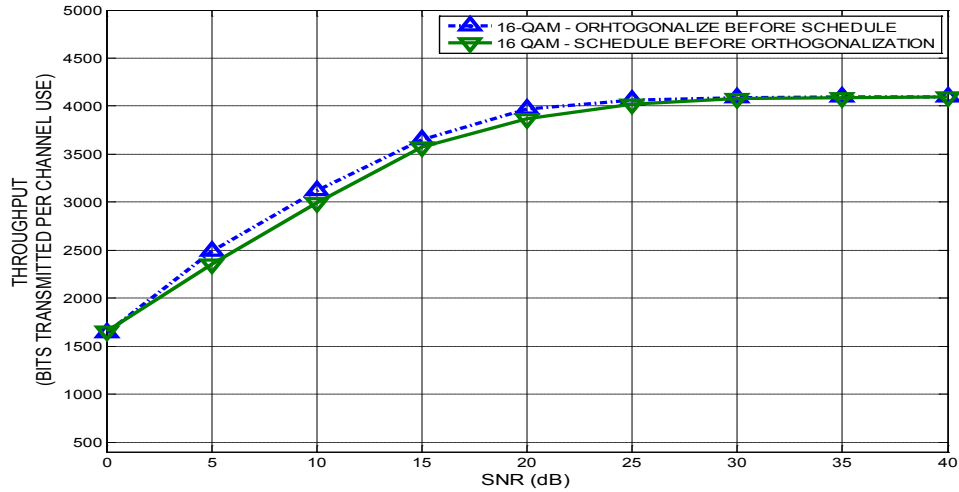


Figure 7.29: Throughput versus SNR for MU scheduling using WF precoding with MaxMinSV scheduling criterion and greedy scheduling algorithm. 4 users are chosen from a set of 16, for a 2x2 MIMO, 128 subcarrier OFDM system with IEEE 802.16m urban macrocell channel model

CHAPTER 8

CONCLUSIONS AND FUTURE

WORK

8.1 CONCLUSIONS

In this thesis, HP has been proposed. HP shows throughput gains of up to 33% at 0dB over WF precoding. FR-HP_{0.5} shows the highest throughput gains, followed by C-HP₄ with a throughput gain of 16% at 0dB over WF. At high SNRs of over 25 dB, both FR-HP and C-HP converge to the WF throughput performance. This gain comes at the cost of deteriorated BER performance. For a BER of 10^{-3} , FR-HP_{0.5} loses 2 dB for BPSK and 1.5 dB with 4 QAM.

In order to overcome the BER deterioration caused by HP, AEMR is proposed. AEMR provides a BER performance versus throughput trade-off. AEMR using SNR cutoff of 15 dB has a lower throughput loss when compared to AEMR using BER cutoff of 10^{-3} , both being compared with WF throughput.

Next, the effect of feedback reduction is studied on the SU-MIMO-OFDM system with WF and HP applied. First, the effect of feedback reduction using WF precoding on a SU-MIMO-OFDM system is studied. The BER results show that feedback in time is more important than feedback in frequency. Feedback reduction with K equal to 0.01 and $N_{Feedback,F}$ equal to 64 OFDM symbols has better BER performance than K value of 0.1 and $N_{Feedback,F}$ equal to 16 OFDM symbols. For a BER of 10^{-3} and 16 QAM constellation, K equal to 0.1 and $N_{Feedback,F}$ equal to 16 OFDM symbols case needs 3 dB more power than K value of 0.01 and $N_{Feedback,F}$ equal to 64. For SNRs up to 20 dB, throughput performance of $K = 1$. Next, the BER and throughput performance of HP is studied with feedback reduction. The BER results show that C-HP₂ performs better than FR-HP_{0.5}. At 25 dB for BPSK, C-HP₂ has a BER of 10^{-2} , whereas for FR-HP_{0.5}, the BER is 1.7×10^{-2} . However, FR-HP_{0.5} performs better at low SNRs of up to 20 dB in terms of throughput, with a gain of 200 bps/Hz over C-HP₂ at 10 dB SNR.

Finally, the performance of user scheduling with HP precoding, for both SU and MU MIMO-OFDMA systems is studied. For the SU case, it is shown that, in the short term of 10 coherence times, minimum singular value is the most fair to all users, when using greedy and PF scheduling. ORR has the worst BER performance, trading off BER performance with user fairness. In the long term of 100 coherence times, the system is fairer to all users, and asymptotically all users would get a fair chance to transmit, irrespective of the scheduling algorithm or the scheduling criterion applied. Choosing users according to their channel's maximum SNR and minimum eigen spread show the lowest BER performance gain due to user scheduling. On the other hand, choosing users

according to their respective channels' minimum singular values shows the highest gain due to user diversity. For the MU case, orthogonalization before scheduling performs better than scheduling before orthogonalizing across all SNRs, both in terms of throughput and BER, for WF precoding.

8.2 FUTURE WORK

The new algorithms that have been introduced in this research work showed improved performance over the existing precoding algorithms. In this section, we are going to show some of the improvements that could be done to these algorithms. Leaving these improvements as a future work, we believe we can get greater benefit from the proposed algorithms.

In this thesis, the feedback reduction done was assumed fixed. In the future, the effects of changing the feedback according to the variations in the channel can be studied, using the proposed precoding algorithms. In the user scheduling chapter, just one scheduling criterion is used at a time. In the future, multiple user selection criteria can be used in an iterative way by grouping users together according to one criterion, and then applying a second criterion to select users from a given group. Also, synchronous channel knowledge is assumed at the transmitter in this thesis. A more general case would be when the channel knowledge at the transmitter is out of sync by a few symbols at all times. Finally, imperfect channel knowledge at receiver will cause performance deterioration, and this effect on performance can also be accounted for during precoding.

APPENDIX

LIST OF ABBREVIATIONS

Acronym	Definition
AEMR	adaptive eigen mode reduction
AGC	automatic gain control
AoA	angle of arrival
AoD	angle of departure
AS	angular spread
AWGN	additive white Gaussian noise
BER	bit error rate
bps/Hz	Bits per second per Hertz
BS	Base station
BW	Bandwidth
CDF	Cumulative distribution function
C-HP	Capacity-based Hierarchical Precoding
CIR	Carrier to interference ratio
CP	Cyclic prefix
CSI	Channel state information
CSIR	Channel state information at the receiver
CSIT	Channel state information at the transmitter
DMMT	Discrete matrix multi-tone
DSL	Digital subscriber line
EGNR	Eigen gain to noise ratio
EMD	Evaluation methodology document
FDM	Frequency division multiplexing
FFT	Fast Fourier transform
FIR	Finite impulse response

FR-HP	Fixed ratio-hierarchical precoding
HP	Hierarchical precoding
IID	Independent identically distributed
ISI	Inter symbol interference
LOS	Line of sight
MIMO	Multiple input multiple output
MMSE	Minimize mean square error
MS	Mobile station
MU	Multiple users
NGR	Noise to gain ratio
NLOS	Non line of sight
OFDM	Orthogonal frequency division multiplexing
OFDMA	Orthogonal frequency division multiple access
ORR	Opportunistic round robin
PBG	Projection based greedy
PDF	Probability density function
PF	Proportional fair
PSD	Power spectral density
QoS	Quality of service
RF	Radio frequency
RR	Round robin
SDMA	Space division multiple access
SINR	Signal-to-interference plus noise ratio
SISO	Single input single output
SMSE	Sum of mean square error
SNR	Signal to noise ratio
SU	Single user
SVD	Singular value decomposition
VBLAST	Vertical-Bell labs layered space time
WF	Waterfilling
WIMAX	Worldwide Interoperability for Microwave Access

REFERENCES

- [1] A. Ghosh, D. R. Wolter, J. G. Andrews, and R. Chen, "Broadband wireless access with WiMax/802.16: current performance benchmarks and future potential," *IEEE Communications Magazine*, vol. 43, no. 2, pp. 129-136, 2005.
- [2] S. J. Vaughan-Nichols, "Achieving wireless broadband with WiMax," *Computer*, vol. 37, no. 6, pp. 10-13, 2004.
- [3] J. Zhuang, L. Jalloul, R. Novak, and J. Park, "IEEE 802 . 16 Broadband Wireless Access Working Group IEEE 802 . 16m Evaluation Methodology Document (EMD)," 2009.
- [4] Z. Wang and G. B. Giannakis, "Wireless Multicarrier Communications where Fourier Meets Shannon," *IEEE Signal Processing*, vol. 17, no. 3, 2000.
- [5] L. Xiao, A. Wang, S. Zhou, and Y. Yao, "A Dynamic Resource Scheduling Algorithm For OFDM System," in *The 9th Asia-Pacific Conference on Communications*, 2003, pp. 21-24.
- [6] G. G. Raleigh and J. M. Cioffi, "Spatio-temporal coding for wireless communication," *IEEE Transactions on Communications*, vol. 46, no. 3, pp. 357-366, Mar. 1998.
- [7] B. Sklar, "Rayleigh fading channels in mobile digital communication systems. I. Characterization," *IEEE Communications Magazine*, vol. 35, no. 7, IEEE, pp. 90-100, 1997.
- [8] S. Al-ghadhban, "Performance Evaluation of Opportunistic Round Robin Scheduling for V_BLAST Users over MIMO Channels," in *International Conference on Telecommunications*, 2009, pp. 82-86.

- [9] K. B. Letaief, J. C.-I. Chuang, and M. L. Liou, "M-PSK and M-QAM BER computation using signal-space concepts," *IEEE Transactions on Communications*, vol. 47, no. 2, pp. 181-184, 1999.
- [10] H. Bolcskei, D. Gesbert, and A. J. Paulraj, "On the capacity of OFDM-based spatial multiplexing systems," *IEEE Transactions on Communications*, vol. 50, no. 2, pp. 225–234, 2002.
- [11] A. Goldsmith, S. Member, S. A. Jafar, S. Member, and N. Jindal, "Capacity Limits of MIMO Channels," *IEEE Journal on Selected Areas in Communications*, vol. 21, no. 5, pp. 684-702, 2003.
- [12] W. Yu, W. Rhee, and J. M. Cioffi, "Optimal power control in multiple access fading channels with multiple antennas," in *IEEE International Conference on Communications, 2001. ICC 2001.*, 2001, pp. 575-579.
- [13] S. Hemrungle, T. Hori, M. Fujimoto, and K. Nishimori, "Channel capacity characteristics of multi-user MIMO systems in urban area," *IEEE Antennas and Propagation Society International Symposium*, pp. 1-4, 11-17, 2010.
- [14] M. Maw and I. Sasase, "Resource allocation scheme in MIMO-OFDMA system for user's different data throughput requirements," in *Wireless Communications and Networking Conference, 2007*, pp. 1708-1712.
- [15] E. Visotsky and U. Madhow, "Space-time transmit precoding with imperfect feedback," *IEEE Transactions on Information Theory*, vol. 47, no. 6, pp. 2632–2639, 2001.
- [16] H. Sampath and A. Paulraj, "Joint Transmit and Receive Optimization for High Data Rate Wireless Communication Using Multiple Antennas," in *Conference Record of the Thirty-Third Asilomar Conference on Signals, Systems, and Computers, 1999.*, 1999, pp. 215-219.
- [17] H. Sampath, P. Stoica, and A. Paulraj, "Generalized Linear Precoder and Decoder Design for MIMO Channels Using the Weighted MMSE Criterion," *IEEE Transactions on Communications*, vol. 49, no. 12, pp. 2198-2206, 2001.
- [18] C. Windpassinger, R. F. H. Fischer, T. Vencel, and J. B. Huber, "Precoding in multi-antenna and multiuser communications," *IEEE Transactions on Wireless Communications*, vol. 3, no. 4, pp. 1305–1316, 2004.
- [19] Y. Jiang, M. Shen, and Y. Zhou, "Two-dimensional water-filling power allocation algorithm for MIMO-OFDM systems," *Science China Information Sciences*, vol. 53, no. 6, pp. 1242-1250, Apr. 2010.

- [20] G. Munz, S. Pfletschinger, and J. Speidel, "An efficient waterfilling algorithm for multiple access OFDM," in *Global Telecommunications Conference, 2002. GLOBECOM'02. IEEE*, 2002, vol. 1, pp. 681–685.
- [21] H. Karaa, R. S. Adve, and A. J. Tenenbaum, "Linear precoding for multiuser MIMO-OFDM systems," in *IEEE International Conference on Communications*, 2007, pp. 2797–2802.
- [22] L. Zhou, X. Li, Y. Hei, and G. Yu, "Channel orthogonalization precoding algorithms for multiuser MIMO downlink systems," in *International Conference on Communications and Signal Processing*, 2011, no. 60702060, pp. 339-343.
- [23] Y. H. Yang, S. C. Lin, and H. J. Su, "Multiuser MIMO Downlink Beamforming Design Based on Group Maximum SINR Filtering," *IEEE Transactions on Signal Processing*, vol. 59, no. 4, pp. 1746–1758, 2011.
- [24] X. Li and N. Park, "Differential Precoding Scheme of LTE Systems over Temporally Correlated Channels," in *IEEE Vehicular Technology Conference*, 2011.
- [25] C. Zhong, L. Yang, and M. You, "Dynamic Resource Allocation for Downlink Multiuser MIMO-OFDMA/SDMA Systems," *Circuits, Systems, and Signal Processing*, vol. 29, no. 6, pp. 1061–1074, 2010.
- [26] J. Choi and R. W. Heath Jr, "Interpolation Based Transmit Beamforming for MIMO-OFDM With Limited Feedback," *IEEE Transactions on Signal Processing*, vol. 53, no. 11, pp. 4125–4135, 2005.
- [27] P. Tejera, W. Utschick, G. Bauch, and J. A. Nossek, "Subchannel Allocation in Multiuser Multiple-Input-Multiple-Output Systems," *IEEE Transactions on Information Theory*, vol. 52, no. 10, pp. 4721–4733, 2006.
- [28] H. Wang, L. Li, J. Wang, and L. Song, "A Transmit Precoding Scheme for Downlink Multiuser MIMO Systems," in *IEEE Vehicular Technology Conference*, 2011.
- [29] P. W. C. Chan and R. S. Cheng, "Capacity Maximization for Downlink Systems with Multiuser Diversity," *IEEE Transactions on Communications*, vol. 6, no. 5, pp. 1880-1889, 2007.
- [30] V. Tralli, P. Henarejos, and A. Perez-Neira, "A low complexity scheduler for multiuser MIMO-OFDMA systems with heterogeneous traffic," in *International Conference on Information Networking*, 2011, no. 1, pp. 251–256.

- [31] M. Esslaoui, F. Riera-Palou, and G. Femenias, "Opportunistic multiuser MIMO for OFDM networks," in *8th International Workshop on Multi-Carrier Systems & Solutions (MC-SS)*, 2011, pp. 1–5.
- [32] G. Dimic and N. D. Sidiropoulos, "On Downlink Beamforming With Greedy User Selection: Performance Analysis and a Simple New Algorithm," *IEEE Transactions on Signal Processing*, vol. 53, no. 10, pp. 3857–3868, 2005.
- [33] G. Liu, J. Zhang, F. Jiang, and W. Wang, "Joint Spatial and Frequency Proportional Fairness Scheduling for MIMO OFDMA Downlink," in *International Conference on Wireless Communications, Networking and Mobile Computing*, 2007, pp. 491-494.
- [34] E. Lo, P. Chan, and V. Lau, "Adaptive resource allocation and capacity comparison of downlink multiuser MIMO-MC-CDMA and MIMO-OFDMA," *IEEE Transactions on Wireless Communications*, vol. 6, no. 3, pp. 1083-1093, 2007.
- [35] Z. Shen, J. G. Andrews, and B. L. Evans, "Adaptive resource allocation in multiuser OFDM systems with proportional rate constraints," *IEEE Transactions on Wireless Communications*, vol. 4, no. 6, pp. 2726- 2737, 2005.
- [36] C. Mohanram and S. Bhashyam, "Joint subcarrier and power allocation in channel-aware queue-aware scheduling for multiuser OFDM," *IEEE Transactions on Wireless Communications*, vol. 6, no. 9, pp. 3208–3213, 2007.
- [37] V. D. Papoutsis, I. G. Fraimis, and S. A. Kotsopoulos, "Resource allocation algorithm for MIMO-OFDMA systems with minimum resources guarantee," in *17th IEEE International Conference on Electronics, Circuits, and Systems*, 2010, pp. 363–366.
- [38] N.-D. Đào and Y. Sun, "User-selection algorithms for multiuser precoding," *IEEE Transactions on Vehicular Technology*, vol. 59, no. 7, pp. 3617–3622, 2010.
- [39] E. Conte, S. Tomasin, and N. Benvenuto, "A simplified greedy algorithm for joint scheduling and beamforming in multiuser MIMO OFDM," *IEEE Communications Letters*, vol. 14, no. 5, pp. 381–383, 2010.
- [40] T. Thomas, B. Mondal, and K. Baum, "User Selection for SDMA Beamforming with Imperfect CSI in MIMO-OFDM Systems," in *IEEE International Conference on Communications*, 2007, pp. 5419-5422.

- [41] N. Shrivastava, S. P. Singh, and A. Trivedi, “Joint scheduling and random beamforming with reduced feedback in multiuser MIMO-OFDM,” in *Wireless Advanced (WiAd)*, 2011, pp. 66–69.

VITA

- Name: Siddharth Nair
- Date of Birth: 12th June, 1985
- Nationality: Indian
- Received Bachelor of Technology (B.Tech) with honors in Electronics and Communications Engineering from Allahabad Agricultural Institute - Deemed University, Allahabad, India, 2008.
- Joined Electrical Engineering Department at King Fahd University of Petroleum and Minerals (KFUPM), Dhahran, Saudi Arabia, Research Assistant in October 2009.
- Received Master of Science (M.S) in Telecommunication from KFUPM in January 2012.
- Present Address: Bldg.802, Room 311, P.O. Box No. 8613, KFUPM, Dhahran 31261, Saudi Arabia.
- Permanent Address: M-67/M.I.G., Ganga Vihar, Jajmau, Kanpur, India - 208010
- E-mail: nairsiddarth.85@gmail.com
- Mobile Number: 00966544646247